Noise Coupling Effect in Multi-antenna Systems

Snezana Krusevac

November 2007

A thesis submitted for the degree of Doctor of Philosophy
of the Australian National University

To my mother and the loving memory of my father

Declaration

November 14, 2007

The contents of these thesis are the results of original research and have not been submitted for a higher degree to any other university or institution.

Much of the work in this thesis has been published or has been submitted for publication as journal paper or conference paper. These papers are:

1. S. Krusevac, P. B. Rapajic and R. A. Kennedy, Mutual Coupling Effect on Thermal Noise in Multi-antenna Communication System, Progress in Electromagnetics Research (PIER) Journal PIER 59, pages 325-333, 2006.

2. S. M. Krusevac, P. B. Rapajic and R. A. Kennedy, Thermal Noise Mutual Coupling Effect on the Capacity of MIMO Wireless Systems, Wireless Personal Communications Journal, Springer, volume 40 (3), pages 317-328, Feb. 2007.

3. S. Krusevac, P. B. Rapajic and R. A. Kennedy, Method for MIMO Channel Capacity Estimation for Electro-Magnetically Coupled Transmit Antenna Elements, Proc. 5th Australian Communications Theory Workshop, AusCTW'2004, pages 122-126, Newcastle, Australia, Feb. 2004.

4. S. Krusevac, P. B. Rapajic and R. A. Kennedy, Channel Information Capacity for Mutually Coupled Transmittal Antennas, Proc. 2004 Progress in Electromagnetics Research Symposium, PIERS 2004, pages 639-642, Pisa, Italy, Mar. 2004.

5. S. Krusevac, P. B. Rapajic and R. A. Kennedy, The Method for MIMO Channel Capacity Estimation in the Presence of Spatially Correlated Noise, Proc. 2004 IEEE International Symposium on Spread Spectrum Techniques and Applications, ISSSTA 2004, pages 511-514, Sydney, Australia, Sep. 2004.

6. S. Krusevac, P. B. Rapajic, R. A. Kennedy and P. Sadeghi, Mutual Coupling Effect on Thermal Noise in Multi-antenna Communication

Systems, Proc. 6th Australian Communications Theory Workshop, AusCTW'2005, pages 192-197, Brisbane, Queensland, Australia, Feb. 2005

7. S. Krusevac, P. B. Rapajic and R. A. Kennedy, Capacity Bound of MIMO Systems in the Presence of Spatially Correlated Noise, Proc. 8th International Symposium on Communication Theory and Applications, ISCTA05, pages 298-303, Ambleside, Lake District, UK, July 2005.

8. S. Krusevac, P. B. Rapajic and R. A. Kennedy, Effect of Mutual Coupling on the Performance of Multielement Antenna Systems, Proc. 2005 IEEE International Symposium on Antennas and Propagation, ISAP05, pages 565 - 568, Seoul, Korea, Aug. 2005.

9. S. Krusevac, P. B. Rapajic and R. A. Kennedy, Mutual Coupling Effect on Thermal Noise in Multi-antenna Communication System, Proc. 2005 Progress in Electromagnetics Research Symposium, PIERS 2005, pages 53-57, Honzhou, China, Aug. 2005.

10. S. Krusevac, P. B. Rapajic and R. A. Kennedy, Channel Capacity of Multi-antenna Communication Systems with Closely Spaced Antenna Elements, Proc. The 16th Annual IEEE International Symposium on Personal Indoor and Mobile Radio Communications, IEEE PIMRC 2005, pages 2366-2370, Berlin, Germany, Sep. 2005.

11. S. Krusevac, P. B. Rapajic and R. A. Kennedy, Thermal Noise Mutual Coupling Effect on the Capacity of MIMO Wireless Systems, Proc. Wireless Personal Multimedia Communications Symposia 2005, WPMC'05, pages 466 - 470, Aalborg, Denmark, Sep. 2005.

12. S. Krusevac, P. B. Rapajic and R. A. Kennedy, SNR Estimation for Multi-antenna Communication Systems with Closely Spaced Antenna Elements, Proc. The Eight IEEE International Symposium on Signal Processing and Its Applications, ISSPA 2005, pages 423-426, Sydney, Australia, Sep. 2005.

13. S. Krusevac, P. B. Rapajic and R. A. Kennedy, Channel Capacity of MIMO Wireless Systems with Correlated Noise, Proc. 2005 IEEE Global Telecommunications Conference, IEEE GLOBECOM 2005, pages 2812-2816, St. Louis, Missouri, USA, Dec. 2005.

14. S. Krusevac, P. B. Rapajic, Channel Capacity of MIMO Systems with Closely Spaced Terminated Antennas , ISIT 2007, pages 1076-1080, 24 - 29 June 2007, Nice, France

The research represented in this thesis has been performed jointly with Professor Predrag B. Rapajic and Professor Rodney A. Kennedy. The substantial majority of this work is my own.

Snežana Krusevac

November 14, 2007

Acknowledgements

I would like to extend my sincere thank to my supervisors Prof. Rodney A. Kennedy and Prof. Predrag B. Rapajic for letting me dictate the pace of my research, giving me freedom to a large extent on the choice of topics, their invaluable guidance and encouragement, and for giving me invaluable insight into my research.

I would also like to thank A. Prof. Thushara Abhayapala and A. Prof. Rodica Roamer for many fruitful discussions during my research. Although no results from these interactions become part of this thesis, the experience was invaluable and their energy and enthusiasm was infectious.

My friends and colleagues at the University of New South Wales, National ICT Australia and Australian National University, for providing fruitful and pleasant research environment.

I would like thank to my family and friends who make it all worth while. My mother Stojanka for believing in me (if I ever become as good as you believe in me - it will be purely a result of good genes). My sister Sladjana has supported me with her endless love, caring and patience. My dearest nephew Nikola and nice Hristina have enhanced my life in every respect. My brother-in-low Zvezdan for being friend out of ordinary.

Finally, no words are sufficient to express my love and gratitude to my husband Zarko and my baby daughter Nevena. Zarko has supported and encouraged me in pursuing my dreams, and has always been there to make sure they become realities. Nevena is the sunshine in my universe - each day is brighter because of her love and sweetness. I am incredibly lucky to share my life with these two special people.

This work was founded by the Australia Research Council and National ICT Australia.

Abstract

Close antenna spacing, less than a half of a wavelength, in multi-antenna systems results in mutual coupling which affects the capacity performance of multi-antenna systems. In contrast to previous studies which study mutual coupling's effect on signals, this thesis examines the effect of mutual coupling on thermal noise.

We investigate noise correlation in closely spaced multiple antennas, and find that noise is correlated due to the mutual coupling. We calculate the noise covariance matrix, and the corresponding total thermal noise power in multi-antenna systems by applying the Nyquist thermal noise theorem. Then, we calculate the receive signal-to-noise ratio in the coupled antenna system to complete the quantitative analysis.

By taking into account the noise correlation effect, we provide an analysis of the ergodic channel capacity with equal power allocation and water-filling power allocation schemes of the transmitted power. We show that ergodic capacity of MIMO systems is underestimated if the noise correlation due to the mutual coupling on thermal noise is neglected. Furthermore, we confirm that the water-filling allocation scheme is superior to the equal-power allocation scheme, which is more significant when multiple antennas with non-uniformly spaced antennas are used at the receiver. In that case the noise coupling affects the signal-to-noise ratio of individual antennas differently.

In order to provide an analysis of the full distribution of the mutual information over fading channels, we examine the outage capacity which indicates the variance of the mutual information. Our numerical investigation of the outage capacity shows that the multi-antenna systems with small antenna spacing up to 0.2 λ provides almost $4 - 6$ % better performance in terms

of outage capacity when the mutual coupling on the noise is accounted for. We look at the effective degrees of freedom in the MIMO systems in order to isolate the noise correlation effect on the channel capacity. We show that for a very small antenna spacing ($d \longrightarrow 0$), when the number of effective subchannels drops to 1, the water-filling allocation scheme is superior as it reconfigures to the optimal situation of allocating the total power to only one receiving antenna. We extract the contribution from the noise correlation in the channel capacity formula by deriving the noise correlation factor. It enables us to derive of the upper bound on channel capacity of MIMO system in the presence of correlated noise. This is a significant result as it further enables us to estimate the channel capacity of the multiple antennas with closely spaced antennas avoiding complex matrix computations, which are time-consuming for large numbers of antenna elements. We conclude that noise coupling is a substantial parameter in determining the channel capacity of closely spaced multiple antennas.

In order to accurately calculate the received correlated noise power, we consider the antenna mismatching impedance effect. We analyze the noise covariance matrix for the three most common antenna terminated matching networks. We show that multi-port conjugate match acts not only as the optimal match in terms of maximal delivered signal power, but also as the whitening filter for the coupled thermal noise.

Based on the results of our termination network analysis we conclude that an adequate matching decoupling network design has to be based on the signal-to-noise ratio analysis rather than on the signal power analysis alone. This is especially important for wireless systems operating in the low signal-to-noise regime such as mobile handheld devices.

Contents

List of Figures

Notation and terminology

Notation

B	bandwidth in Hz
$(\cdot)^T$	Matrix transpose
$(\cdot)^\dagger$	Hermitian matrix transpose
$(\cdot)^*$	Complex conjugate of argument
$\lvert\cdot\rvert$	Determinant of Matrix
$\det(\cdot)$	Determinant of matrix argument
$\mathrm{diag}(\cdot)$	Diagonal operator - retaining only the diagonal elements of the matrix
$\mathrm{Tr}(\cdot)$	Trace operator
$\mathbf{I}_m$	$(m \times m)$ identity matrix
$E\{\cdot\}$	Statistical expectation operator
$\mathbf{H}$	Channel matrix
$\hat{\mathbf{H}}$	Channel matrix - elements are spatially correlated
$\mathbf{C}$	Coupling matrix
C_{eq}	Calculated channel capacity with equal power allocation scheme at transmitter

C_{wf}	Calculated channel capacity with water-filling allocation scheme at transmitter
$\mathbf{N}$	Uncorrelated noise matrix
$\mathbf{N}_c$	Correlated noise matrix
$\hat{\mathbf{N}}_c$	Noise coupling matrix
P_T	Radiated power
$\mathbf{Q}_x$	Covariance matrix of transmitted signals
Z_{mn}	Impedance between ports m and n
Y_{mn}	Admittance between ports m and n
E_{mn}	thermal noise voltage between ports m and n
J_{mn}	thermal noise current from port m to port n
$\mathbf{Z}$	Mutual impedance matrix
$\mathbf{Y}$	Mutual admittance matrix
$\mathbf{e}$	Thermal noise voltage vector
$\mathbf{j}$	Thermal noise current vector
f	frequency in Hz
h	Planck's constant $h = 6.6260692 \times 10^{-34} Js$
i	Imaginary unit
k	Boltzmann's constant $1.3806503 \times 10^{-23} J/K$
$k_\omega = 2\pi/\lambda$	angular wavenumber
n_T	number of transmitting antennas
n_R	number of receiving antennas

T	absolute temperature in K
ω	angular frequency

Terminology

AoA	Angle of Arrival
AWGN	Additive White Gaussian Noise
BER	Bit-Error-Rate
BLAST	Bell labs LAyered Space Time
D-BLAST	Diagonally LAyered Space Time
H-BLAST	Horizontal LAyered Space Time
BS	Base station
CDF	Cumulative Distribution Function
DoA	Direction of Arrival
DoD	Direction of Departure
DSPU	Digital Signal Processing Unit
EDOF	Effective Degrees of Freedom
EQ	Equal (power allocation scheme)
i.i.d.	Independent and Identically Distributed
IF	Intermediate Frequency
LNA	Low-Noise Amplifier
SISO	Single Input Single Output
MIMO	Multiple Input Multiple Output

MLSE	Maximum Likelihood Sequence Estimation
MMSE	Minimum Mean-Square Error
MS	Mobile Station
MISO	Multiple Input Single Output
NF	Noise Factor
SIMO	Single Input Multiple Output
RX	Receiving unit
QAM	Quadrature Amplitude Modulation
UCA	Uniform Circular Array
ULA	Uniform Linear Array
WF	Water-Filling (power allocation scheme)
ZF	Zero-Forcing

Part I

Mutual Coupling in Multi-antenna System

Chapter 1

Introduction

1.1 Motivation and Background

The ability to communicate with people on the move has evolved remarkably since Guglielmo Marconi first demonstrated radio's ability to provide continuous contact with ships sailing the English channel. This was in 1897, and since then new wireless communication methods and services have been enthusiastically adopted by people throughout the world. This has enormous implications on the growth of the mobile radio communication industry in the last few decades. The growth and diversity of applications in addition to the increase of the number of users keep raising new challenges over all aspects of mobile communication system design.

Ever-increasing demand for high speed communications and steadily increasing miniaturization of mobile hand-held devices place additional, but often conflicting, requirements on the mobile communication system design. The proposed solution based on using multiple antennas at both ends of wireless links, known as Multiple Input Multiple Output (MIMO) systems, emerges as a promising solution for the demand for high information throughput [1, 2]. Namely, a single user system with n_T transmit and n_R receive antennas could theoretically achieve $\min(n_T, n_R)$ separate channels in a multipath propagation environment. It means that capacity scales linearly with $\min(n_T, n_R)$ relative to a system with just one transmit and one receive antenna known as a SISO (Single Input Single Output) system.

However, this linear capacity scaling in MIMO systems is achievable only under certain assumptions. First of all, the wireless channel should be the independent and identically distributed (i.i.d.) Rayleigh fading channel [1]. This channel scenario corresponds to the wireless channel with the majority of the generated transmission paths being mutually independent. Such a wireless channel barely reflects reality, and hence it forces the research community to search for more realistic channel models. Further investigations have found that the achievable information rate in the real-case scenario, of a more realistic channel model environment, is less than one predicted in [1,2].

The calculated high capacity gain of MIMO systems is also implicitly based on the assumption that antennas are widely spaced in the multi-antenna systems. Antennas should be spaced at least a at the half of a the wavelength apart from each other. However, this condition is directly opposed to the miniaturization trend of the mobile hand-held devices. Therefore, the potential implications on the capacity performance should be thoroughly investigated if multiple antennas with small antenna spacing are intended to be used in mobile hand-held devices.

Small antenna spacing in multi-antenna system results in high signal correlation. It appears that signal correlation is consequence of two phenomena. One is the electromagnetic coupling [3–5] between antennas, and another is scattering effects [6–8] in wireless channel. However, the focus in these studies has been signal behavior in multiple antennas, while studies omit thermal noise despite the fact that it is also electromagnetic radiation. Therefore, in this thesis we provide an analysis of thermal noise behavior in multi-antenna system.

First of all, we question the noise correlation in multiple antennas. We have found that if antenna spacing is less than a half of a wavelength, thermal noise at each antenna port will appear as a correlated noise, and the correlation is due to mutual coupling. Then, we estimate the noise correlation effect on the MIMO channel capacity.

1.2 Multiple Antennas

A significant improvement in the capacity performance can be achieved by using multiple antennas. The potential capacity improvement is based on the processing technique that exploits space as a new degree of freedom.

In general, by utilizing multiple antennas, one or more of the following benefits can be achieved:

- *Spatial diversity* - multiple antennas can be used to counteract the channel fading due to multipath propagation. This is based on the fact that multiple copies of the transmitted signals can be received in the multipath propagation environment, and those copies of the transmitted signals are affected by different fading conditions. This can be utilized to obtain a higher data throughput or to decrease the transmission power.

- *Multiplexing gain* - by using multiple antennas, a higher data throughput can be achieved. The rate increase over the single antenna channel capacity is known as the multiplexing gain.

- *Array gain* - by forming an assembly of radiating elements, an equivalent antenna gain can be significantly increased. In such a way, range and coverage of such device can be enlarged. Furthermore, the transmit power of the mobile hand-held devices can be reduced due to the increased gain, or sensitivity of the receiving antenna array;

- *Interference suppression* - by using the spatial dimension provided by multiple antennas, superior interference suppression can be obtained in comparison with a single antenna system. Hence, the system can be tuned to be less susceptible to interference improving the system capacity;

Three major applications, beamforming, diversity combining and spatial multiplexing, have been established demonstrating the benefits of utilizing multiple antennas. In the following, those applications will be discussed.

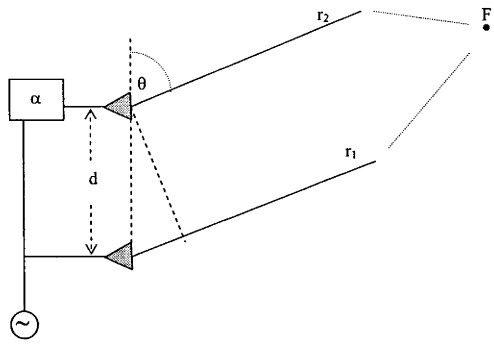

Figure 1.1: Beamforming technique with two-antenna array

Typical Applications

The *beam-forming* technique exploits the differential phase between different antennas normally at RF level to modify the antenna pattern of the whole array.

In order to get better insight into the beamforming technique, we present a simple example by calculating the radiation pattern for a two-antenna array. The aim is to calculate the strength of the electric field E at point F due to the radiation from the antennas as shown in Fig. 1.1. At point F, which belongs to the antenna far-field, the narrowband received field is given by

$$\begin{aligned} E_F &= E_0 e^{-ir_1} + E_0 e^{i\alpha - ir_2} \\ &= E_0 e^{-ir_1} + E_0 e^{i(-r_1 + k_\omega d\cos\theta + \alpha)} \\ &= E_0 e^{-ir_1}(1 + e^{i(k_\omega d\cos\theta + \alpha)}) \end{aligned}$$

where $r_1, r_2, d, \alpha, \theta$ are defined as in Fig. 1.1; Block denoted by α represents a multiplier $e^{i\alpha_j}$ $k_\omega = 2\pi/\lambda$ is the angular wavenumber.

Further the modulus of the electric field E received at point F can be calculated as

$$\begin{aligned} |E_F| &= |E_0| \cdot \left|(1 + e^{i\psi})\right| \\ \psi &= k_\omega d\cos\theta + \alpha \end{aligned}$$

where $|E_0|$ is the modules of the radiation pattern of a single antenna when it is used on its own. This radiation pattern is called unit radiation pattern,

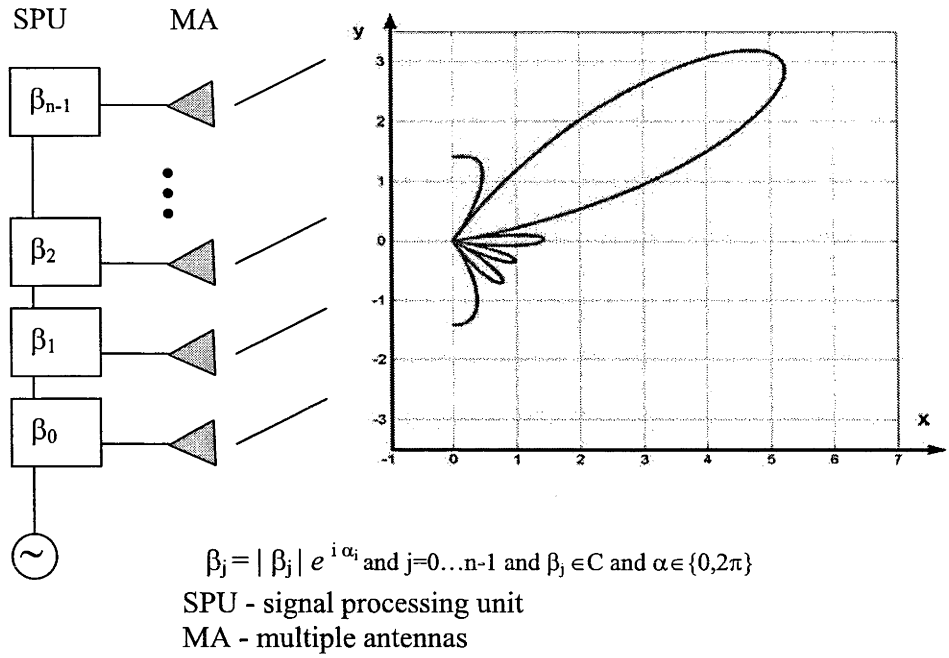

Figure 1.2: Beamforming technique with n-antenna array

while $|(1+e^{i\psi})|$ is the array factor. Similarly, the calculation can be repeated for the general case of phase beamforming, i.e., the antenna array with n antennas shown in Fig. 1.2. Then, the antenna array radiation pattern is given by

$$|E_F| = |E_0| \cdot \left| \frac{\sin n\psi/2}{\sin \psi/2} \right|$$

In the beamforming arrangement, once the signals are combined, the whole array has a single antenna pattern as graphically presented in Fig. 1.2.

For the beamformer to steer the radiation in a particular direction and to place the nulls in the interfering directions, the directions of arrival has to be known beforehand. In particular, by processing the received signal at the output of the array, the directions of arrivals of the incoming signals are computed. Then, this angle information is fed into the beamforming network to compute the complex weight vectors, phase delay coefficients α_j and weightings $|\beta_j|$, for beam steering as illustrated in Fig. 1.2.

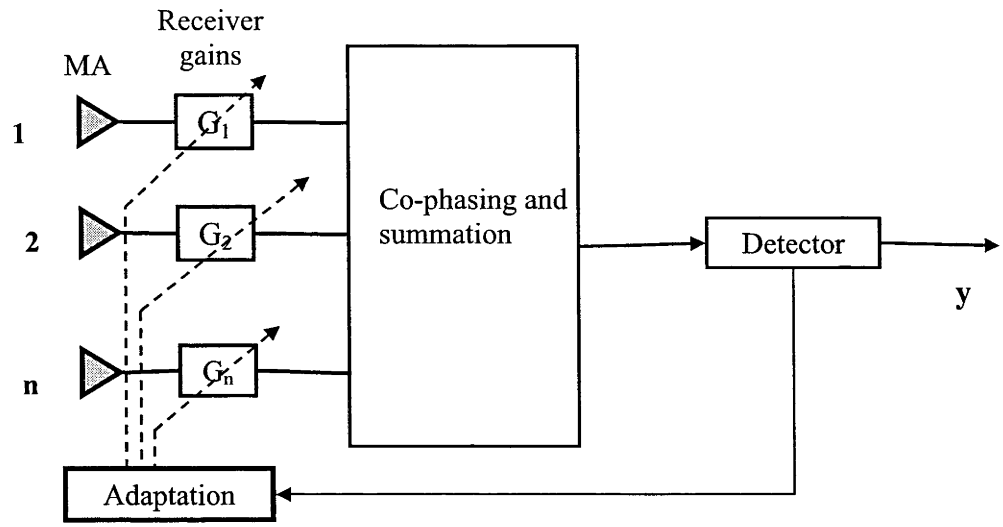

Figure 1.3: Diversity combining technique

Beamforming techniques can be broadly divided into two categories: conventional (fixed) beamformers and adaptive beamformers. In the *conventional* beamforming technique, a fixed set of weightings $|\beta_j|$ and phase shifts $e^{i\alpha_j}$ is used to combine the signals from the antennas in the multiple antenna system. Based on the information about the locations of the antennas in space and the wave directions of interests, the fixed weights β_j are calculated in the signal processing unit (SPU). In the case of *adaptive* beamforming techniques, the weights are automatically updated by using the information about the antenna locations and wave directions, as well as the information extracted from the received signals. As the name indicates, in an adaptive beamforming technique, the response is automatically adapted and updated to different channel conditions and received signals variations.

Diversity combining is employed to overcome the problem of fading in radio channels by utilizing the fact that the signals arriving at different locations fade under different conditions. The signals are combined at the baseband or at the intermediate frequency (IF) level to increase the signal level without affecting the individual antenna patterns. Three common diversity combining techniques are elaborated below: selection diversity, equal-ratio combining and maximum ratio-combining.

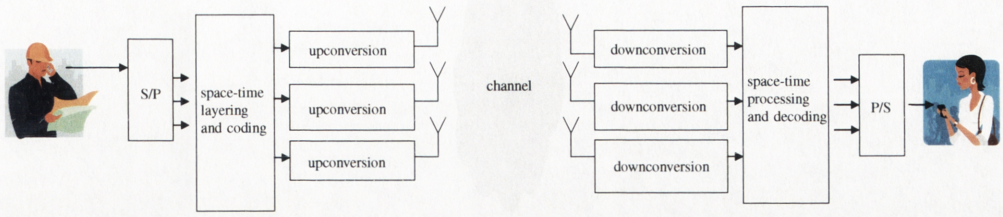

Figure 1.4: Spatial multiplexing technique

Selection diversity is the simplest of these methods. From a collection of n antennas the branch with the largest signal-to-noise ratio (SNR) at any time is selected and connected to the receiver. As one would expect, the larger the value of n the higher the probability of having a larger SNR at the output.

Maximal SNR ratio combining takes a better advantage of all the diversity branches in the system, and its block scheme is presented in Fig. 1.3. All n branches are weighted with their respective instantaneous signal-to-noise ratios. The branches are then co-phased prior to summing in order to ensure that all branches are added in phase for maximum diversity gain. The summed signals are then used as the received signal. The maximal SNR ratio combiner has advantages over selection diversity but is more complicated. Proper care has to be taken in order to ensure that signals are cophased correctly and gain coefficients are constantly updated.

A variation of maximal ratio combining is equal gain combining. An equal gain combiner adjusts the phases of the desired signals and combines them in-phase after equal weighting. The output is a cophased sum of all the branches.

Finally, *spatial multiplexing* uses multiple antennas at the transmitter for transmission of parallel data streams as illustrated in Fig. 1.4. An original high-rate data stream is multiplexed into several parallel streams, each of which is sent from one transmit antenna element. The channel "mixed up" these data streams, so that each of the receive antenna element "sees" a combination of them. If the channel is "well-behaved", the received signals represent linearly independent combinations of the transmitted data streams.

In this case, an appropriate signal processing technique at the receiver can separate the downstream signals. A basic condition is that the number of receive antenna elements is at least as large as the number of transmit antennas. This technique allows the data rate to be increased by a factor equals to the minimum between the number of transmitting and receiving antennas. The spatial multiplexing technique will be further investigated later in this thesis.

1.3 Closely Spaced Multiple Antennas

1.3.1 Mutual Coupling Effect

When antennas are closely spaced to one other, some of the energy that is primary intended for one antenna ends up at the adjacent antennas. Thus, the received signal of each antenna reflects not only the magnitude of direct incoming electromagnetic waves, but also some portion of the signals induced by the adjacent antennas. The effect is known as *mutual coupling.*

The portion of signal that will be induced from the adjacent antennas depends on a number of parameters. We summarize the most important parameters affecting mutual coupling.

- *Separation between antenna elements* is the most crucial parameter affecting mutual coupling. Analytical studies [5] have shown that if the antenna spacing is equal to or greater than a half of a wavelength, mutual coupling is negligible. This implies that mutual coupling will also depend on the frequency of the signals being received since the distance is expressed in terms of the wavelength;

- In addition to the separation of antenna elements, *array geometry* and the *positions* of the antenna elements in the array also affect mutual coupling. The impact of the placement of antenna elements on the capacity performance of portable devices has been investigated in [9], and it has been found that a single antenna element is differently affected by the mutual coupling in a nonuniform array comparing to a uniform

array. Elements on the periphery of the antenna array are less affected by the reradiated signals than the other antenna elements;

- *Radiation characteristics of antenna* is one of the factors determining mutual coupling level among the multiple antennas. This can be illustrated by the following example which considers the two antennas case. If both antennas are transmitting, some of the energy radiated from each will be received by other because of the nonideal directional characteristic of practical antennas. Part of the incident energy on one or both antennas may be rescattered in different directions allowing them to behave as secondary transmitters [4]. Similar analysis can be obtained for the receiving mode of antennas;

- *Relative orientation of antennas* in the multi-antenna array plays an important factor determining the level of mutual coupling. As an example, mutual coupling could almost vanish if dipoles are orthogonally positioned to each other, as it has been shown in [10];

- Another parameter that affects mutual coupling is *direction of arrival* (DoA). Studies have shown that mutual coupling and DoA are strongly coupled [11]. This effect mostly occurs in adaptive antenna arrays. In order to direct the antenna beam to a specific angle, the phase shifters in feeding network need to be adjusted, resulting in a different feeding network and hence different mutual coupling scenarios. Moreover, waves impinging on antennas from different angles generate surface waves in different directions, which results in different mutual coupling;

- *Surrounding objects* in the near field of the antenna elements affect mutual coupling. Re-radiated signals from antenna elements can be reflected back from the near-field scatterers and be coupled back to the other elements, resulting in more coupling.

Based on the previous discussion, it is difficult to predict the mutual coupling, using closed form expressions, if all these parameters are to be accounted for. Furthermore, the results can not be generalized to any configuration of multiple antennas. However, mutual coupling must be taken into

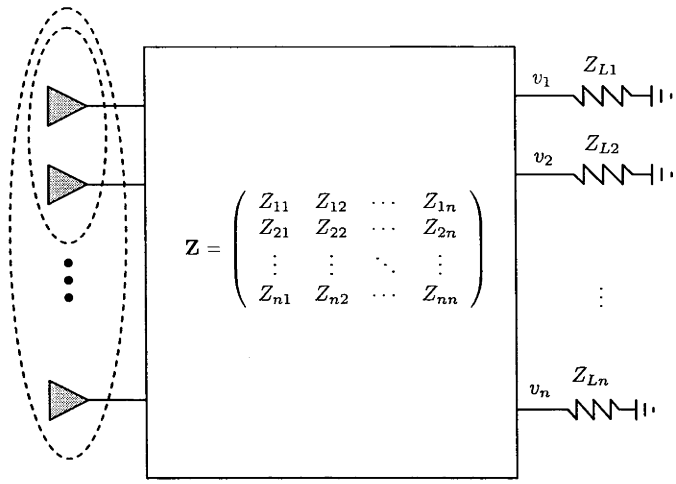

Figure 1.5: Network representation of multi-antenna system with coupled antennas

account because of its significant impact on system performance. Therefore, we discuss network modeling and simulation methods that account for mutual coupling in the next section. We also outline the method used for simulation analysis in this thesis.

1.3.2 Modeling of Closely Spaced Multiple Antennas

The multi-antenna array can be regarded as a n port network with n terminals (shown in Fig. 1.5). If the vector of induced currents is written as

$$\mathbf{i} = [i_1, i_2, ..., i_n]^T$$

where $(.)^T$ denotes transpose, and the vector of terminal voltages is given by

$$\mathbf{v} = [v_1, v_2, ..., v_n]^T$$

the circuit relation at the n-port network can be written as

$$\mathbf{v} = \mathbf{Z}^T\mathbf{i} \tag{1.1}$$

where $\mathbf{Z}$ is the impedance matrix. If multiple antennas are widely spaced, the interaction between the antennas are negligible, and thus the impedance

matrix is a diagonal matrix defined by

$$\mathbf{Z} = Z_A \mathbf{I}_n$$

where Z_A is antenna impedance and $\mathbf{I}_n$ is the identity matrix of order n.

However, in the presence of mutual coupling, the matrix becomes full rank, known as the mutual impedance matrix, and is defined by

$$\mathbf{Z} = \begin{pmatrix} Z_{11} & Z_{12} & \dots & Z_{1n} \\ Z_{21} & Z_{22} & \dots & Z_{2n} \\ \vdots & \vdots & \ddots & \vdots \\ Z_{n1} & Z_{n2} & \dots & Z_{nn} \end{pmatrix}$$

Here, Z_{jl} is antenna self-impedance for $j = l$, while Z_{jl} is the mutual impedance for $j \neq l$.

In order to calculate the mutual and self impedances, one should employ mathematical techniques and tools of the electromagnetic (EM) analysis. The EM analysis is a complex task, and there is no need to describe it in details here. However, understanding of the basic methods used in the EM analysis is of crucial importance, as it enables the most appropriate choice of parameters for analysis and accurate interpretation of the obtained results. Therefore, we present three basic methods often used in the EM analysis. In the order of increasing accuracy and complexity these methods are:

- the induced electromotive force (EMF)
- the method of moments
- the full-wave electromagnetic numerical computation

In each method, an n_A-element antenna array is represented as an N-port network. For induced EMF, $N = n_A$, while for the method of moments, N is an integer multiple of n_A, i.e., each antenna is subdivided into equal-length increments, each corresponding to a port. Full-wave electromagnetic numerical computation assumes that the entire antenna is represented by a three-dimensional (3-D) computer-aided design model, and subdivided into N surface patches.

The calculation of the driving point impedance of each port by using those three methods is presented in the following.

Induced EMF

Induced EMF is a classical method of computing the self and mutual impedances of a $N-$port network representation of an antenna array. Here, the Poynting vector, created from the electric and magnetic fields, is integrated over the array elements. This method is restricted to straight and parallel elements in formation and does not account for radii of the wires and the gaps at the feeds. The advantage of induced EMF is that it leads to closed-form solutions providing a simple analysis. As an example, following the approach of King [12], the elements of the mutual impedance matrix $\mathbf{Z}$, can be calculated as

$$Z_{mn} = \begin{cases} 30(0.5772 + \ln(2k_\omega l) - \mathrm{Ci}(2k_\omega l)) + 30(\mathrm{Si}(2k_\omega l)), & m = n \\ R_{mn} + iX_{mn}, & m \neq n \end{cases} \tag{1.2}$$

$$\begin{aligned} R_{mn} = {} & 30\cos(2k_\omega l)(\mathrm{Ci}(u_0) + \mathrm{Ci}(v_0) - 2\mathrm{Ci}(u_1) - 2\mathrm{Ci}(v_1) + 2\mathrm{Ci}(k_\omega d)) \\ & + 30\sin(2k_\omega l)(-\mathrm{Si}(u_0) + \mathrm{Si}(v_0) + 2\mathrm{Si}(u_1) - 2\mathrm{Si}(v_1)) \\ & + 30(-2\mathrm{Ci}(u_1) - 2\mathrm{Ci}(v_1) + 4\mathrm{Ci}(kd)) \end{aligned}$$

$$\begin{aligned} X_{mn} = {} & 30\cos(2k_\omega l)(-\mathrm{Si}(u_0) - \mathrm{Si}(v_0) + 2\mathrm{Si}(u_1) + 2\mathrm{Si}(v_1) - 2\mathrm{Si}(k_\omega d)) \\ & + 30\sin(2k_\omega l)(-\mathrm{Ci}(u_0) + \mathrm{Ci}(v_0) + 2\mathrm{Ci}(u_1) - 2\mathrm{Ci}(v_1)) \\ & + 30(2\mathrm{Si}(u_1) + 2\mathrm{Si}(v_1) - 4\mathrm{Si}(k_\omega d)) \end{aligned}$$

$$\begin{aligned} u_0 &= k_\omega(\sqrt{d^2 + 4l^2} - 2l) \\ u_1 &= k_\omega(\sqrt{d^2 + l^2} - l) \\ v_0 &= k_\omega(\sqrt{d^2 + 4l^2} + 2l) \\ v_1 &= k_\omega(\sqrt{d^2 + l^2} + l) \\ \mathrm{Ci}(u) &= \int_\infty^u \frac{\cos(x)}{x} dx \\ \mathrm{Si}(u) &= \int_\infty^u \frac{\sin(x)}{x} dx \end{aligned}$$

where $1 \leq m, n \leq n_A$ and where d is the horizontal distance between vertically-oriented dipole antennas m and n, l is a half of the length of the

dipole antenna, and $k_\omega = 2\pi/\lambda$ is the wave number. Since the above expressions only depends on interelement distances, arbitrary arrangements of array elements can be considered.

Method of Moments

For greater accuracy, we may partition each antenna of the array into equal-length segments and apply the method of moments. The method of moments is a general technique for converting a set of linear integrodifferential equations into an approximating set of simultaneous algebraic equations suitable for solving on a computer. Using electromagnetic theory and assuming unidirectional current flow, the current and charge densities are approximated by viewing the antenna arrays as filaments of current and charge of the wire axis. Using the method in [13], an expression for the mutual impedance matrix elements $1 \leq m, n \leq N$ is shown to be

$$
\begin{aligned}
Z_{mn} &= i\omega\mu\Delta\overrightarrow{l_n} \cdot \overrightarrow{l_m}\psi(n,m) \\
&\quad + \frac{1}{i\omega\varepsilon}[\psi(n^+,m^+) - \psi(n^-,m^+) - \psi(n^+,m^-) + \psi(n^-,m^-)] \\
\psi(n,m) &= \frac{1}{\Delta l_n}\int_{\Delta l_n} \frac{e^{-ik_\omega R_m}}{4\pi R_m} dl \\
R_m &= \begin{cases} \sqrt{\varrho^2 + (z - z_m)^2}, & m \neq n \\ \sqrt{a^2 + z^2}, & m = n \end{cases}
\end{aligned}
$$

where ϱ is the horizontal distance between the antennas containing points n and m, a is the dipole antenna radius, k_ω is the wave number, z_m is the vertical distance between the points n and m, μ is the permeability, ε is the permittivity, Δl_n the length of the n^{th} increment, ω is the frequency of operation (in radians per second), and n^- and n^+ denotes the starting and terminating points of the n^{th} increment, respectively.

Full-wave Electromagnetic Numerical Computation

Full-wave electromagnetic numerical computation models both the electric current on a metallic structure and the magnetic current representing the field distribution on a metallic aperture. An element of the mutual impedance

matrix $\mathbf{Z}$, Z_{mn} is given as

$$Z_{mn} = \int_S \{Z_s \overrightarrow{B_m} \cdot \overrightarrow{B_n}\} ds + \int_S ds \int_S \{\overrightarrow{B_m} \cdot \overrightarrow{G}(\overrightarrow{r} \mid \overrightarrow{r}') \cdot \overrightarrow{B_n}\} ds' \quad (1.3)$$

where Z_s is the surface of the antenna increment with surface S, $\overrightarrow{B}_n(\overrightarrow{r})$ is a basis function, and $\overrightarrow{G}(\overrightarrow{r} \mid \overrightarrow{r}')$ is Green's function. The differences among full-wave electromagnetic numerical computation formulations are based on the choice of basis functions $\overrightarrow{B}_n(\overrightarrow{r})$ for the current distribution representation and Green's functions $\overrightarrow{G}(\overrightarrow{r}|\overrightarrow{r}')$.

SONNET® software uses a sum of sines and cosines as Green's function, while some other electromagnetic software such as Zetland IE3D, uses the Sommerfield integral as a Green's function [14]. Although, it is hard to make a comparison between different techniques and tools for the EM analysis, for a simple antenna array structure such as uniform linear array with half-wave dipoles, sufficiently accurate results can be obtained by using any of previously mentioned software, *SONNET*®, Zeland IE3D, or other similar software. On the other hand, for complex antenna structures, multiple EM tools are required in order to efficiently solve Maxwell's equations. In any case, the understanding of the used method is essential as it enables the most appropriate choice of parameters for calculation, and the correct interpretation of the simulation results.

1.4 Summary of Approach

In this chapter, we first summarized the theoretical and practical features of multiantenna elements for use in mobile wireless communication networks. Then, we indicated on the potential limitations caused by implementing multi-antenna systems with small antenna spacing.

Closely spaced antennas result in mutual coupling. The effect of the mutual coupling in multiple antennas has been extensively studied by the research community. In this thesis, we extended the analysis of the mutual coupling effect in the multiple antenna systems by including one missing parameter - thermal noise.

In order to investigate the signal and noise coupling, we elaborated on the mutual coupling effect in this chapter. We presented a model of mutual coupling effect in multi-antenna systems (used in this thesis). Then, we discussed the three basic methods often used for mutual impedance matrix calculation, including the full-wave electromagnetic numerical computation, that has been used in this thesis.

1.5 Structure of this Thesis

In this thesis, we provide an analysis of the mutual coupling effect on thermal noise. Then, we estimate the channel capacity of multi-antenna systems with small inter-element spacings.

In order to provide a better insight into the thesis topics, and to improve the clarity of presentation of the research results, the thesis is divided into two parts. The first part is focused on the signal processing theory, more precisely, the signal and noise coupling in the multi-antenna systems. In the second part, the achievable information rate of a wireless communication link is estimated when a coupled multi-antenna system is used at one side, or on both sides of the link.

1.5.1 Questions to be Answered in this Thesis

In this thesis the following open questions are addressed:

1. Part I
    - Does mutual coupling affect thermal noise?
    - What is the impact of mutual coupling on thermal noise power in closely spaced multiple antennas?
    - What is the overall effect of mutual coupling on signal-to-noise ratio in multi-antenna systems?
    - What is the critical antenna spacing beyond which the combined mutual coupling can be neglected?
2. Part II

- How does correlated noise affect ergodic channel capacity of MIMO wireless systems?
- How does correlated noise impact outage channel capacity, and cumulative distribution function of channel capacity?
- What is the minimum antenna spacing beyond which the channel capacity is not affected by mutual coupling?
- How many effective degrees of freedom can be formed in MIMO wireless system with coupled antennas?
- Could we separately estimate the total contribution of the noise correlation on the channel capacity?

1.5.2 Content and Contributions of Thesis

In the following, the chapters of the thesis are outlined with emphasis on contributions made within:

Part I

Chapter 1 is the introduction chapter into the first part of the thesis. The system with multiple antennas, its advantages and typical applications, is elaborated. The mutual coupling effect is considered in the multi-antenna systems. The modeling of the coupled multiple antennas, and the calculation method of the elements of the mutual impedance matrix are also presented.

Chapter 2 introduces the concept of the noise correlation due to mutual coupling in the mobile wireless communication systems. Noise covariance matrix and correlated noise power matrix are calculated for the two antenna array. This is followed by the derivation of the closed form solution for the noise covariance matrix and the correlated noise power matrix in the general case - multi-antenna system with n antennas. Simulation results indicate that the coupled thermal noise power is reduced in comparison with the thermal noise power of isolated dipole.

Chapter 3 examines the combined effect of noise and signal coupling in the multi-antenna systems. We investigate the combined effect of mutual coupling on signal and noise on the signal-to-noise ratio performance. Our simulation results indicate that the signal-to-noise ratio in coupled multiple antennas is underestimated if the noise coupling effect is not accounted for.

Chapter 4 is the concluding chapter of the first part of the thesis.

Part II

Chapter 5 represents the introduction into a wireless communication theory. We examine the MIMO channel models found in the literature. In particular, we elaborate on the channel model that has been found as the most suitable for our analysis. We present the correlation model which introduces the signal coupling into the MIMO channel model.

Chapter 6 - the concept of noise coupling is introduced into the channel capacity calculations of MIMO systems with small antenna spacings. Channel capacity performance of the MIMO systems is estimated by varying the antenna spacing which has the greatest influence on the coupling level in the multi-antenna systems. Ergodic channel capacity is investigated by applying equal power allocation and water-filling power allocation schemes at the transmitters. Furthermore, capacity outage and its cumulative distribution function are presented for very small antenna spacing along with the case when antennas are separated for more than a half of wavelength. The number of effective degrees of freedom is then examined. Noise correlation factor is derived, enabling the quantification of the noise correlation contribution to the channel capacity. Finally, an upper bound of the channel capacity of the coupled multi-antenna systems is defined.

Chapter 7 explores the effect of mismatching impedance due to the combined mutual coupling effect on signal and noise on the capacity performance of the MIMO systems. Three most widely used matching networks are analyzed, and it has been confirmed that the multi-port

conjugate matching network is optimal in terms of signal power, and it also acts as the whitening filter on the coupled thermal noise. Further, the capacity of MIMO systems is estimated when the coupled multi-antenna systems is used at both sides of the link, receiver and transmitter. Our simulation results confirm that the transmit coupling degrades the capacity performance compared to the case with no constraint on the emitted power.

Chapter 8 is the concluding chapter of the second part of the thesis.

Chapter 2

Correlated Noise

2.1 Introduction

Mobile wireless communication system design comprises a comprehensive setup of tasks with the core objective to attain the minimum achievable received signal power level to enable reliable transmission over a wireless channel. In a noise limited environment, the minimum received signal power level P_S can be defined as

$$P_S[dBm] = SNR_{min}[dB] + P_n[dBm] \tag{2.1}$$

where SNR_{min} is a minimum signal-to-noise ratio and P_n is a noise power level.

Therefore, the transmission quality criterion for the wireless system design can be defined as a minimum signal-to-noise ratio (SNR) at the receiver to achieve a pre-defined threshold for reliable communications. For digital systems, the transmission quality is defined in terms of the bit error rate (BER) and is driven by a range of factors such as modulation schemes, coding, etc. However, the SNR still persists as an essential parameter in determining the transmission quality of digital systems.

In a multi-user setting, an additional limitation is placed on the design of wireless systems where the interference from other users can significantly reduce the capacity performance of wireless systems. The presence of strong interferences is generally equated to a very noisy environment when the in-

terference attains the AWGN characteristic, and it has been an established belief, prior to 1988 [15], that correct detection and demodulation is impossible. However, it was demonstrated in [15, 16] and other papers that by using multiuser detection it is possible to combat multiuser interference in mobile wireless communication systems. Multiuser detection is based on the idea of detecting interference, and exploiting the resulting knowledge to mitigate its effect on the desired signal. Using such techniques, interference becomes less detrimental then noise [17].

From the previous discussions, one can conclude that the noise becomes a crucial factor in determining the transmission quality over the wireless channels even for multi-user mobile communications. In this context, we provide an analysis of the received noise in a multi-antenna system, while we examined the effects of signal-to-noise ratio at the receiver in Chapter 3.

In the next section, antenna noise is elaborated. This is followed by an interpretation of the noise coupling effect in the multi-antenna systems in Section 2.3. An analytical evaluation of the correlated noise in the multi-antenna system is given in Section 2.4, while, simulation results are presented in Section 2.6. Concluding remarks and contributions are listed in Section 2.7.

2.2 Antenna Noise

The noise appearing at the output of a receiver has its origin partially in the receiver and partially outside the receiver. The external noise is picked up by the antenna and is generally referred to as "antenna noise". This type of noise is largely either man-made or environmental in origin.

Antenna noise at microwave frequencies (1GHz - 300 GHz) is largely thermal in origin. It has been found experimentally that with a few exceptions (e.g., radiation from fluorescent lights) antenna noise at microwave frequencies could be traced to thermal radiation emitted by surrounding objects [18]. In such a way, the thermal radiation intercepted by an antenna depends upon the object at which the antenna is pointed. Further, the limiting sensitivity of a receiver depends upon the nature of the objects at which the antenna is directed.

In summary, the dominant antenna noise for mobile wireless applications is thermal noise. However, impulse noise may be a predominant disturbance for some indoor situations. Therefore, both the thermal and impulse noise will be elaborated in the following.

2.2.1 Thermal Noise

Noise is the result of the random motion of charged particles in a conductor. In general, the mechanical motions of these charged particles are coupled with other forms of energy such as the incident radiation energy on an antenna. When the charged particles are in thermal equilibrium with all other forms of energy with which they might be coupled, the noise is called thermal noise.

Because of the continuous thermal agitations of the charged particles, a random current $I(t)$ exists. If a sufficiently sensitive ammeter is placed across the conductor's terminal, a fluctuating reading would be observed. In similar way, a voltmeter would show a fluctuating voltage $V(t)$. Schematically, this conductor can be represented as a noiseless resistance in series with a voltage source, with a spectral intensity proportional to that of the current generated therein as depicted in Fig. 2.1(a). Similarly, the conductor as a current source in parallel with a noiseless resistance can be presented as shown in Fig. 2.1(b).

The noiseless resistance in either instance has the same numerical measure as the actual, noisy one. Since $V(t) = I(t)R$, the spectral intensities are (in steady or equilibrium state) related by

$$W_V(f) = R^2 W_I(f) \tag{2.2}$$

where $W_I(t)$ and $W_V(t)$ are current and voltage spectral densities, respectively. They were derived in two ways:

1. Directly on the basis of a kinetic-theory model of conduction process. Originally, it was presented in [19–21];

2. By appropriate thermodynamical arguments, which do not depend on the detailed mechanism of conduction. This was done originally by Nyquist [22].

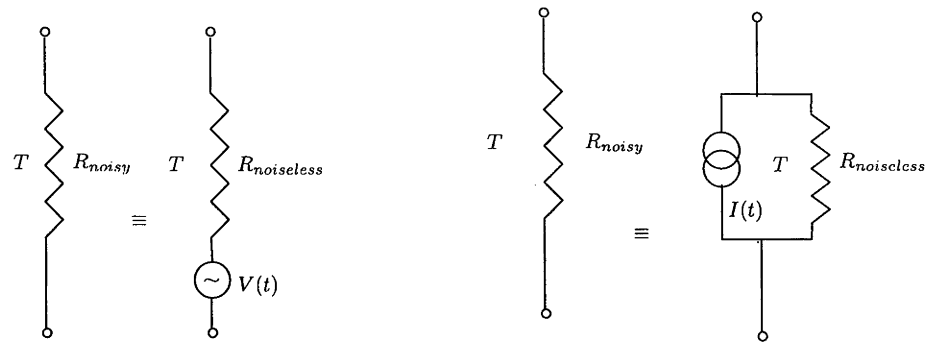

(a) (b)

Figure 2.1: Equivalent representations of a resistance (at temperature T): (a) resistance represented as a noiseless resistance in series with a voltage source (b) resistance represented as a current source in parallel with a noiseless resistance

The former has the advantage of explicitness. The later is more abstract, while avoiding some of the technical difficulties inherent in any detailed model of the conduction process. Then, the voltage spectrum becomes

$$W_V(f) = 4kTR \tag{2.3}$$

where $k = 1.3806503 \times 10^{-23} J/K$ is the Boltzmann constant, and T is the absolute temperature in K.

The result (2.3) is strictly speaking, valid only for the low-frequency end of the spectrum. If this relation were used for all frequencies, the power spectrum $W_V(f)/R = 4kT$ would then be independent of frequency in this model and one would have an infinite total power. In his original paper [22], Nyquist indicates that the difficulty can be overcome by replacing the equipartition value kT for the energy per mode of one-dimensional transmission line by Planck's expression, as follows

$$hf(e^{hf/kT} - 1)^{-1}$$

where $h = 6.6260692 \times 10^{-34} Js$ is Planck's constant, and f is frequency.

Then, the voltage spectral density becomes

$$W_V(f) = \frac{4Rhf}{e^{hf/kT} - 1} \tag{2.4}$$

Thus, the spectrum departs noticeably from its constant low-frequency value at about $f = (k/h)T = 2.1 \times 10^{10}T$ Hz.

Now, the mean power $\overline{P}$ dissipated in the resistive element can be calculated as

$$\overline{P} = \int_0^\infty W_I(f)R(f)df = 4kT \int_0^\infty R(f)^2|Y(i\omega)|^2 df \tag{2.5}$$

$$= \int_0^\infty W_V(f)|Y(i\omega)|^2 df \tag{2.6}$$

where $Y(iw)$ is admittance, and ω is angular frequency. Here, the finite power is due to the frequency selective properties of the circuit, and not to the actual high-frequency behavior of the resistive element, since the "low-frequency" approximation is assumed.

Additionally, the general Nyquist's formula for voltage and current spectral density is valid for a general (linear passive) network when different resistances in the network are no longer at the same temperature. Then the spectral distribution of the total mean squared current fluctuations is the sum of the current spectral densities of each resistance [23]

$$W_I(f) = 4k \sum_i \frac{T_i R_i}{|Z_{ei}|^2} \tag{2.7}$$

where Z_{ei} is an equivalent resistance of the source E_i [24]. This result is experimentally confirmed in [25].

2.3 Noise Coupling

In this Section, we investigate the electromagnetic coupling of the thermal radiation intercepted by antenna elements.

First of all, the generalized Nyquist noise theorem is presented. Then, the noise coupling for the simplest case, two dipole antennas, will be elaborated. This is followed by the more general case where the noise coupling in multiple antenna systems will be examined.

2.3.1 Thermal Noise Electromagnetic Radiation

Thermal noise electromagnetic radiation results in self-induced noise, also known as self-radiated thermal noise of an antenna element [26]. Furthermore, when an antenna element is placed in the close proximity of other radiated bodies, including the adjacent antenna elements, thermal noise is induced from the closely spaced radiated bodies [26]. It was predicted by [27] that the partially correlated noise is induced into two closely spaced antennas with isolated receivers. Theoretical formulation of this effect is given by the Nyquist thermal noise theorem [28].

2.3.2 Nyquist Thermal Noise Theorem

The generalized Nyquist thermal noise theorem [28] allows us to determine thermal noise power of coupled antennas in a multi-antenna system. The theorem states that for a passive network in thermal equilibrium it is possible to represent the complete thermal-noise behavior by applying Nyquist's theorem independently to each element of the network.

In general, a network (even nonreciprocal) with a system of n_A internal thermal generators all at absolute temperature T is equivalent to the source-free network together with a system of noise voltage generators $E_m, m = 1, ..., n_A$ with zero internal impedance [27]. Noise generator voltages are correlated and spectral density of their cross-correlation is given by (relates to the two coupled antenna case in Fig. 2.2(a))

$$W_{E_m E_n^*}(f) = 2kT(Z_{mn} + Z_{nm}^*) \tag{2.8}$$

where $\overline{(\cdot)}$ denotes expectation, Z_{mn} and Z_{nm} are the mutual impedances, and k is Boltzmann's constant and T is absolute temperature. Similarly, spectral density of the nodal current cross-correlation is

$$W_{I_m I_n^*}(f) = 2kT(Y_{mn} + Y_{nm}^*) \tag{2.9}$$

where Y_{mn} and Y_{nm} are the mutual admittances. Correlation is zero when the mutual coupling is purely reactive. Furthermore, the expressions (2.8) and (2.9) can be generalized, and matrix of spectral densities for network

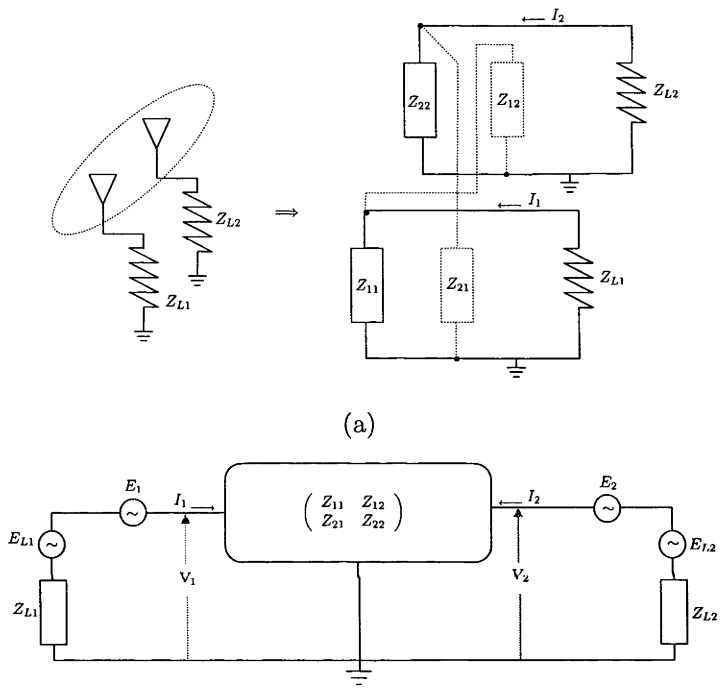

Figure 2.2: (a) Two coupled antennas and corresponding representation of their self (Z_{11}, Z_{22}), mutual (Z_{12}, Z_{21}) and load (Z_{L1}, Z_{L2}) impedances (b) Network representation for two antenna array with voltage noise generators associated with antennas E_1, E_2 and load E_{L1}, E_{L2} impedances

system can be written as

$$W_{\mathbf{ee}^\dagger} = 2kT(\mathbf{Z} + \mathbf{Z}^*) \tag{2.10}$$

where $(\cdot)^\dagger$ denotes conjugate transpose or Hermitian transpose. Further, matrix of current's spectral densities is

$$W_{\mathbf{jj}^\dagger} = 2kT(\mathbf{Y} + \mathbf{Y}^*) \tag{2.11}$$

where $\mathbf{Z}$ and $\mathbf{Y}$ are the mutual impedance and admittance matrices, respectively; $\mathbf{e}$ and $\mathbf{j}$ are voltage and current vectors, respectively.

From (2.11) and (2.10), one can conclude that the cross-correlations between the voltages/currents of open thermal noise sources are directly proportional to the real part of their mutual impedances and admittances. Based upon these properties, total exchangeable thermal noise power between the multi-antenna systems and load network will be calculated.

2.4 Noise in Multi-antenna Systems

Based on the Nyquist Thermal Noise theorem, the noise correlation matrix for the closely spaced antenna can be derived. The correlated noise current and associated noise power for the simplest case, the two-dipole array, are calculated [29]. Then, for the generalized case, the noise covariance matrix and correlated noise power for the multi-antenna system with n antennas, is presented [30].

2.4.1 Two-antenna Case

One can write the noise voltage spectral densities as in Fig. 2.2(b) for the two-antenna array in terms of its current spectral densities W_{J_k} and spectral densities of noise voltage generators W_{E_k} by

$$W_{V_1} = Z_{11}W_{J_1} + Z_{12}W_{J_2} = W_{E_{L1}} + W_{E_1} - Z_{\mathrm{L1}}W_{J_1} \tag{2.12}$$

$$W_{V_2} = Z_{21}W_{J_1} + Z_{22}W_{J_1} = W_{E_{L2}} + W_{E_2} - Z_{\mathrm{L2}}W_{J_2} \tag{2.13}$$

where W_{J_l}, $l = 1, 2$ are the noise current spectral density and W_{V_l}, $l = 1, 2$ the associated noise voltage spectral density of l^{th} antenna element. The

terms $W_{E_{Ll}}$, $l = 1, 2$ are the voltage spectral density of the noise generator associated with the load impedance of receiver Z_{Ll}, $l = 1, 2$ and W_{E_l}, $l = 1, 2$ are the voltage spectral density of the noise generator associated with the input impedance of the l^{th} antenna element, respectively.

Furthermore, the spectral density of noise currents can be expressed as

$$W_{J_1} = \frac{1}{|\mathbf{Z}_A|}\Big((Z_{22} + Z_{L2})(W_{E_{L1}} + W_{E_1}) - Z_{21}(W_{E_{L2}} + W_{E_1})\Big)$$
$$W_{J_2} = \frac{1}{|\mathbf{Z}_A|}\Big((Z_{11} + Z_{L1})(W_{E_{L2}} + W_{E_2}) - Z_{12}(W_{E_{L1}} + W_{E_1})\Big) \qquad (2.14)$$

where $|\mathbf{Z}_\mathrm{A}| = \det(\mathbf{Z}_A)$ is determinant of the receiver front-end impedance matrix $\mathbf{Z}_\mathrm{A}$ given by

$$\mathbf{Z}_\mathrm{A} = \begin{pmatrix} Z_{11} + Z_{\mathrm{L1}} & Z_{12} \\ Z_{21} & Z_{22} + Z_{\mathrm{L2}} \end{pmatrix} \qquad (2.15)$$

The power spectral density of thermal noise absorbed in the receiver load of the first antenna - $W_{N1}(f)$ is

$$W_{N1}(f) = \frac{1}{2}(Z_{\mathrm{L1}} + Z^*_{\mathrm{L1}})W_{J_1 J_1^*} \qquad (2.16)$$

Similarly, for the second antenna:

$$W_{N2}(f) = \frac{1}{2}(Z_{\mathrm{L2}} + Z^*_{\mathrm{L2}})W_{J_2 J_2^*} \qquad (2.17)$$

Substituting the expressions (2.12) in (2.16) yields

$$W_{N1}(f) = \frac{(Z_{\mathrm{L1}} + Z^*_{\mathrm{L1}})}{2|\mathbf{Z}_\mathrm{A}||\mathbf{Z}^*_\mathrm{A}|}\Big((Z_{22} + Z_{L2})(Z^*_{22} + Z^*_{L2})(W_{E_{\mathrm{L1}}E^*_{\mathrm{L1}}} + W_{E_1 E_1^*})$$
$$- Z_{21}(Z^*_{22} + Z^*_{\mathrm{L2}})W_{E_1 E_2^*} - Z^*_{21}(Z_{22} + Z_{\mathrm{L2}})W_{E_1^* E_2}$$
$$+ Z_{21}Z^*_{21}(W_{E_{\mathrm{L2}}E^*_{\mathrm{L2}}} + W_{E_2 E_2^*})\Big) \qquad (2.18)$$

Using (2.8) for the cross-correlation of noise voltage spectral density, the expression (2.18) becomes

$$W_{N1}(f) = kT\frac{(Z_{\mathrm{L1}}+Z^*_{\mathrm{L1}})}{|\mathbf{Z}_\mathrm{A}||\mathbf{Z}^*_\mathrm{A}|}\Big((Z_{22}+Z_{\mathrm{L2}})(Z^*_{22}+Z^*_{\mathrm{L2}})\big((Z_{\mathrm{L1}}+Z^*_{\mathrm{L1}}) + (Z_{11}+Z^*_{11})\big)$$
$$- Z_{21}(Z^*_{22} + Z^*_{\mathrm{L2}})(Z_{12} + Z^*_{12}) - Z^*_{21}(Z_{22} + Z_{\mathrm{L2}})(Z_{12} + Z^*_{12})$$
$$+ Z_{21}Z^*_{21}\big((Z_{\mathrm{L2}} + Z^*_{\mathrm{L2}}) + (Z_{22} + Z^*_{22})\big)\Big) \qquad (2.19)$$

The spectral density of total collected noise power in the received load of the first antenna consists of two parts:

1. its internal thermal noise from its own resistance; and
2. the externally received noise that is accumulated from space.

Further, the external noise consists of two parts:

1. one that its own antenna amasses directly; and
2. the part that is indirectly gathered through adjacent closely-spaced antenna [31].

Similarly, the spectral density of thermal noise power of second antenna is

$$\begin{aligned} W_{N2}(f) = kT\frac{(Z_{L2}+Z_{L2}^*)}{|\mathbf{Z}_A||\mathbf{Z}_A^*|}\Big((Z_{11}+Z_{L1})(Z_{11}^*+Z_{L1}^*)\big((Z_{L2}+Z_{L2}^*)+(Z_{22}+Z_{22}^*)\big) \\ - Z_{12}(Z_{11}^*+Z_{L1}^*)(Z_{21}+Z_{21}^*) - Z_{12}^*(Z_{11}+Z_{L1})(Z_{21}+Z_{21}^*) \\ + Z_{12}Z_{12}^*\big((Z_{L1}+Z_{L1}^*)+(Z_{11}+Z_{11}^*)\big)\Big) \end{aligned} \tag{2.20}$$

For a given receiver bandwidth B, the thermal noise powers accumulated in the receiver loads of the first and second antennas can be written as

$$\overline{P}_{N1} = \int_B W_{N1}(f)\,df \tag{2.21}$$

$$\overline{P}_{N2} = \int_B W_{N2}(f)\,df \tag{2.22}$$

where $\overline{(\cdot)}$ denotes the mean value.

The closed-form solution for the mutual impedance of two infinitely thin antennas in echelon is given in [12]. However, by implementing the closed form solution, the analytically obtained results will be restricted to only a few applications. Therefore, numerical methods for calculating the mutual impedance matrix are proposed, and results are presented in Section 2.6.

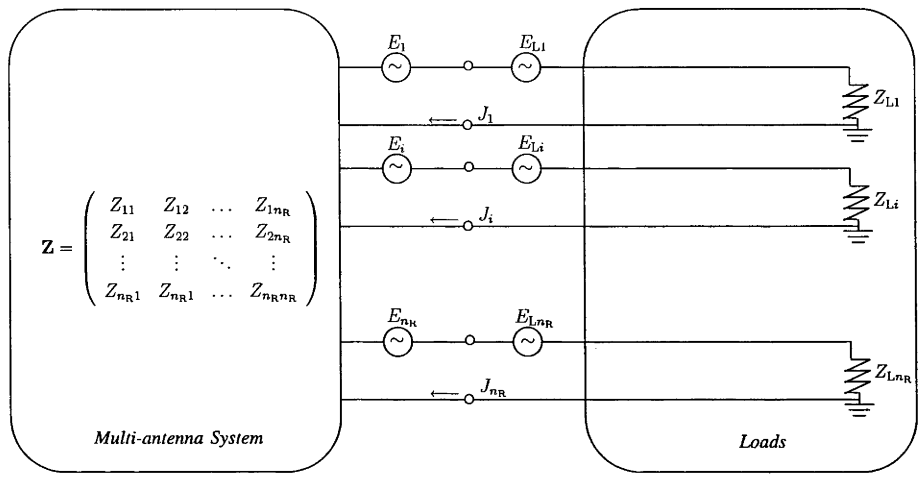

Figure 2.3: Block diagram of the receive subsystem including coupled antenna array and loads

2.4.2 General Case

An equivalent linear network representation with internal noise sources of the multi-antenna system with n_R antennas is presented in Fig. 2.3. Based on block diagram in Fig. 2.3, the vector of the noise current $\mathbf{j}$ can be written as

$$\mathbf{j} = (\mathbf{Z} + \mathbf{Z}_L)^{-1} \cdot \mathbf{e}_T \tag{2.23}$$

where $\mathbf{e}_T$ is thermal noise voltage vector contributions from antenna's and load's system impedances, $\mathbf{Z}$ is the mutual impedance matrix, and $\mathbf{Z}_L$ is load impedance matrix.

Then, the cross-covariance matrix of thermal noise current spectral densities is given by

$$\mathbf{W}_j(f) = (\mathbf{Z} + \mathbf{Z}_L)^{-1}\mathbf{W}_{eT}^T(f)((\mathbf{Z} + \mathbf{Z}_L)^{-1})^\dagger \tag{2.24}$$

By applying the Nyquist thermal noise theorem (2.10) for the network in Fig. 2.3, the matrix of the voltage cross-spectral densities is the contribution from the thermal noise from antennas and termination impedances, and can be calculated as

$$\mathbf{W}_{eT}^T(f) = 2kT\big((\mathbf{Z} + \mathbf{Z}_L) + (\mathbf{Z} + \mathbf{Z}_L)^*\big) \tag{2.25}$$

Then, the matrix of the spectral densities of the nodal noise currents can be rewritten as

$$\mathbf{W_j} = 2kT(\mathbf{Z}+\mathbf{Z_L})^{-1}\big((\mathbf{Z}+\mathbf{Z_L})+(\mathbf{Z}+\mathbf{Z_L})^*\big)((\mathbf{Z}+\mathbf{Z_L})^{-1})^\dagger \tag{2.26}$$

Further, the matrix of the thermal noise cross-power spectral densities can be written as

$$W_{P_N} = 2kT\mathrm{diag}\Big((\mathfrak{Re}(\mathbf{Z_L})(\mathbf{Z}+\mathbf{Z_L})^{-1}\big((\mathbf{Z}+\mathbf{Z_L})+(\mathbf{Z}+\mathbf{Z_L})^*\big)((\mathbf{Z}+\mathbf{Z_L})^{-1})^\dagger\Big) \tag{2.27}$$

where $\mathrm{diag}(\cdot)$ is diagonal operator, and $\mathfrak{Re}(\cdot)$ denotes real part of complex value.

The total thermal noise power dissipated at loads $\mathbf{Z_L}$ is

$$\overline{P}_N = 2kTB\mathrm{Tr}\Big(\mathfrak{Re}(\mathbf{Z_L})(\mathbf{Z}+\mathbf{Z_L})^{-1}\big((\mathbf{Z}+\mathbf{Z_L})+(\mathbf{Z}+\mathbf{Z_L})^*\big)((\mathbf{Z}+\mathbf{Z_L})^{-1})^\dagger\Big) \tag{2.28}$$

where $\mathrm{Tr}(\cdot)$ denotes the trace operator.

The solution in (2.27) is general, and is valid for any multi-antenna systems. When the antennas are widely spaced, the mutual impedances are negligible, and the total thermal noise power becomes the sum of individual antenna thermal noise powers, as one can see from (2.27).

$$\overline{P}_N = 4n_R kTB \tag{2.29}$$

note that it is assumed that isolated antenna are matched to the loads impedance $\mathbf{Z} = \mathbf{Z}_L^*$.

Based on this analysis, one can conclude that the noise current correlation matrix (2.24) directly reveals the noise correlation. On the other hand, the correlated noise power matrix is the diagonal matrix composed of the coupled antenna noise powers. Yet, each element of the correlated noise power matrix consists of noise intercepted by its own antenna, and the noise dissipated due to the mutual coupling from the adjacent antennas.

2.5 Noise Correlation Matrix - Definition

In order to provide an comparative analysis of the signal-to-noise ratio and channel capacity performance (presented in Chapter6) when the noise is cor-

related versus uncorrelated noise, we used the normalized noise correlation matrix - noise coupling matrix.

We define here the noise coupling matrix. But, in order to be able to define it, we have previously defined uncorrelated and correlated noise matrices as they will be referred in our analysis.

Definition 2.1. Let the number of antennas in the multi-antenna systems be n_A. Further, antennas are widely spaced and noise is uncorrelated AWGN. If the thermal noise power of isolated antenna is $\mathbf{N}$, the *uncorrelated* noise matrix is given by

$$\mathbf{N} = N\mathbf{I}_n \tag{2.30}$$

where $\mathbf{I}_n$ identity matrix of order n, and N is the thermal noise power of uncoupled antenna element.

Definition 2.2. Let the number of antennas in the multi-antenna systems be n_A. Further, antennas are closely spaced imposing noise correlation. If coupled thermal noise power of i^{th} antenna is denoted by P_{Ni}, as calculated in (2.21), then the *noise correlation matrix* is given by

$$\mathbf{N}_c = \begin{pmatrix} P_{N1} & 0 & 0 & 0 \\ 0 & P_{N2} & 0 & 0 \\ \cdots & \cdots & \ddots & \vdots \\ 0 & 0 & 0 & P_{Nn} \end{pmatrix} \tag{2.31}$$

Definition 2.3. Let the number of antennas in the multi-antenna systems be n_A. Furthermore, antennas are closely spaced and noise is correlated. If the thermal noise power of i^{th} coupled antenna is denoted by P_{Ni}, as calculated in (2.21), the matrix *noise coupling matrix* can be defined as

$$\hat{\mathbf{N}}_c = \mathbf{N}^{-1}\mathbf{N}_c \quad = \begin{pmatrix} P_{N1}/N & 0 & 0 & 0 \\ 0 & P_{N2}/N & 0 & 0 \\ \cdots & \cdots & \ddots & \vdots \\ 0 & 0 & 0 & P_{Nn}/N \end{pmatrix} \tag{2.32}$$

The effect of noise coupling on channel capacity performance of MIMO system used in mobile wireless communication will be investigated based on the above definitions in the second part of this thesis.

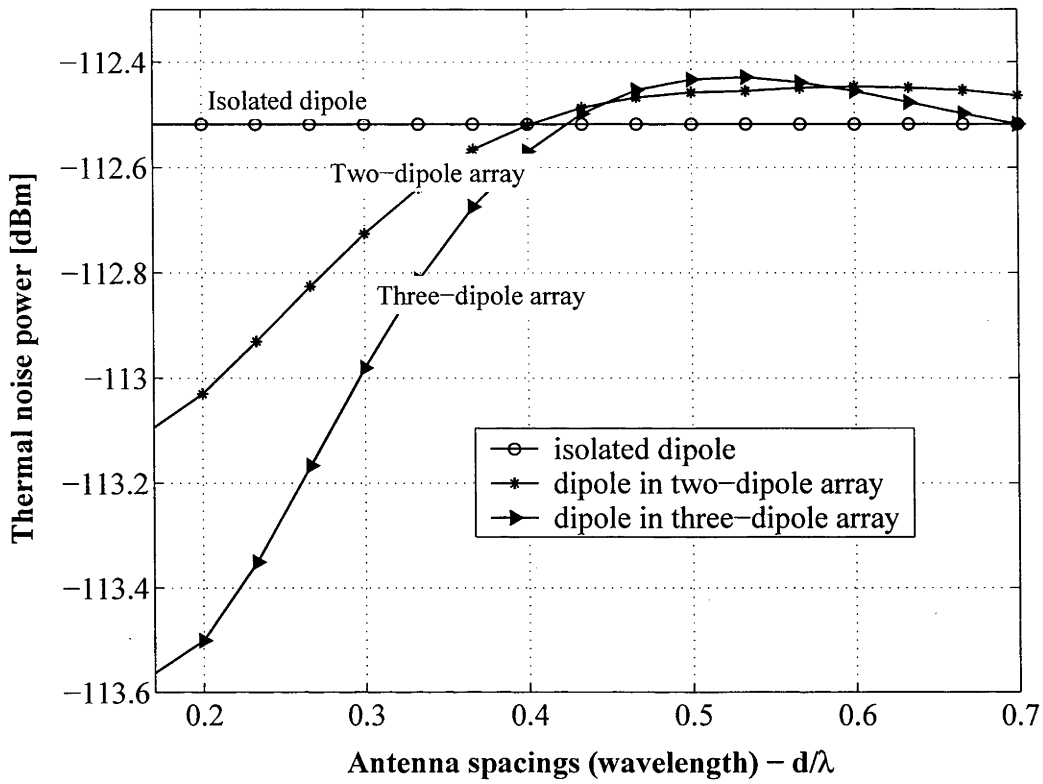

Figure 2.4: Effect of mutual coupling on average thermal noise power per antenna element in the multiple element antenna systems

2.6 Simulation Experiments

In this section we use the computer simulation to confirm the results of the presented analysis. Our simulation models are based on the calculations for uniform linear arrays (ULA) with two and three half-wave dipoles. Mutual- and self impedances are calculated by using SONNET® [32] software.

Fig. 2.4 depicts mutual coupling effects upon thermal noise power in multiple element antenna systems [29]. Simulation analysis shows a decrease in thermal noise power for antenna spacing below 0.5λ if mutual coupling of thermal noise is considered in comparison with traditional approach which ignores the coupling interaction for thermal noise. Results are given for antenna spacing below 0.7λ.

In order to understand the effect presented in Fig. 2.4, lets first recall the

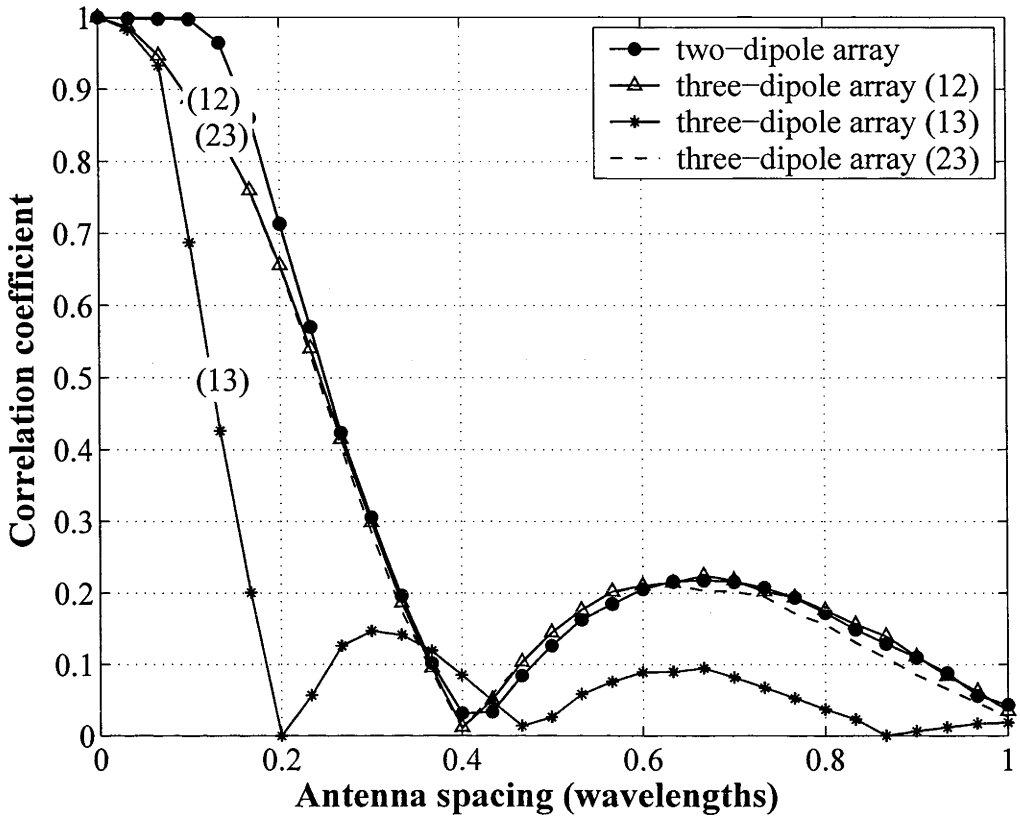

Figure 2.5: Correlation coefficients of thermal noise voltages due to mutual coupling effect

origin of thermal noise. As previously elaborated thermal noise has its origin (internal) partially in the receiver and partially outside of the receiver (external). By decreasing the antenna spacing between the antenna elements, the effective antenna aperture of each elements will be reduced. Thus, the power of noise that is picked up by each antenna element will have a tendency to decline. The adjacent antenna partially blocks the incidents waves. In general, it is expected that for the overlapping case, when all antenna elements can be seen as one element, the external thermal noise approaches the value of a noise pick up by a single, isolated element with an equivalent radiated resistance.

Furthermore, we compare thermal noise power of a single dipole in a two- and three-dipole array. It was shown in Fig. 2.4 that thermal noise power

of a single dipole in three-dipole array is lower than in two-dipole array at the same interelement spacing. This is due to asymmetrical placement of dipoles in the uniform linear array. In other words, a dipole placed in the middle position of the uniform three-dipole array will be more affected by the mutual coupling than the other two dipoles in the array.

Additionally, we estimate the noise correlation coefficients in order to draw conclusions about mutual coupling effect on noise correlation [29]. We compute correlation coefficients of complex thermal noise voltages within antenna spacing range $[0, 1\lambda]$ in two- and three-antenna arrays. Voltage correlation coefficient is computed as

$$\begin{aligned}\gamma_{12} &= \langle V_1, V_2 \rangle \\ &= \frac{E\{[V_1 - E\{V_1\}][V_2 - E\{V_2\}]^*\}}{\sqrt{E\{|V_1 - E\{V_1\}|^2\}E\{|V_2 - E\{V_2\}|^2\}}}\end{aligned}$$

where, V_i, $i = 1, 2$ is the voltage at the output port of i^{th} antenna element. Thermal noise voltages for the two- and three-antenna arrays are calculated by using (2.12) and (2.13). Similar expressions can be easily derived for the case of three-antenna array.

Fig. 2.5 plots the resulting magnitude of the correlation coefficients versus antenna spacing, for both, two-dipole and three-dipole arrays. The correlation coefficients are calculated for the adjacent dipoles (12), (23)(Fig. 2.5) and dipoles set $2 \times d$ apart(13)(Fig. 2.5). The results from Fig. 2.5 confirm that thermal noise between the adjacent antenna elements in the multi-antenna system is highly correlated for antenna spacing up to 0.5λ.

Uncorrelated white noise is usually presupposed in antenna array applications. However, the results from Fig. 2.5 corroborate our theoretical analysis that mutual coupling strongly correlates thermal noise when antennas are closely spaced. The noise depends on the inter-element spacing of the array elements. Additionally, for the asymmetrical arrangement of antennas in the antenna array such as uniform three-antenna array, the correlation will be affected by their mutual placement.

2.7 Summary and Contributions

This chapter outlines a procedure for thermal noise analysis of the multi-antenna system with coupled antennae. We provide an analysis of electromagnetic coupling effect on thermal noise in an antenna array. We calculate the thermal noise power of an antenna in the coupled antenna array. We confirm the partial correlation of thermal noise for antenna spacing below a half of a wavelength.

Specific contributions made in this chapter are:

1. We calculate thermal noise power in an antenna array when antenna elements are closely spaced presupposing strong electromagnetic coupling between the elements. In order to gain better insight of noise coupling affecting closely spaced antennas, we first provide an analysis for the simplest case — two-antenna array. Then, the general case is presented when the number of antennas is n_A;

2. The closed-form expression of total thermal noise power for coupled multi-antenna system is derived;

3. We corroborate our theoretical analysis of thermal noise in the coupled antenna array with the simulation results. The results indicate that thermal noise power of a dipole in the two- and three-dipole arrays is lower than noise power of isolated dipole. The statement is true when the antenna spacing in the two- and three-dipole arrays is lower than 0.4 λ;

4. Finally, we use the simulation to confirm the correlation of thermal noise due to the mutual coupling in an antenna array with antenna spacing up to 0.4 λ.

Chapter 3

Signal-to-Noise Ratio Analysis

3.1 System Overview

The ever-increasing demand for wireless services with steadily increasing number of applications and users force the wireless research community to investigate all possible ways to increase information throughput [17]. The methods based on more effective exploitation of spatial dimension of wireless channel, such as the multiple antenna systems when used as spatial multiplexers, might be seen as a promising solution [1].

Spatial multiplexing allows direct improvement of capacity by simultaneous transmission of multiple datastreams. While information-theoretic limits of these systems will be examined in Part II of this thesis, a practical realization of parallel datastream transmission is presented in the following. In order to provide an analysis of the SNR of multi-antenna systems, a typical front-end receiver of such a system is outlined. This is followed by the SNR analysis when strong electromagnetic coupling among the antennas is presupposed. It will be shown and quantitatively evaluated that the SNR is underestimated if the effect of noise coupling is omitted from the analysis.

3.1.1 Layered Space-time Structure

Spatial multiplexing is a technique for transmission of several datasteams in parallel. One possible realization is joint encoding of the datastreams. These datastreams are then transmitted from different antennas, and joint

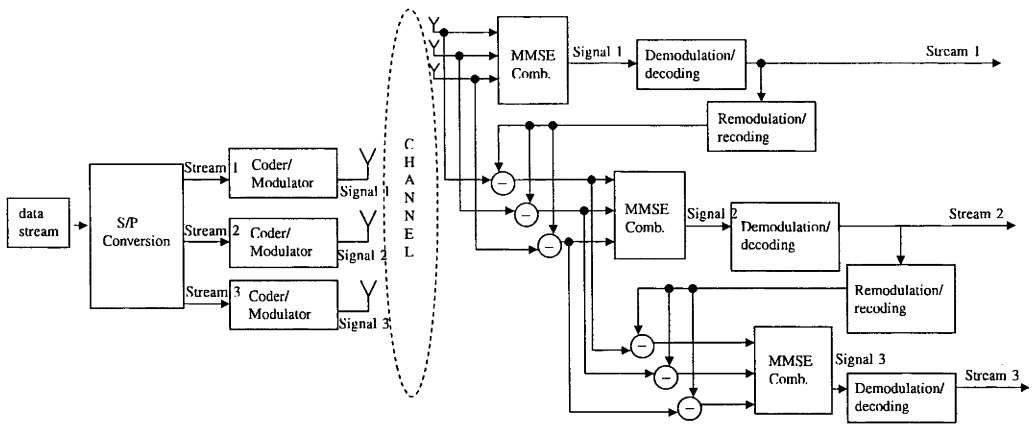

Figure 3.1: Block diagram of a horizontal BLAST trensceiver

maximum likelihood detection is used at the receiver. However, for most practical cases, the complexity of joint maximum likelihood sequence estimation (MLSE) is too high [17]. For this reason, so-called layered space-time structures have been proposed [33]. This technique decomposes the demodulation process into several separate layers, each of which has a lower complexity. These structures are also known under the name of BLAST (Bell labs LAyered Space Time) architectures.

The diagonally-layered space-time architecture proposed by Foschini [33], known as D-BLAST, uses multielement antenna arrays at both transmitter and receiver. It is based on the diagonally-layered coding structure in which code blocks are dispersed across diagonals in space-time. In an independent Rayleigh scattering environment, this processing structure leads to theoretical information rates which grow linearly with the number of transmit and receive antennas.

A simpler layered space-time structure is Horizontal BLAST (H-BLAST), and the block diagram is presented in Fig. 3.1. The transmitting unit consists of a vector encoder and n_T QAM (Quadrature Amplitude Modulation) transmitters. Signals are coded, modulated and sent to individual antenna elements. Each antenna is fed by the power that is proportional to $1/n_T$ so that the total radiated power is constant and independent of n_T. The channel mixes up the different datastreams. The n_R receivers consist of conventional QAM receivers. A discrete-time baseband detection process for

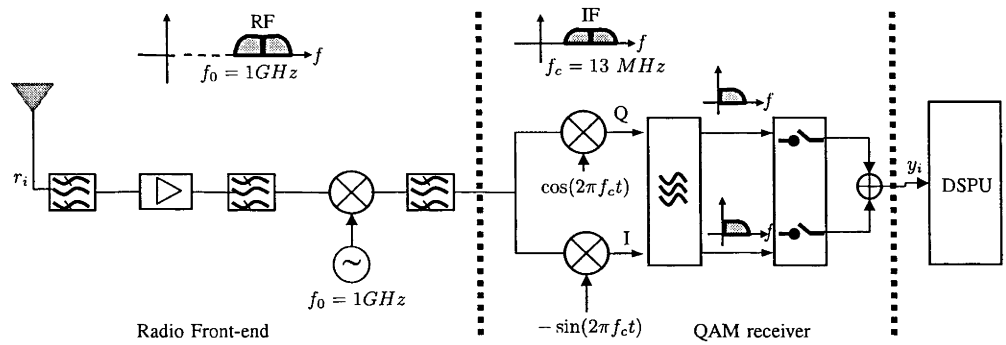

Figure 3.2: Single Receiving Element

a single transmitted vector signal is then applied. The detection process depends on the chosen detection criterion. The most common choices are minimum mean-square error (MMSE) and zero-forcing (ZF). Overall, the scheme is similar to multiuser detection [15–17].

3.1.2 Receiving Unit

This section describes a typical receiving unit (RX) of the multiple antenna system when it is integrated in hand-held devices. In particular, the radio front-end of the receiver is outlined.

A single receiving unit is presented in Fig. 3.2. Signal received by antenna is firstly filtered, and then it is amplified by an ultra-low noise amplifier. The amplified signal is then mixed down to the first intermediate frequency (IF) stage (13 MHz) and sent to QAM receiver. Digitized baseband signals is then sent to digital signal processing unit (DSPU) that performs the detection process [34].

The receiver is fully integrated from LNA (low-noise amplifier) input to the analog-to-digital convertor, and the receiver chain can achieve very low noise factor (NF) by using an advanced SiGe BiCMOS technology [35].

In general, the sensitivity of the radio front-end receiver is driven by noise power intercepted by an antenna, the total noise factor of the radio front-end part of the receiver, and minimum required SNR determined by the required bit-error-rate (BER) for QAM modulation. Thereby, one can

conclude that the sensitivity of radio front-end receiver can be precisely defined only if the antenna thermal noise power and signal-to-noise ratio are accurately determined. While the noise coupling effect upon thermal noise has been elaborated in Section 2.4, here we provide an analysis of SNR at the antenna port. It is our intention to examine the possible directions to improve the design of front-end receiver of the multiple antenna system when it is integrated in the mobile hand-held devices.

3.2 Coupling Effect on Average SNR

This analysis is based on the discrete-time observation of the received signal [36] in the following form

$$\widetilde{\mathbf{y}} = \mathbf{CHx} + \widetilde{\mathbf{n}} \tag{3.1}$$

where $\widetilde{\mathbf{y}}$ is the $n_R \times 1$ vector of the receiving signals, $\mathbf{H}$ is the $n_R \times n_T$ channel matrix, $\mathbf{C}$ is the $n_R \times n_R$ coupling matrix, $\mathbf{x}$ is the $n_T \times 1$ vector of transmitted signals and $\widetilde{\mathbf{n}}$ is $n_R \times 1$ noise vector. Here, the correlation between the elements of some vector $\mathbf{a}$ is denoted by $\widetilde{\mathbf{a}}$.

The effect of mutual coupling is taken into account in the system model (3.1) by using the coupling matrix which is defined as [37]

$$\mathbf{C} = (Z_A + Z_L)(\mathbf{Z} + \mathbf{Z}_L)^{-1} \tag{3.2}$$

where Z_A is the antenna impedance, $\mathbf{Z}_L$ is the load impedance matrix, and $\mathbf{Z}$ is the mutual impedance matrix.

The coupling matrix approach is commonly used to take account of the signal coupling at the receiver in multi-antenna arrays [38]. Other methods have also been proposed. For example, the effect of mutual coupling can be incorporated into the signal power formula by using the scattering (S) parameters [39, 40]. The measurement results in [41] confirm that sufficient accuracy can be achieved by using the coupling matrix, and hence it is adopted here for the purpose of our analysis.

In our analysis, we use the channel model for outdoor environment $\mathbf{H}$ which is defined in [42]. Then, the channel matrix used in the system

model (3.1) can be replaced by

$$\mathbf{H} = \frac{1}{\sqrt{n_S}} \mathbf{R}_{\theta_r,d_r}^{1/2} \mathbf{G}_r \mathbf{R}_{\theta_S,2d_s/n_S}^{1/2} \mathbf{G}_t \mathbf{R}_{\theta_t,d_t}^{1/2} \tag{3.3}$$

where $\mathbf{G}_r$ and $\mathbf{G}_t$ are i.i.d. Rayleigh fading matrix of size $n_R \times n_S$ and $n_S \times n_T$ respectively; while n_S is the number of scatterers; θ_r and d_r are the angular spread and the antenna spacing at the receiver; θ_t and d_t are the angular spread and the antenna spacing at the transmitter; θ_S and d_s are the corresponding angular spread and the spacing between the scatterers positioned between the receiver and transmitter; $\mathbf{R}_{\theta_r,d_r}$ is the $n_S \times n_R$ receive correlation matrix; $\mathbf{R}_{\theta_S,2D/S}$ is the $n_S \times n_S$ correlation matrix and $\mathbf{R}_{\theta_t,d_t}$ is the $n_R \times n_S$ transmit correlation matrix.

If it is considered that signals are correlated at the receiver side only, the channel matrix becomes

$$\mathbf{H} = \mathbf{R}_{\theta_r,d_r}^{1/2} \mathbf{G}_r \tag{3.4}$$

In general, the correlation in $\mathbf{R}_{\theta,d}$ is due to the nonrichness of the scattering environment and/or noninfinite separation between the elements d.

By considering only the correlation matrix at the receiver side, we take into account just the scatterers surrounding the receiving antenna system. It is physically plausible because the electromagnetic coupling phenomenon which is the major concern of this analysis exists only locally around the receiving antennas. In such a way only those scatterers acting in conjunction with the mutual coupling could significantly affect the result.

The distribution of the scatterers affects the correlation. For example, in the case of the uniform power azimuthal distribution, the spatial correlation between two waves is equal to the Bessel function of the first kind of order zero $J_0(.)$. In the next section, we will discuss other commonly used power azimuth distributions in the literature.

3.2.1 Signal Spatial Correlation

The spatial correlation between the waves impinging on two antenna elements has been studied in numerous references. Mathematically, the spatial

correlation coefficient between two antennas can be expressed as [43,44]

$$\rho_c = \frac{\mid \int_0^{2\pi} \int_0^{\pi} E_1^*(\theta,\phi) E_2(\theta,\phi) P(\theta,\phi) \sin\theta d\theta d\phi \mid^2}{\prod_{i=1}^{2} \left(\int_0^{2\pi} \int_0^{\pi} E_i^*(\theta,\phi) E_i(\theta,\phi) P(\theta,\phi) \sin\theta d\theta d\phi \right)} \tag{3.5}$$

where $E_i(\theta,\phi)$ is the electric field antenna pattern of i^{th} antenna, $P(\theta,\phi)$ is the distribution of angle of arrival (AoA), and θ and ϕ are the azimuth and elevation angles, respectively. Hence, the evolution of the correlation coefficients as a function of the distance between antenna elements mostly depends on the AoA distribution and on the radiation pattern.

The statistical distribution of the AoA defines the electromagnetic waves arrive on the antennas from different direction. It describes the AoA of the electromagnetic waves after collisions with the scatterers.

The choice of AoA distribution depends on the environment, and different distributions of AoA result in different correlation values. For example, indoor offices can create a three-dimensional (3D) diffusive medium as there are sufficient horizontal and vertical scatterers [45]. For the 3D environment the spatial correlation is investigated when scatterers are uniformly distributed around antennas, and when scatterers are uniformly placed within certain angular sector [8].

On the other hand, the urban and suburban cellular environments are primarily two-dimensional (2D) due to the planar distribution of mobile phone users, the vertical nature of dominant scatterers (building) and the planar sensitivity patterns of high gain cell site antennas [36]. In the 2D case, the spatial correlation primarily depends upon the power azimuth distribution. In the following, we have outlined several distributions that have been reported in the literature.

For the channel model presented in [46], the n^{th} power of a cosine function is used as a model of the power azimuth spectrum. However, this model has been regarded as inconvenient, since it does not enable closed-form derivation [47] of spatial correlation functions. Hence, two other distributions, a truncated Gaussian and a uniform, have been introduced in [48] and in [49]. More recently, a Laplacian distribution has been proposed in [50] as the best fit to measurement results in urban and rural areas. Cross-correlation

functions of the received signals at two antennas have been derived for the truncated Laplacian and the truncated Gaussian distributions in [7]. In addition, the von-Mises azimuthal distribution is investigated in [8].

The spatial correlation between signals received by coupled antennas placed in a 3D scattering environment with the Gaussian AoA distribution is investigated in [51]. The combined effect of the mutual coupling and scattering on signal correlation in two- and three-dimensional environments with uniform AoA distributions was investigated in [36]. Their simulation results indicate on the lower level of signal correlation in coupled antenna arrays in comparison with uncoupled antenna arrays. Namely, the mutual coupling modifies the radiation pattern of each antenna, decreasing its maximum effective area and resulting in a lower level of the spatial correlation. Although the conclusion is based on the uniform and Gaussian AoA distributions, it is believed to be indicative of the general trend.

In the next section, we use the uniform AoA distribution in the two-dimensional case for the SNR analysis. Although the uniform AoA distribution is very often used as an approximation because of its simplicity, it is believed that the result will be valid for a great variety of situations.

3.2.2 SNR Analysis

In this Section, we extend our study of the effect of mutual coupling in multiple antennas, and provide an analysis of the signal-to-noise ratio. For the purpose of this analysis the receive signals are taken to be correlated due to the mutual coupling, in addition to the correlation due to the scattering effect. Uncorrelated transmitted signals are considered.

Based on the system model (3.1), the total received signal power $\overline{P}_R$ can be calculated as [37, 52, 53]

$$\begin{aligned}\overline{P}_R &= \frac{P_T}{n_T}\mathrm{Tr}(\mathbf{C}\mathbf{H}\mathbf{H}^\dagger\mathbf{C}^\dagger) \\ &= \frac{P_T(Z_A+Z_L)^2}{n_T}\mathrm{Tr}\Big(\big((\mathbf{Z}+Z_L\mathbf{I}_{n_R})^{-1}\big)^\dagger(\mathbf{Z}+Z_L\mathbf{I}_{n_R})^{-1}\mathbf{H}\mathbf{H}^\dagger\Big) \qquad (3.6)\end{aligned}$$

where P_T is total transmitted power at antenna's output and $\mathrm{Tr}(\cdot)$ denotes the trace operator.

When the correlation due to the scattering effect is considered at the receiver only, the channel matrix can be simplified, and the average (or expected) received signal power becomes

$$\begin{aligned}\overline{P}_R &= \frac{P_0}{n_T}\mathrm{Tr}(\mathbf{C}\mathbf{R}_{\theta_r,d_r}\mathbf{C}^\dagger) \\ &= \frac{P_0}{n_T}\mathrm{Tr}\Big((\mathbf{Z}+\mathbf{Z}_L)^{-1})^\dagger(\mathbf{Z}+\mathbf{Z}_L)^{-1}\mathbf{R}_{\theta_r,d_r}\Big)\end{aligned} \tag{3.7}$$

where the receive correlation matrix due to the scattering environment is $\mathbf{R}_{\theta_r,d_r}$.

Then, the signal-to-noise ratio can be calculated as

$$\begin{aligned}\rho_r &= \frac{\overline{P}_{ri}}{N_{total}} \\ &= \frac{P_0(Z_A+Z_L)^2}{n_T P_N}\mathrm{Tr}\Big(((\mathbf{Z}+\mathbf{Z}_L)^{-1})^\dagger(\mathbf{Z}+\mathbf{Z}_L)^{-1}\mathbf{H}\mathbf{H}^\dagger\Big)\end{aligned} \tag{3.8}$$

where the average noise power $\overline{P}_N$ is defined in (2.28) of Chapter 2 as

$$\overline{P}_N = 2kTB\mathrm{Tr}\Big(\mathfrak{Re}(\mathbf{Z}_L)(\mathbf{Z}+\mathbf{Z}_L)^{-1}\big((\mathbf{Z}+\mathbf{Z}_L)+(\mathbf{Z}+\mathbf{Z}_L)^*\big)((\mathbf{Z}+\mathbf{Z}_L)^{-1})^\dagger\Big) \tag{3.9}$$

where $\mathfrak{Re}(\cdot)$ denotes real part of complex value.

Finally, the received signal-to-noise ratio (SNR) when both signal and noise are coupled is [54]

$$\rho_r = \frac{P_0(Z_A+Z_L)^2}{2n_T kTB}\frac{\mathrm{Tr}\Big((\mathbf{Z}+\mathbf{Z}_L)^{-1}\big((\mathbf{Z}+\mathbf{Z}_L)^{-1}\big)^\dagger\mathbf{R}_{\theta_r,d_r}\Big)}{\mathrm{Tr}\Big(\mathfrak{Re}(\mathbf{Z}_L)(\mathbf{Z}+\mathbf{Z}_L)^{-1}\big((\mathbf{Z}+\mathbf{Z}_L)+(\mathbf{Z}+\mathbf{Z}_L)^*\big)((\mathbf{Z}+\mathbf{Z}_L)^{-1})^\dagger\Big)} \tag{3.10}$$

The result in (3.10) represents the mean SNR value per receiving antenna element. One can see that the SNR per isolated antenna element is

$$\rho_r = \frac{P_0}{4n_T n_R kTB} \tag{3.11}$$

In other words, the antenna elements are sufficiently placed apart from each other that the mutual coupling effect and spatial correlation due to the scattering are negligible.

However, if the antenna spacing in the receiving antenna systems is less than 0.5λ, the combined signal and noise coupling effects have to be accounted for in order to correctly calculate the mean signal-to-noise ratio. The results of the numerical analysis, given in the next section, will indicate on the potential error level if the combined mutual coupling effect is not accounted for.

3.3 Simulation Results

In this section, we use simulations to demonstrate the effect of noise coupling on the SNR performance of multi-antenna systems [54, 55]. We consider uniform linear arrays (ULA's) with two, three and four dipoles where the dipole length is $d = \lambda/2 = 150\ mm$. For the purpose of calculating the self and mutual impedances we use the SONNET® [32] software.

In Fig. 3.3, the average signal-to-noise ratio is calculated for the two and three dipole arrays when the antenna interelement spacing varied within the $[0, \lambda/2]$ range.

SNR is calculated when both the signal and noise are affected by the mutual coupling (3.10), denoted in Fig. 3.3 as (mctn) and this is compared with traditional approach which ignores the coupling interaction for thermal noise, denoted by (nmctn). Simulation analysis confirms that the actual SNR (nmctn) is underestimated if the noise coupling is not accounted for. In particular, the maximum SNR underestimation is about 0.5dB and 1dB for the two-dipole and three-dipole array, respectively.

Another interesting result from Fig. 3.3 is that if the mutual coupling is taken into account for both the signal and noise, the uniform linear dipole array starts to act as a single antenna with an equivalent resistance, when the antenna spacing approaches zero.

Fig. 3.4 depicts the variation in the mean signal-to-noise ratio (SNR) per MIMO sub-channel (branch) due to the mutual coupling on thermal noise for antenna spacing up to 0.5 λ. The variations in the mean SNR are calculated in relation to the SNR of isolated antennas as

$$\varsigma = \frac{SNR^{coupled} - SNR^{isolated}}{SNR^{isolated}}[\%] \tag{3.12}$$

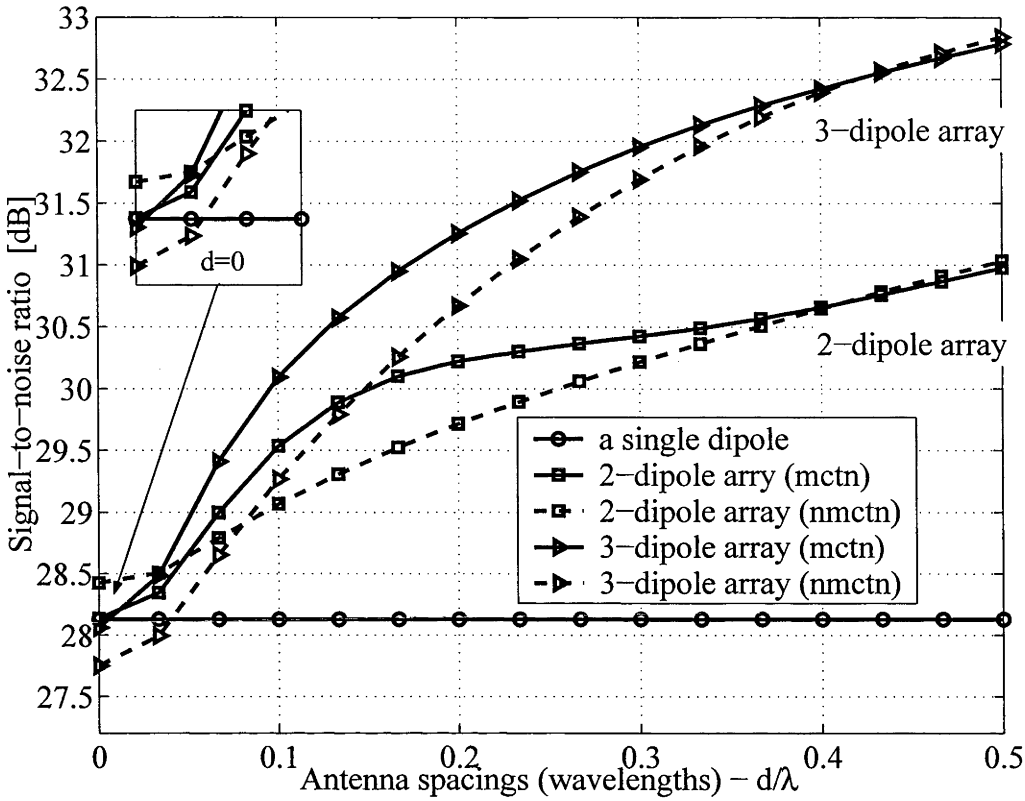

Figure 3.3: The SNR value verus antenna spacing for two-dipole and three-dipole arrays assuming mutual coupling for both signal and noise

The variations in mean SNR are calculated for the uniform linear antenna array with two, three, and four dipole antennas. One can see that the variations can be as large as 7% for very small antenna spacing equal to 0.1λ. For such a small antenna spacing, the electromagnetic interactions between the antennas are very strong. Further, for up to 0.35λ antenna spacing, the mutual coupling is still very high, and coupled SNR is higher than SNR for the isolated antennas.

For the range $(0.35 - 0.5)\ \lambda$ antenna spacing, the thermal noise power of coupled antenna is slightly below the thermal noise power of isolated antenna, and the curves are below zero. In other words, the thermal noise power level and the signal power level oscillates around the SNR for isolated antennas for the antenna spacing around 0.35λ. Consequently, the coupled SNR slightly

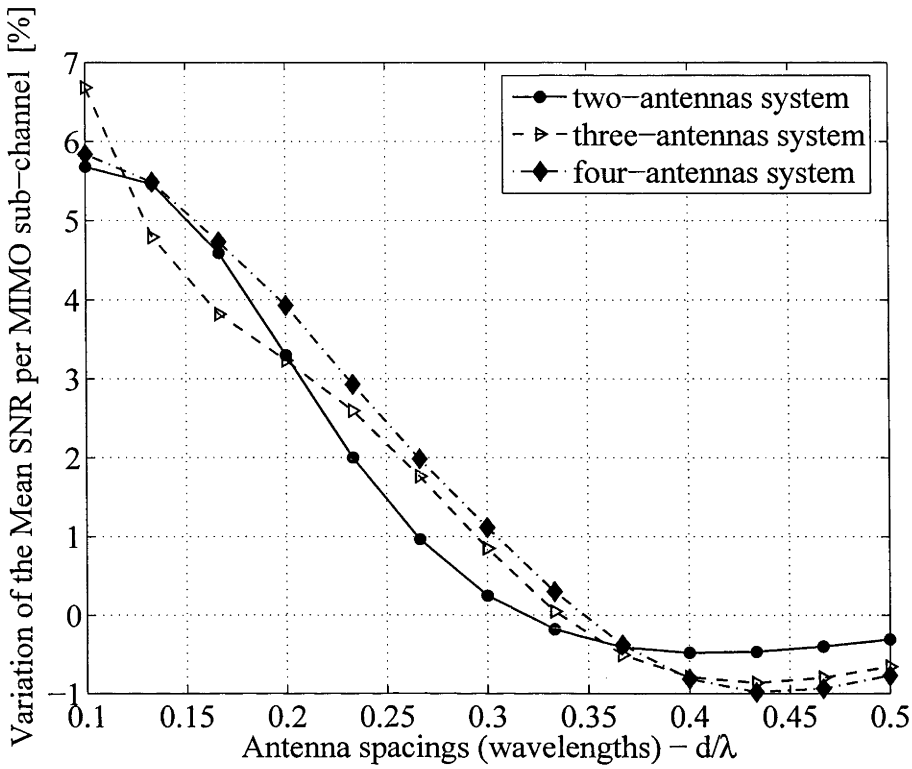

Figure 3.4: The SNR value verus antenna spacing for two-dipole and three-dipole array assuming mutual coupling for both signal and noise

drops below the isolated SNR case. For even greater antenna spacings, the coupled thermal noise power approaches the thermal noise power level of isolated antennas, and the curves merge into one.

The result is presented for the ULA's with two, three and four antennas. However, it should be noted that the curves are not overlapping as one can expect. The reason is that a ULA with more than two antennas is not a symmetrical configuration. For example, the dipole positioned in the middle slot of three-dipole array will be exposed to higher level of the mutual interaction than the dipole at the edge position of the array. A similar conclusion can be derived for the ULA with four antennas.

3.4 Summary and Contributions

In this chapter, we investigated the combined mutual coupling effect on signal and thermal noise in the multi-antenna systems with closely spaced antennas. We provided an analysis of the SNR for coupled antennas. We showed and quantitatively evaluated that the SNR is underestimated if the effect of noise coupling is omitted from the analysis. Finally, we compared the error made by traditional thermal noise consideration with the presented method and showed that the maximum SNR underestimation is about 0.5dB for a two-dipole array and 1dB for a three-dipole array, for antenna spacings below 0.5 λ.

Chapter 4

Conclusions and Future work

This chapter draws together the conclusions from Part I of the thesis. The summary of contributions can be found at the end of each chapter and is not repeated here.

4.1 Conclusions

This part has been concerned with the mutual coupling effect in multiple antenna systems. Motivated by the trend of increasing number of antennas in the physically restricted volume of hand-held devices, this part of thesis investigated the signal and noise correlation in multi-antenna systems with small interelement spacings.

By introducing the previously ignored noise correlation into the system model of MIMO wireless communication systems, more realistic estimates of the signal-to-noise ratio performance can be computed. The most significant result was that noise is affected by the mutual coupling just as mutual coupling affects the signal. Consequently, it has been shown that the thermal noise power of coupled antenna is lower than the noise power of isolated antennas. Further, the average received signal-to-noise ratio per receiving antenna might be underestimated for very small antenna spacings if the noise coupling is neglected.

This part has shown that the implementation of the multi-antenna systems in the already small hand-held devices will bring up some new effects,

as yet to be fully exploited, such as the noise coupling effect. Therefore, it is crucial to fully ascertain those effects in order to get the most accurate estimation of the capacity performance for such systems.

4.2 Future Directions of Research

Although this part of the thesis has given valuable insights into the signal and noise correlation in the closely spaced multi-antenna systems, there are many more research directions one could follow to further broaden the understanding of signal and noise correlation effects. Outlined below is a small subset of a much larger group of possible research projects pertinent to this thesis.

Noise correlation theory: As outlined in Chapter 2 noise correlation requires further investigation, especially if directional antennas are to be implemented in future mobile handheld devices. Some foundation has been laid in Section 2.2 about the impulse noise, however, there is a significant amount of work required to fully develop the theory.

Signal correlation theory: As outlined in Chapter 3 spatial signal correlation in the coupled antenna array requires further investigation. The impact of AoA distributions on the signal spatial correlation of the coupled antennas, in both two- and three-dimensional environments, will provide a valuable insight into the correlation mechanisms. Some foundation has been laid in Section 3.2.1 about the possible distributions which have been already studied in the literature. Further, signal spatial correlation due to the scatterers placed in the far-field of antenna are studied in the literature, while the impact from the near-field scatters has to be examined. In such a way, there is a significant amount of work required to examine the spatial signal correlation due to the near- and far-field scatterers in the coupled antenna arrays.

Implementation: The implementation of the multiple antenna systems could significantly increase data throughput in personal mobile communications. Following that, a full investigation of the noise coupling

effect has to be done for the other types of antennas used in personal mobile communication such as patch antennas. In addition, the noise coupling effects have to be tested for more practical realizations of multi-antenna systems, and possibly confirmed by measurement results of the SNR's of mobile hand-held devices.

Part II

Multiple Antenna Channel Capacity

Chapter 5

Introduction

5.1 Wireless Communication Channels

The wireless channel places fundamental limitations on the performance of wireless communication systems. The transmission path between the transmitter and the receiver ranges from simple line-of-sight to complex environments with obstructions from mountains, foliage, and man-made objects such as buildings. Additionally, any motion of the transmitter or receiver affects the performance of the wireless communication system.

The mechanisms behind electromagnetic wave propagation through the wireless channel are many and varied, and can generally be attributed to reflection, diffraction and scattering. Wireless communications systems typically operate in urban area with no line-of-sight, and diffraction and scattering are dominant propagation mechanisms. The electromagnetic waves propagate along various paths of differing lengths. The presence of multiple paths along which a signal can travel, between the transmitter and receiver, is known as *multipath propagation.*

A simplified picture of a multipath environment is shown in Fig. 5.1. At the receiver, the incoming waves arrive from many different directions with different propagation delays. The signal received at any point in space may consist of a large number of plane waves with random distributed amplitudes, phases, and angle of arrivals. The received signal will typically be a superposition of these many multipath components thereby creating a rapid

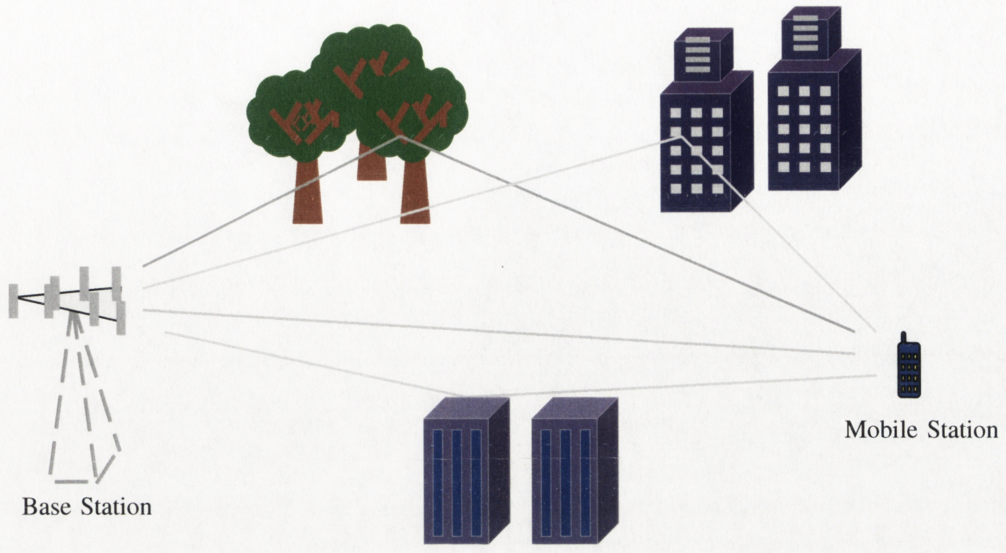

Figure 5.1: Multipath Scattering Environment

fluctuation in signal strength at the receiver, known as *multipath fading.*

The traditional approach to mitigate fading effects is to simply allow for deep fades by increasing the transmit power. However, this simple approach leads to a majority of the time transmitting many times the actual required power for reliable communication, therefore causing high power consumption and considerable interference to other users.

A more recent and successful scheme to overcome the effects of signal fading is to exploit channel diversity. The principle idea is for the receiver to obtain several independent copies of the signal of interest transmitted over independent fading channels, thus the probability that all the signal components will fade simultaneously is considerably reduced. For successful exploitation of diversity schemes in fading channels the different received branches must, on average, exhibit low mutual correlations. Following that, different diversity schemes for obtaining several replicas of signal have been proposed: time, frequency, polarization and spatial diversity.

Time diversity repeatedly transmits information at a time spacing that exceeds the coherence time of the channel, where the coherence time is the minimum time separation between independent channel fades.

Frequency diversity simply transmits information on more than one carrier frequency. Provided the frequency are separated by more then the coherence bandwidth of the channel they will experience independent fades. The coherence bandwidth of the channel is the minimum frequency separation between independent fades and is inversely proportional to the delay spread of channel.

Polarization diversity consists of transmitting information over orthogonally polarized branches. It has been shown that by exploiting electromagnetic polarizations, an increase in the number of degrees of freedom and hence transmission information rate over wireless channels can be achieved [56]. Further, experimental results by using antenna with orthogonal polarizations has been reported in [57].

Finally, spatial diversity could improve SNR, BER (bit-error-rate) and capacity performance of mobile wireless systems under certain channel modeling assumptions. Namely, in the presence of multipath the received power-level is a random function of the user location and, at times, experiences fading. By using spatially separated antennas we can reduce the probability of losing the signal by combining the antenna signals.

This thesis is mostly concerned with spatial diversity, in particular the performance improvement that can be achieved when multiple antennas are used. However, with decreasing sizes of mobile handheld and portable devices, the employment of multiple antennas is becoming more difficult. In particular, the effects arising from the case when the multiple antennas are placed in small volume have been addressed in the first part of thesis. The second part of thesis examines of MIMO channel capacity when the multi-antenna systems with small antenna spacing are used.

The use of multiple transmit and receive antennas to increase capacity is known as spatial multiplexing. When it is employed in a rich scattering environment multiple data pipes can be created to yield a linear (in number of antennas) increase in capacity. The multiple date pipes are transmitted at the same bandwidth. Spatial multiplexing operates by breaking up the symbol stream into several parallel streams which are then transmitted simultaneously within the same frequency band. At the receiver, information from each of the transmit antennas has a unique spatial signature due

to the multipath propagation, which is exploited to separate the individual data streams. With the increase in capacity obtained at no extra bandwidth or power consumption under certain channel modeling assumptions, MIMO system is an attractive solution to the capacity demands of next generation wireless systems. An early version of this outstanding result was also presented in [58] for its application to broadcast digital TV. However, the first results hinting at the capacity gains of MIMO were published by J. Winter in [59].

MIMO System Model

For a MIMO communication system shown in Fig. 5.2 with n_T transmit and n_R receive antennas, and for a narrowband frequency-flat fading system, the system model is given by

$$\mathbf{y} = \mathbf{H}\mathbf{x} + \mathbf{n} \tag{5.1}$$

where $\mathbf{x} = [x_1, x_2, ..., x_{n_T}]'$ is the $n_T \times 1$ vector of transmitted signals, $\mathbf{y} = [y_1, y_2, ..., y_{n_R}]'$ is the $n_R \times 1$ vector of received signals and $\mathbf{n}$ the $n_R \times 1$ noise vector, while $[\cdot]'$ denotes the vector transpose. The channel can be described by a $n_R \times n_T$ channel matrix $\mathbf{H}$

$$\mathbf{H} = \begin{pmatrix} h_{11} & h_{12} & \cdots & h_{1n_T} \\ h_{21} & h_{22} & \cdots & h_{2n_T} \\ \vdots & \vdots & \ddots & \vdots \\ h_{n_R1} & \cdots & \cdots & h_{n_Rn_T} \end{pmatrix}$$

with elements $\mathbf{H}|_{r,t} = h_{r,t}$ representing the complex gain between the t^{th} transmit and the r^{th} receive antenna, assumed constant over a symbol period.

5.2 Channel Capacity

The analysis of information theoretic channel capacity gives very useful, although often idealistic, bounds on the maximum information transfer rate realizable between two points of a wireless communication link.

It is important to note that the information theoretic capacity is an upper limit on the possible error-free bit rate, and this limit can only be approached

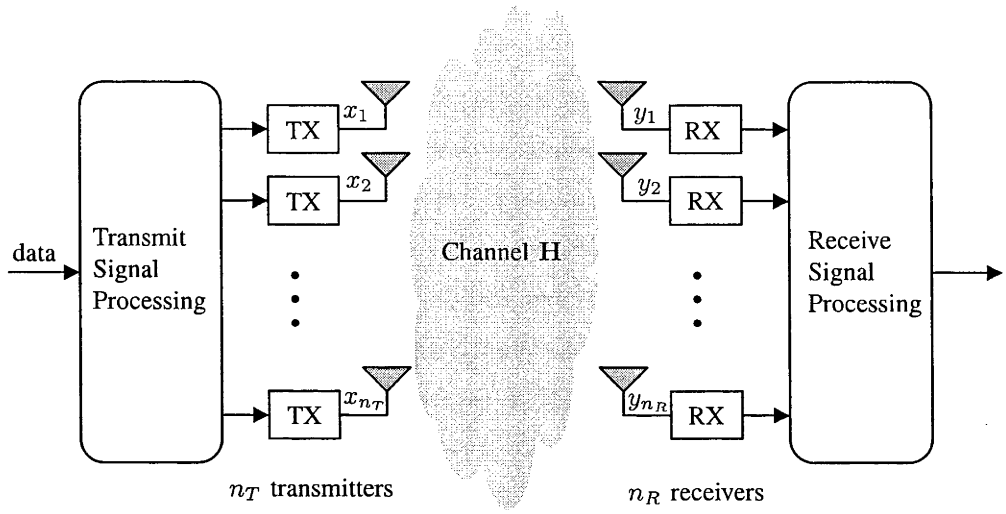

Figure 5.2: A MIMO wireless transmission system with n_T transmit antennas and n_R receive antennas. The transmit and receive signal processing includes coding, modulation, mapping, etc. and may be realized jointly or separately

in practice with high complexity. In real system implementations, the achievable bit rate is limited due to coding, detection and constellation complexity. Therefore, any practical system usually achieves a bit rate (at some desired small BER) that is a fraction of information theoretic capacity.

The capacity is defined as the maximum of the average mutual information rate $\mathcal{I}(\mathbf{x}, \mathbf{y})$ between the input and output of the channel with respect to all possible transmitter statistical distributions $p(\mathbf{x})$ [60, 61]

$$C = \max_{p(\mathbf{x}):\mathrm{Tr}(\mathbf{Q})\leq P_T} \mathcal{I}(\mathbf{x}, \mathbf{y}) \tag{5.2}$$

where $\mathbf{Q}$ is the covariance matrix of the transmitted signals, P_T is the total transmitted power, and $\mathrm{Tr}(\cdot)$ denotes the trace operator.

Here, the mutual information rate between the transmitted and received signals is given by

$$\begin{aligned}\mathcal{I}(\mathbf{x}, \mathbf{y}) &= \mathcal{H}(\mathbf{y}) - \mathcal{H}(\mathbf{y}|\mathbf{x}) \\ &= \mathcal{H}(\mathbf{y}) - \mathcal{H}(\mathbf{H}\mathbf{x} + \mathbf{n}|\mathbf{x}) \\ &= \mathcal{H}(\mathbf{y}) - \mathcal{H}(\mathbf{n}|\mathbf{x})\end{aligned}$$

$$= \mathcal{H}(\mathbf{y}) - \mathcal{H}(\mathbf{n}) \tag{5.3}$$

where $\mathcal{H}$ denotes the entropy rate of a random variable, and gives a measure of uncertainty. It is assumed that the transmitted signals $\mathbf{x}$ and the noise $\mathbf{n}$ are independent. From (5.3) maximizing $\mathcal{I}(\mathbf{x}, \mathbf{y})$ is equivalent to maximizing $\mathcal{H}(\mathbf{y})$. For example, this can occur if $\mathbf{y}$ and $\mathbf{x}$ are circularly symmetric complex Gaussian variables. The entropy rate $\mathcal{H}(\mathbf{y})$ is then equal to $\mathcal{H}(\mathbf{y}) = \log_2 |\pi e \mathbf{Q}_y|$, with covariance matrix $\mathbf{Q}_y = E\{\mathbf{y}\mathbf{y}^\dagger\}$ [2]. In this case the mutual information rate is given by

$$\begin{aligned} \mathcal{I}(\mathbf{x}, \mathbf{y}) &= \log_2 |\pi e \mathbf{Q}_y| - \log_2 |\pi e \mathbf{Q}_n| \\ &= \log_2 |\frac{\mathbf{Q}_y}{\sigma^2}| \\ &= \log_2 \left| \mathbf{I}_{n_R} + \frac{\mathbf{H}\mathbf{Q}_x\mathbf{H}^\dagger}{\sigma^2} \right| \end{aligned} \tag{5.4}$$

One can define

$$C(\mathbf{Q}_x) = \log_2 \left| \mathbf{I}_{n_R} + \frac{\mathbf{H}\mathbf{Q}_x\mathbf{H}^\dagger}{\sigma^2} \right| \tag{5.5}$$

as the capacity achieved by transmitting independent complex circular Gaussian symbols along the eigenvectors of $\mathbf{Q}_x$. Now the capacity of the channel becomes a transmitter optimization problem. The capacity is subject to the transmitter power constraint, and it is required to find the optimal input covariance matrix to maximize $C(\mathbf{Q}_x)$

$$C = \max_{\mathbf{Q}_x : \mathrm{Tr}(\mathbf{Q}_x) \leq P_T} C(\mathbf{Q}_x) \tag{5.6}$$

Optimization of the input covariance matrix will be discussed in more detail in Section 5.3, where water-filling and equal power allocation scheme are presented as commonly used techniques to optimize the input covariance matrix under the constraint of channel state information availability.

5.2.1 Single Input Single Output (SISO) System

The channel capacity of SISO wireless systems is considered here in the presence of additive white Gaussian noise (AWGN) only. The discrete-time system model is given by

$$y(n) = x(n) + n(n) \tag{5.7}$$

where x is the transmitted signal, y is the corresponding received signal, and n is a white Gaussian noise random process at time n. If the received signal power is P, the occupied bandwidth is B, the received signal-to-noise ratio SNR is then given by $\rho = P/BN_0$, where $N_0/2$ is the power spectral density of the noise. Then, the channel capacity of SISO wireless communication system is given by

$$C = \log_2(1 + \rho) \tag{5.8}$$

where the capacity unit is bits per second per Hz (b/s/Hz). The capacity of SISO system (5.8) is the well known Shannon's formula.

5.3 MIMO Fading Channel Capacity

We consider a MIMO wireless communication system shown in Fig. 5.2 with n_T transmit and n_R receive antennas and channel model given by (5.1). For channel matrix $\mathbf{H}$ with random independent complex elements, it was shown in [1,2] that the capacity is given by

$$C = \log_2 \left| \mathbf{I}_{n_R} + \frac{\rho}{n_T} \mathbf{H}\mathbf{H}^\dagger \right| \tag{5.9}$$

where ρ is the average SNR at any receive antenna, $(\cdot)^\dagger$ is the complex conjugate transpose. It is assumed that the perfect channel information is known at the receiver but not at the transmitter.

Here, we consider a random channel model represented by a stochastic channel matrix $\mathbf{H}$, hence the capacity given by (5.9) is also random and represents an instantaneous capacity for a particular realization of $\mathbf{H}$. With the capacity defined as a random variable, it is necessary to consider how to best characterize it. Two simple characteristics are often used: *ergodic capacity* [2,62] and the *outage capacity* [1,63,64].

5.3.1 Erodic Capacity

The average or *ergodic* capacity is the mean value of all occurrences of capacity C and is defined as

$$C_{erg} = E_{\mathbf{H}}\{C\} = E_{\mathbf{H}}\left\{ \log_2 \left| \mathbf{I}_{n_R} + \frac{\rho}{n_T} \mathbf{H}\mathbf{H}^\dagger \right| \right\} \tag{5.10}$$

where $E_{\mathbf{H}}$ is the expectation over all possible channel realization $\mathbf{H}$. The ergodic capacity gives information on the average data rate offered by the link and gives a useful measure of the possible performance for a randomly fading channel.

To indicate the potential performance of MIMO systems, consider the special case of $n_T = n_R$. Then for a large number of antennas, by the law of large numbers $\mathbf{H}\mathbf{H}^{\dagger}/n_T \longrightarrow \mathbf{I}_{n_R}$, the ergodic capacity increases linearly with n_R

$$C_{erg} = n_R \log_2(1+\rho) \tag{5.11}$$

In general, the capacity grows linearly with the smaller number of antennas, $\min(n_T, n_R)$, hinting at the significant capacity gains of MIMO systems.

5.3.2 Outage Capacity

Another measure of channel capacity that is frequently used is *outage* capacity. The outage capacity C_{out} is defined as the data rate that can be guaranteed with a high level of certainty. If the channel capacity falls below the outage capacity, there is no possibility that the transmitted block of information can be decoded with no errors, whichever coding scheme is employed.

Let p be the outage threshold (say 1% or 0.01), then define the outage capacity $C_{out,p_{out}}$ for which [33, 65]

$$Prob\{C \leq C_{out,p_{out}}\} = p_{out} \tag{5.12}$$

The outage capacity is often presented in the form of a cumulative distribution function (CDF). Sometimes, it is useful to study the opposite question and ask how often the channel capacity is above the outage threshold. Then, the complementary cumulative distribution function (CCDF) is used.

5.3.3 Channel Unknown at the Transmitter

When there is no feedback in the system, the channel is known at the receiver but unknown at the transmitter. Then, one way to distribute transmit output power is to apply the equal power allocation scheme. The covariance matrix

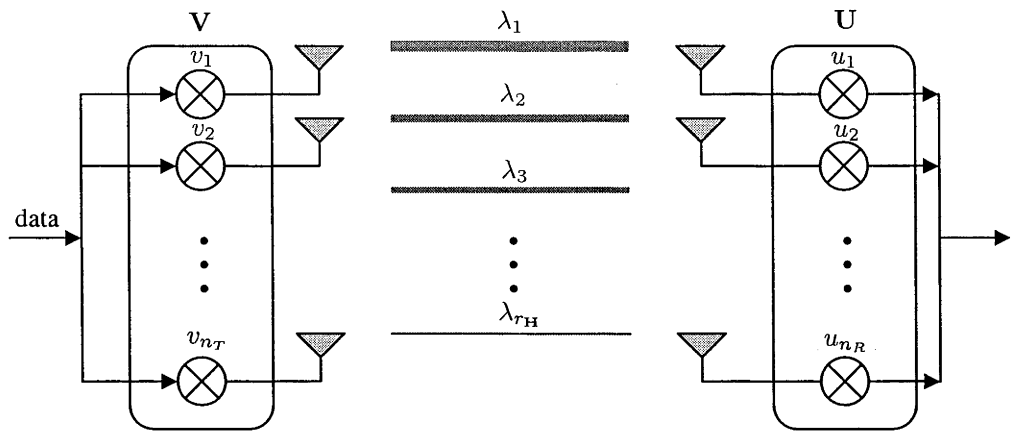

Figure 5.3: Illustration of parallel eigen-channel of a MIMO system for the singular value decomposition $\mathbf{H} = \mathbf{UDV}^\dagger$. The width of the line indicates the different eigen-power gains λ_n

of transmitted signals is then given by $\mathbf{Q}_x = (P_T/n_T)\mathbf{I}_{n_T}$. The channel capacity becomes

$$C_{eq} = \log_2 \left| \mathbf{I}_{n_R} + \frac{\rho}{n_T} \mathbf{H}\mathbf{H}^\dagger \right| \tag{5.13}$$

where $\rho = P_T/\sigma^2$ is the average SNR at any receive antenna. To emphasize the capacity growth, one can apply the singular value decomposition (SVD) of the channel matrix $\mathbf{H}$. The MIMO channel is then decomposed into an equivalent system of parallel AWGN SISO channels. Let $\mathbf{H} = \mathbf{UDV}^\dagger$ be the SVD of $\mathbf{H}$, then $\mathbf{U} = [u_1, ..., u_{n_R}] \in \mathbb{C}^{n_R \times n_R}$ and $\mathbf{V} = [v_1, ..., v_{n_T}] \in \mathbb{C}^{n_T \times n_T}$ are unitary and $\mathbf{D} = \text{diag}(\sqrt{\lambda_1}, \sqrt{\lambda_2}, ..., \sqrt{\lambda_{r_\mathbf{H}}}, 0, ..., 0)$, where $\sqrt{\lambda_n}, n = 1, ..., r_\mathbf{H}$, are the singular values of the channel matrix, and $r_\mathbf{H} = \text{rank} \leq \min(n_T, n_T)$. Then (5.1) can be written as

$$\widetilde{\mathbf{y}} = \mathbf{D}\widetilde{\mathbf{x}} + \widetilde{\mathbf{n}} \tag{5.14}$$

where $\widetilde{\mathbf{y}} = \mathbf{D}\mathbf{y}, \widetilde{\mathbf{x}} = \mathbf{V}^\dagger\mathbf{x}$ and $\widetilde{\mathbf{n}} = \mathbf{U}^\dagger\mathbf{x}$. Therefore, we have a system of $r_\mathbf{H}$ equivalent parallel SISO eigen-channels, as illustrated in Fig. 5.3 for the case $n_T = n_R$, with signal power given by the non-zero eigenvalues $\{\lambda_1, \lambda_2, ..., \lambda_{r_\mathbf{H}}\}$. Hence, the channel capacity (5.13) can be expressed as the sum of the ca-

pacities of the individual subchannels:

$$C_{eq} = \sum_{n=1}^{r_{\mathbf{H}}} \log_2 \left(1 + \frac{\rho}{n_T}\lambda_n\right) \tag{5.15}$$

Clearly, with a reduced number of significant eigenvalues in (5.15) the capacity of the MIMO channel will be reduced because of a rank deficient channel matrix. This situation can occur when the signals and noises intercepted by antennas become correlated due to scattering and mutual coupling. This is an important issue of this thesis.

5.3.4 Channel Known at the Transmitter

If the channel is fading slowly enough it may remain constant long enough for timely feedback of the channel state to the transmitter. In this case, when the channel is known at the transmitter (and at the receiver) then the optimal Q_x is called the waterfilling solution [60, 66–68]. In the waterfilling power allocation scheme, the power which is allocated to each MIMO sub-channel is determined by the strength of that sub-channel and is given by

$$P_n = (\mu - \lambda_n^{-1})^+ \tag{5.16}$$

where λ_n is the n^{th} eigenmode of the channel, μ is the waterfill level chosen such that $\sum_n P_n \leq P_T$, and a^+ denotes $\max\{a, 0\}$. The channel capacity is then given by [60]

$$C_{wf} = \sum_n \log_2 \left(\mu\lambda_n\right)^+ \tag{5.17}$$

Waterfilling allocates more power to those subcahnnels with higher $SNR's$ with the water level μ indicating the amount of power to be poured into the channel formed by the function $\{\lambda_n^{-1},\ n = 1, 2, , N\}$, as illustrated in Fig. 5.3. Each of the sub-channels contributes $\log(\mu\lambda_n)^+$ to the total capacity. Feedback of the channel state and waterfilling provides significant capacity gain over uniform power allocation at low SNR's. However, the gain margin becomes negligible as the SNR increases [69]. The intuition is that when there is a low SNR, it is important to allocate the available transmit power to the strongest sub-channels, while as the SNR increases, there is sufficient power to be distributed evenly over all the sub-channels.

5.4 Channel Modeling

5.4.1 Statistical and Analytical Channel Models

For the design of wireless systems, we need channel model that reflects the important properties of propagation channels, properties that have an impact on system performance. This is usually achieved by a simplified channel model that describes the statistics of the impulse response in parametric form, and could lead to the closed form relations between the channel parameters and system performance. In such a way, particular parameters can be described by using stochastic and analytical channel modeling.

Stochastic methods model the probability density function of the channel impulse response. These methods do not attempt to correctly predict the impulse response in one specific location, but rather to predict the probability density function over a large area. The simplest example of this approach is the Rayleigh fading model.

Analytical channel models are defined based on the mathematical properties of their channel covariance matrix. Channel covariance matrix is fully defined, and hence some analytical channel models could be seen as a simplified representation of physical reality. In particular, the specific characteristics of the channel models can be evaluated by using these models, such as: spatial and/or temporal channel correlation, line-of-sight components, number of interacting objects, keyholes and interferences. In the following, we will examine more carefully spatial channel correlation, and present channel models that will be used as a basis to estimate the effect of signal and noise correlation on the capacity performance in the following chapters.

5.4.2 Spatial Correlation

In multi-antenna system, spatial correlation is a measure of relationship between the waves impinging on two antenna elements. It has been shown that the evaluation of the correlation coefficients as a functions of the distance between the antennas elements mostly depends on the Power Azimuthal Spectrum (PAS), on the radiation pattern of the antenna elements and on the level of electromagnetic coupling which is elaborated in the first part of the

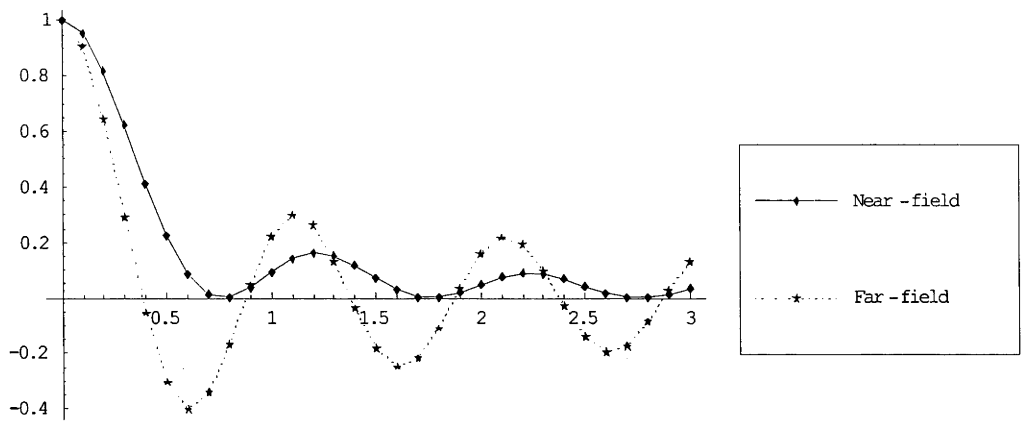

Figure 5.4: Correlation coefficient vs. normalized antenna spacing d/λ, for 2D Uniform PAS distribution

thesis. Antenna elements will be assumed omnidirectional in the following.

Here, the impact of the power azimuthal spectrum on the spatial correlation will be briefly discussed. The azimuthal power distribution is driven by the distribution of the scatterers around the multi-antenna system. The azimuthal power distribution determines the level and the shape of spatial correlation. A narrower azimuthal angular spread in certain directions will result in a higher level of spatial correlation.

The accurate prediction of the azimuthal power distribution in the wireless channels is crucial, as it enables the modeling of the correlation matrix modeling, and hence the modeling of channel matrix. In [46], the n^{th} power of a cosine function is used to model the power azimuth spectrum in outdoor scenarios. A truncated Gaussian distribution and a uniform distribution have been introduced in [48] and in [49]. More recently, a Laplacian distribution has been proposed in [50] as the best fit to measurement results in urban and rural areas. The impact of power azimuthal distribution on spatial correlation is then presented in [7,8]

In order to get a better insight into spatial correlation, we present the spatial correlation due to the uniform distribution of scatterers in Fig. 5.4. The spatial correlation is calculated for the uniform power azimuthal distribution.

In addition, we compare the impact of near-field versus far-field scatterers in Fig. 5.4. The correlation due to the near-field scatterers has a higher

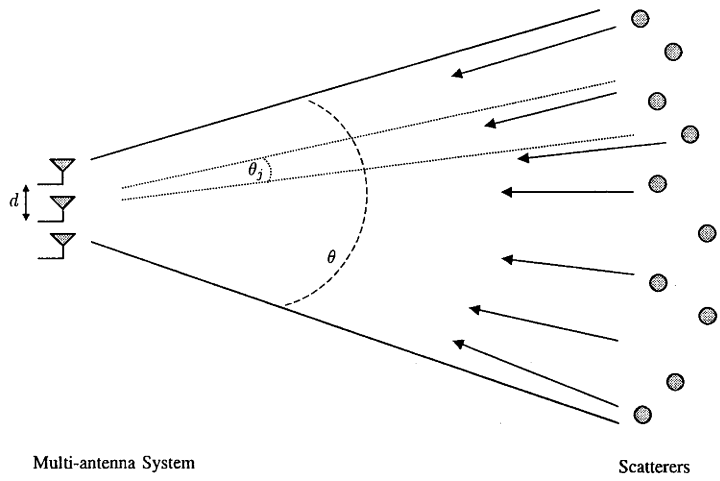

Figure 5.5: Propagation scenarion for spatial correlation due to the scattering. Each scatterers transmit a plane-wave signal to a multi-antenna systems

intensity for small antenna spacings, but it diminishes quickly for greater antenna spacings where the influence of the near-field scatterers fades.

Outdoor Channel Model

A model for the MIMO outdoor wireless channel is presented in [42]. It is more realistic than the usual i.i.d. model, and takes into consideration the scattering radii at transmitter and receiver, antennas spacing, antenna beamwidth and distance between transmitter and receiver. In this channel model, a number of distributed scatterers are placed in the vicinity of the multi-antenna system, but still sufficiently far away from the antennas that the impinging waves to the multi-antenna system behave as plane waves, as it is illustrated in Fig. 5.5. Furthermore, the scatterers are model as perfect omnidirectional antennas, and the electromagnetic waves arrive at the multi-antennas with uniform direction-of-arrivals (DoA). Then, the elements of the correlation matrix are defined as [42]

$$[\mathbf{R}_{\theta,d}]_{m,k} = \frac{1}{n_S} \sum_{j=-((n_S-1)/2)}^{(n_S-1)/2} e^{-2\pi i(k-m)d\cos((\pi/2)+\theta_j)} \tag{5.18}$$

$$\theta = [\theta_{-((n_S-1)/2)}, ..., \theta_{-1}, \theta_0, \theta_1, ..., \theta_{((n_S-1)/2)}]$$

where n_S is the number of scatterers with corresponding DoA denoted by θ_j; d, θ_j and θ are defined in Fig. 5.5. For "large" values of angle spread θ and/or antenna spacing d, $\mathbf{R}_{\theta,d}$ will converge to the identity matrix, which gives uncorrelated fading. For "small" values of θ and d, the correlation matrix becomes rank deficient (eventually rank one), causing (fully) correlated fading.

Now, the MIMO channel model is defined as

$$\mathbf{H} = \frac{1}{\sqrt{S}} \mathbf{R}_{\theta_r,d_r}^{1/2} \mathbf{G}_r \mathbf{R}_{\theta_S,2D/S}^{1/2} \mathbf{G}_t \mathbf{R}_{\theta_t,d_t}^{1/2} \tag{5.19}$$

where $\mathbf{G}_r$ and $\mathbf{G}_t$ are i.i.d. Rayleigh fading matrix of size $n_R \times n_S$ and $n_S \times n_T$ respectively. The matrix $\mathbf{R}_{\theta_S,d_r}$,$\mathbf{R}_{\theta_S,2D/S}$ and $\mathbf{R}_{\theta_t,d_t}$ are the corresponding correlation matrix defined by (5.18) [42].

The presented channel model considers the channel correlation matrix as separable correlation at the receiver and transmitter, and it seems that this assumption is fulfilled for outdoor scenarios based on the measurement results presented in [70].

The separable correlation model is restricted by two more conditions. Firstly, the antennas are tuned to the same polarization. The condition is fulfilled for the multi-antennas systems in our simulations. The second condition is that the antennas should have very similar radiation patterns. It is not satisfied for asymmetrically arranged antennas and when the mutual coupling is strong. This is the case of the uniform linear three- and four-dipoles array, and therefore care should be taken when interpreting these results.

Indoor Channel Model

In contrast to the previously explained channel model, the channel model presented in [71] does not divide the spatial correlation of the channel into separate contributions from the transmitter and the receiver. The joint correlation properties is modeled by describing the average coupling between the eigenmodes of two link ends. The model is given by

$$\mathbf{H} = \mathbf{U}_{RX}(\widetilde{\Omega} \odot \mathbf{G})\mathbf{U}_{TX}^T \tag{5.20}$$

where ($\odot$) denotes the element-wise product of two matrices, $\mathbf{\Omega}$ is power coupling matrix, and $\widetilde{\mathbf{\Omega}}$ is defined as element-wise square root of $\mathbf{\Omega}$. The structure of the power coupling matrix is related to the radio environment. If $\mathbf{\Omega}$ is diagonal, each single direction of departure (DoD) is linked to a single DoA. If $\mathbf{\Omega}$ is of rank one, the model reduces to the separable correlation model. Further, $\mathbf{G}$ is a random matrix with i.i.d. zero-mean complex-normal entries with unit variance, while $\mathbf{U}_{TX}$ and $\mathbf{U}_{RX}$ are the spatial eigenbasis at the transmitter and receiver, respectively.

The presented model is capable of correctly predicting the behavior of channel in indoor environment, as it is confirmed by measured results [71].

5.4.3 Mutual Coupling Effect on Channel Matrix Coefficients

The closely spaced antenna elements result in mutual coupling. The effect is elaborated in the first part of thesis, while here we present the channel correlation matrix where the correlation is due to the mutual coupling.

In the literature, several methods are used to introduce the correlation due to the mutual coupling in the channel matrix. By using the S-parameter representation of a coupled antenna system, the received signal vector is related to the impinging signals at antennas [39, 40]. Then, numerical evaluation of radiation patterns are performed, and the generated results are used for calculating the correlation coefficient derivation and the channel matrix. On the other hand, the coupling matrix method uses the Z-parameters of coupled antennas (mutual impedance matrix) and derives the modified channel matrix [72].

In this thesis, the coupling matrix approach is used to incorporate the coupling into the channel matrix [38]. The modified matrix is then given by

$$\hat{\mathbf{H}} = \mathbf{C}_R \mathbf{H} \mathbf{C}_T \tag{5.21}$$

where $\mathbf{C}_R$ and $\mathbf{C}_T$ are coupling matrices at the receiver and transmitter, respectively, while $\mathbf{H}$ is the channel matrix. In the case of rich scattering environment, the i.i.d. Rayleigh fading matrix might be used for $\mathbf{H}$, otherwise one of the previously defined channel matrices should be applied.

The modified channel matrix is derived under the conditions that the distances between the obstacles and the receive or the transmit arrays are large enough compared to the inter-element distance so that only plane waves are considered.

Using circuit theory, the coupling matrix can be written as [37]

$$\mathbf{C} = (Z_A + Z_T)(\mathbf{Z} + Z_T\mathbf{I}) \tag{5.22}$$

where Z_T is the load impedance of each element, Z_A is the antenna impedance and $\mathbf{Z}$ is the mutual impedance matrix and $\mathbf{I}$ is identity matrix of order n_T and n_R for the transmit and receive matrices, respectively.

The use of coupling matrix is based on several assumption which are verified for dipoles. The main assumption is that the open circuit voltages do not depend on the presence of the other elements. This is correct for half-wavelength dipoles. For other types of antennas, the assumptions may not be verified and the use of numerical method is suggested.

5.4.4 Content and Contributions of the Second Part of the Thesis

Although we have outlined the contributions of the thesis chapters in chapter 1, here we briefly repeat the content and contributions of the chapters of the second part in order to provide an introduction into the rest of the thesis.

Chapter 5 - this chapter gave an introduction into a wireless communication theory. We examined the MIMO channel models found in the literature. In particular, we elaborated an channel model that is the most suitable for our analyzes. We presented the correlation model which introduces the signal coupling into the MIMO channel model;

Chapter 6 introduces the concept of noise coupling into the channel capacity calculations of MIMO systems with small antenna spacings. We estimate the channel capacity performance of MIMO systems. We provide an analysis of ergodic and outage capacities. Then, we examine the

number of effective degrees of freedom of MIMO systems with coupled antennas. We derive the noise correlation factor. Finally, we define the upper bound of the channel capacity of the coupled multi-antenna systems;

Chapter 7 explores the impact of mismatching impedance due to the combined mutual coupling effect on signal and noise on the capacity performance of MIMO systems. Three most widely used matching networks are analyzed, and it has been confirmed that the multi-port conjugate matching network is optimal in terms of signal power, and it also acts as the whitening filter on the coupled thermal noise. Further, the capacity of MIMO systems is estimated when the coupled multi-antenna systems is used at both sides of the link, i.e., at the receiver and transmitter. Our simulation results confirm that the transmit coupling degrades the capacity performance comparing with the case with no constraint on the emitted power;

Chapter 8 is the concluding chapter of the second part of the thesis.

Chapter 6

Channel Capacity Analysis

6.1 Introduction

Multiple input multiple output (MIMO) wireless systems, using multiple antennas at the transmitter and receiver, have demonstrated the potential for increased capacity by exploiting the spatial properties of the multi-path channel [1]. If the channel matrix coefficients are i.i.d. complex Gaussian variables, a linear increase in capacity with the number of antennas has been demonstrated. The statistical independence of the channel coefficients can be achieved if the multiple antennas are sufficiently spaced. However, this is not often practically achievable for example due to limitation in the physical size of mobile hand-held devices.

Close antenna spacing in multi-antenna systems results in electromagnetic coupling. The effect of mutual coupling on the signal-to-interference-plus-noise ratio (SINR) in adaptive antenna arrays has been studied in [37]. It has been shown that SINR and speed of adaptation are overestimated if the effect is omitted. Combined mutual coupling and scattering effect on signal correlation coefficients for both two- and three-dimensional environment was investigated in [36], and the study indicates a lower level of signal correlation in coupled antenna array in comparison with uncoupled antenna array. The mutual coupling effect on radiated power and received signal-to-noise ratio, and its combined effect of decreasing the transmission rate over the MIMO system is presented in [53]. The radiation patterns of five printed dipoles,

and transmission rate over such system were measured in an anechoic chamber in [73]. It has been shown that the measured capacity value is below theoretically obtained capacity of a system with isolated printed dipoles, but still above the calculated capacity of the MIMO system with coupled printed dipoles.

Radiation patterns of coupled antennas and capacity performance of such systems are presented in [72]. Furthermore, losses in antenna loads due to the mutual coupling are included in the capacity analysis in [74]. Spatial signal correlation and antenna gains are examined [51], and it was presented that the mutual coupling reduces the signal correlation and effective antenna gain resulting in a reduction of the estimated transmission rate over the MIMO system. In [75], it was shown that the mutual coupling decreases both the signal spatial correlation and the radiation efficiency of an antenna, and the combined effect resulting in a net capacity reduction is confirmed by simulation results as well as measurement results in a reverberation chamber.

Correlation matrix due to the mutual coupling is formulated in [38], and it was confirmed that the effect acts as an increasing factor on the MIMO channel capacity. Channel capacity performance of compact MIMO wireless systems with small antenna spacing is investigated in [40] where the combined effect of mutual coupling on the SNR, channel coefficient correlation, antenna mismatching impedance and transmitted power is taken into account. Detail network analysis of MIMO wireless system and its channel capacity performance is presented in [39], where power collection capability and radiation patterns are considered in terms of optimal matching impedances along with radiated power constraint due to the mutual coupling.

In order to provide an extensive analysis of the electromagnetic coupling effect on MIMO channel capacity, researchers have investigated a great variety of parameters that are affected by mutual coupling, as was discussed previously, but one important parameter has not been treated—the receiver front-end noise. Although noise power analysis including both internal and external losses and signal-to-noise performance of receiving antenna arrays is presented in [76], the mutual coupling effect on noise power is omitted. Furthermore, receive amplifier noise is included into analysis in [39,77], with the antenna noise taken to be white and Gaussian. The radiation character-

istic of thermal noise was discussed in [26] and the mutual coupling effect on thermal noise in two closely spaced antennas was presented in [27]. However, to our knowledge, the modeling of spatial noise correlation due to mutual coupling and its effect on MIMO channel capacity has not been addressed yet.

An analytical evaluation of the effect on the achievable information rate of the MIMO systems in the outdoor environment is presented in the following. The analytical results are corroborated by the simulation results [30, 78, 79].

6.2 Ergodic MIMO Channel Capacity Analysis

The definition of the ergodic channel capacity is given in Section 5.3.1. While the ergodic channel capacity in Section 5.3.1 was discussed when the noise is AWGN, here we provide an analysis of the ergodic channel capacity with consideration to the noise correlation. Further, the ergodic channel capacity is examined for two cases based on the availability of the CSI. Firstly, the channel capacity is estimated with the CSI available only at the receiver. Then, the channel capacity is evaluated when the CSI is available at the transmitter as well.

6.2.1 Equal-power Allocation Scheme

In this Section we provide an analysis of the channel capacity of MIMO systems with consideration to the signal and the noise correlation at the receiver [78]. We consider the case when the CSI is not available at the transmitter. One technique that might be adopted is the equal power allocation to distribute the total radiated power P_T to the n_T antennas. In addition, we assume that the transmitted signals are independent, with their covariance matrix taken to be

$$\mathbf{Q}_x = \frac{P_T}{n_T}\mathbf{I}_{n_T} \tag{6.1}$$

where P_T is the total transmitted power and $\mathbf{I}_{n_T}$ is a identity matrix of order n_T.

The mutual information for the $n_T \times n_R$ MIMO systems based on [1] becomes [7]

$$C_{eq} = E_{\mathbf{H}}\left\{ \log_2 \left[\det \left(\mathbf{I}_{n_R} + \mathbf{N}_c^{-1} \hat{\mathbf{H}} \mathbf{Q}_x \hat{\mathbf{H}}^\dagger \right) \right] \right\} \tag{6.2}$$

where $\mathbf{N}_c$ is the noise correlation matrix defined in Section 2.5, the channel matrix $\hat{\mathbf{H}}$ is defined by (5.21), and $\mathbf{I}_{n_R}$ is the identity matrix of order n_R. The expectation $E_{\mathbf{H}}\{\cdot\}$ is taken with respect to the channel matrix $\hat{\mathbf{H}}$ and $(\cdot)^\dagger$ denotes the conjugate transpose of a matrix. The channel model which consider correlation due to the scattering in addition to the mutual coupling is presented in Section 5.4.

By using the correlated noise matrix $\mathbf{N}_c = \hat{\mathbf{N}}_c \mathbf{N}$ defined in Chapter 2 in terms of the noise coupling matrix $\hat{\mathbf{N}}_c$, the mutual information becomes

$$C_{eq} = E_{\mathbf{H}}\left\{ \log_2 \left[\det \left(\mathbf{I}_{n_R} + (\hat{\mathbf{N}}_c \mathbf{N})^{-1} \hat{\mathbf{H}} \mathbf{Q}_x \hat{\mathbf{H}}^\dagger \right) \right] \right\} \tag{6.3}$$

It can be rewritten as

$$C_{eq} = E_{\mathbf{H}}\left\{ \log_2 \left[\det \left(\mathbf{I}_{n_R} + \frac{\rho}{n_T} \mathbf{N}_c^{-1} \hat{\mathbf{H}} \hat{\mathbf{H}}^\dagger \right) \right] \right\} \tag{6.4}$$

where ρ/n_T is the average received SNR calculated by considering uncorrelated noise, and ρ is defined by $\rho = P_T/N$.

By applying an eigenvalue decomposition to $\hat{\mathbf{H}}\hat{\mathbf{H}}^\dagger$ and $\hat{\mathbf{N}}_c^{-1}$, the mutual information becomes

$$\begin{aligned} C_{eq} &= E_{\mathbf{H}}\left\{ \log_2 \prod_{i=1}^{r_H} \left(1 + \frac{\rho}{n_T} \frac{\lambda_i}{\nu_i} \right) \right\} \\ &= E_{\mathbf{H}}\left\{ \sum_{i=1}^{r_H} \left(\log_2 \left(1 + \frac{\rho}{n_T} \frac{\lambda_i}{\nu_i} \right) \right) \right\} \end{aligned} \tag{6.5}$$

where λ_i is the i^{th} eigenvalue of matrix $\hat{\mathbf{H}}\hat{\mathbf{H}}^\dagger$ and ν_i is i^{th} eigenvalue of the matrix $\hat{\mathbf{N}}_c$ and $r_H = \text{rank}(\hat{\mathbf{N}}_c^{-1}\hat{\mathbf{H}}\hat{\mathbf{H}}^\dagger) \leq \min(n_T, n_R)$. Also, $\hat{\mathbf{N}}_c$ is a diagonal matrix, and the inverse of a diagonal matrix is a diagonal matrix with its elements inverted $\mathbf{A} = \text{diag}(a_1, \ldots, a_n) \Rightarrow \mathbf{A}^{-1} = \text{diag}(a_1^{-1}, \ldots, a_n^{-1})$. The eigenvalues ν_i of the thermal noise coupling matrix $\hat{\mathbf{N}}_c$ are given by $\nu_i = P_{Ni}/N$.

Fig. 2.4 shows that the coupled thermal noise power P_{Ni} of i^{th} antenna element is lower then the thermal noise power of an isolated antenna element N for antenna spacing $d < 0.4\lambda$. Based on this result the following inequality holds true for antenna spacings lower than 0.4 of the wavelength (λ) [29].

$$\nu_i \leq 1 \Longrightarrow \frac{1}{\nu_i} \geq 1 \tag{6.6}$$

The decrease in the thermal noise power is ascribable to the variation of the radiation pattern. The half-wave dipole ideally has a omnidirectional radiation pattern, while the radiation pattern of the coupled half-wave dipole is directional. The effective area (aperture) is affected reducing the total collected noise power. Note here that the signal and noise are not equally influenced by mutual coupling because the signal and noise directions of arrival at the antenna are different. While the multipath components of the signal arrive from the directions of the surrounding scatterers, the thermal noise is generally picked up by an antenna from the local environment.

Based on (6.5) and (6.6), one can conclude that as the eigenvalues of channel matrix represent virtual channel gains, the eigenvalues of the thermal noise coupling matrix appear as increasing factors of channel gains due to the noise correlations. In Section 3.3 it has been discussed that the combined effect of the signal and noise coupling enhances the SNR per receiving antennas or SNR per MIMO sub-channel. Consequently, it would enable a higher information data rate to be transmitted over the MIMO systems with the coupled multi-antenna system at the receiving side.

6.2.2 Water-filling Power Allocation Scheme

In this Section, we provide an analysis of the information rate over the MIMO system when the CSI is available at transmitter, taking into consideration that the received signal and noise are correlated [78].

When the transmitter has a perfect knowledge about the channel, the transmission technique can be attuned to the channel condition in order to achieve the highest possible transmission rate over the MIMO system. The most efficient transmission technique, discussed in Section 5.3.4, is the water-filling power allocation scheme. Therefore, we present an analysis of

the transmission rate over the MIMO systems with the coupled receiving antennas and when the total transmitted power is allocated based on the water-filling algorithm.

Based on the system model defined by (5.1), the highest achievable information rate transmitted over the MIMO system can be computed as

$$C_{wf} = E_{\mathbf{H}}\left\{ \max_{\mathbf{Q}_x} \log_2 \left[\det\left(\mathbf{I}_{n_R} + \mathbf{N}_c^{-1}\hat{\mathbf{H}}\mathbf{Q}_x\hat{\mathbf{H}}^{\dagger}\right)\right]\right\} \tag{6.7}$$

where $\mathbf{Q}_x$ is the $n_T \times n_T$ covariance matrix of $\mathbf{x}$, and $\mathbf{N}_c$ is the noise correlation matrix defined in Section 2.5 and $\hat{\mathbf{H}}$ is the channel matrix defined in Section 5.4. Additionally, the expectation $E_{\mathbf{H}}\{\cdot\}$ is taken with respect to $\hat{\mathbf{H}}$ and $(\cdot)^{\dagger}$ denotes the conjugate transpose of a matrix.

The covariance matrix $\mathbf{Q}_x$ has to satisfy the average power constraint

$$\mathrm{tr}(\mathbf{Q}_x) = \sum_{i=1}^{n_T} E\{|x_i|^2\} \leq P_T \tag{6.8}$$

The implementation of the water-filling algorithm, illustrated in Section 5.3.4, differs from the case when the noise is taken to be uncorrelated (AWGN). As has been discussed in Section 5.3.4, μ is the "water level" that marks the height of the power that is poured into the "water vessel" formed by the function $\{1/\lambda_i,\ i = 1, 2, \ldots, n\}$. The "water" level μ is computed based on the estimated signal-to-noise ratio per receiving antenna. It means that if the noise is uncorrelated, the eigenvalues of the channel matrix λ_i directly determine the "water" level [60], as is presented by

$$\sum_{i=1}^{r_H'} \left(\mu - \frac{1}{\lambda_i}\right)^{+} = \rho \tag{6.9}$$

where $r_H' = \mathrm{rank}(\hat{\mathbf{H}}\hat{\mathbf{H}}^{\dagger}) \leq \min(n_T, n_R)$ and $\rho = \frac{P_T}{N}$.

Additionally, $(x)^{+}$ denotes the positive part of x, i.e.,

$$(x)^{+} = \begin{cases} x & \text{if } x \geq 0, \\ 0 & \text{if } x < 0, \end{cases}$$

However, if the noise is correlated, and full CSI is available at the transmitter enabling correct estimation of the signal-to-noise ratio per receiving

antenna, the "water" level is determined by the channel matrix eigenvalues λ_i and eigenvalues of the noise coupling matrix ν_i

$$\sum_{i=1}^{r_H} \left(\mu - \frac{\nu_i}{\lambda_i}\right)^+ = \rho \tag{6.10}$$

where $r_H = \text{rank}(\mathbf{N}_c^{-1}\hat{\mathbf{H}}\hat{\mathbf{H}}^\dagger) \leq \min(n_T, n_R)$ and $\rho = P_T/N$ is the received SNR calculated for the case when the noise is uncorrelated.

In such a way, the channel capacity of the MIMO systems can be calculated based on the following formula

$$C_{wf} = E_{\mathbf{H}}\left\{\sum_{i=1}^{r_H} \log_2\left(\frac{\lambda_i}{\nu_i}\mu\right)^+\right\} \tag{6.11}$$

Intuitively, the results presented in (6.11) suggest that the original MIMO channel can be decomposed into r_H parallel independent subchannels, and we allocate more power to the subchannels with higher signal-to-noise ratio.

Each of these subchannels contributes to the total capacity though

$$\log_2((\lambda_i/\nu_i)\mu)^+$$

If $\lambda_i/\nu_i\mu \gg 1$, we say that this subchannel provides an effective mode of transmission and is called a strong eigenmode.

Now, based on inequality (6.6), the eigenvalues of the thermal noise coupling matrix ν_i represent the additional subchannel capacity gain over the case when the mutual coupling effect on thermal noise is negligible, and ν_i becomes equal to 1.

In summary, by considering the noise coupling, a better estimate of the MIMO sub-channel gain can be obtained. Hence, the transmitted power could be allocated even more efficiently compared to the case when the noise coupling is omitted from the analysis. Consequently, a higher information rate can be achieved over such MIMO systems.

6.2.3 Simulation Results

In this section, a simulation analysis is performed to corroborate our analytical results. The single-user MIMO system is studied in the outdoor environment. The transmitting antennas are taken to be widely placed in most

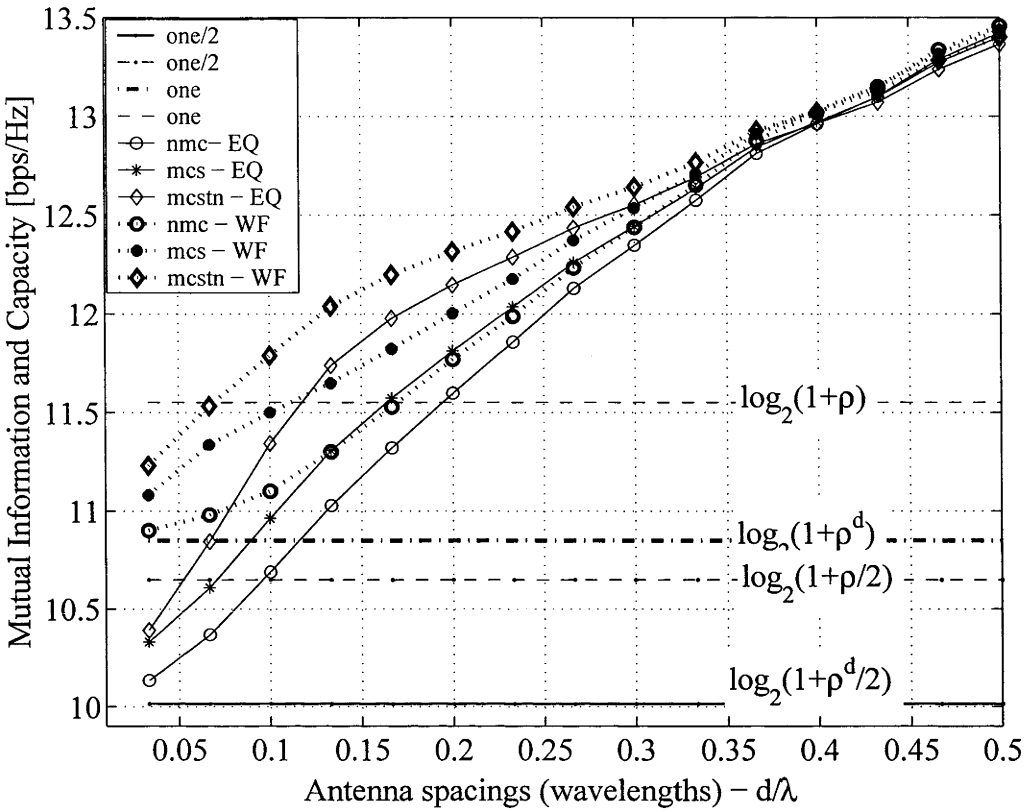

Figure 6.1: Mean (ergodic) capacity with water-filling C_{wf} and equal-power allocation C_{eq} versus antenna element spacings, for 2×2 MIMO Systems

cases, if not specified otherwise. The receiving multi-antenna system with interelement distance d is used, where d is varied within the range $[0, \lambda/2]$. The outdoor channel is simulated by using the MIMO outdoor channel model given in the Section 5.4.2. In addition, the receiver is placed sufficiently far away from the transmitter, and the mobile unit is surrounded by S scatterers placed at the circumference of the circle with $R_S = 30m$ radius. The mutual coupling effect on the received signal vector is modeled with the coupling matrix, presented in Section 5.4.3. The channel capacity is calculated over 10000 channel realizations. Uniform linear arrays (ULA's) with two- and three dipoles are considered. The dipoles are half-wave dipoles and the mutual impedance and admittance matrices are calculated by using the $SONNET^{®}$ [32] software.

Fig. 6.1 depicts the 2×2 MIMO channel capacity as a function of antenna element spacing — a metric of correlation due to the mutual coupling effect. We study the case of achievable information rate when the equal power allocation scheme is used at the transmitter C_{eq} (6.5) and compared it with the transmission rate over the MIMO system when the transmitter applies the water-filling allocation scheme C_{wf} (6.11). In order to explore the noise correlation effect due to mutual coupling on the channel capacity, we estimate the capacity under three assumptions: 1) mutual coupling affects both the signal and thermal noise (mcstn), 2) mutual coupling affects only the signal (mcs) and finally 3) we neglect mutual coupling on both the signal and thermal noise (nmc).

Fig. 6.1 shows that the correlated noise due to the mutual coupling increase the estimated information rate over MIMO system. This confirms the major outcome from our theoretical analysis that correlated noise increases the eigenvalues of channel matrix, by increasing the intensity of each subchannel. Furthermore, we show that the channel capacity calculated under the assumption that mutual coupling correlates both the signal and noise (mcstn) is higher comparing with the case when the noise coupling effect is neglected (mcs).

Fig. 6.1 depicts channel capacity performance for very small antenna element spacings $d \leq 0.1$ (antenna elements almost overlap $d \rightarrow 0$). We use the effective dimensionality approach [80] to estimate the channel capacity for $d \rightarrow 0$. In the WF case, for $d \rightarrow 0$, the transmitter receives information that only one active subchannel exists, and thus transmits all power in that subchannel. The signal-to-noise ratio is then ρ. The WF capacity declines to its lower limit $\log_2(1+\rho)$. However, for the equal-power allocation model, the transmitter does not have any information about the effective number of subchannels and it continues its transmission into the two subchannels. The EQ channel capacity declines towards the lower limit $\log_2(1+\rho/n_T)$, $n_T = 2$.

In addition, for $d \rightarrow 0$, the signal-to-noise ratio of one subchannel becomes ρ^d because the equivalent resistance is doubled in the thermal noise calculation. It is denoted by 'one' (SNR is calculated with doubled impedance) and 'one/2' (SNR is calculated with antenna's impedance) in Fig. 6.1. Then, the lower limits drop to $\log_2(1+\rho^d)$ and $\log_2(1+\rho^d/2)$ for WF and EQ,

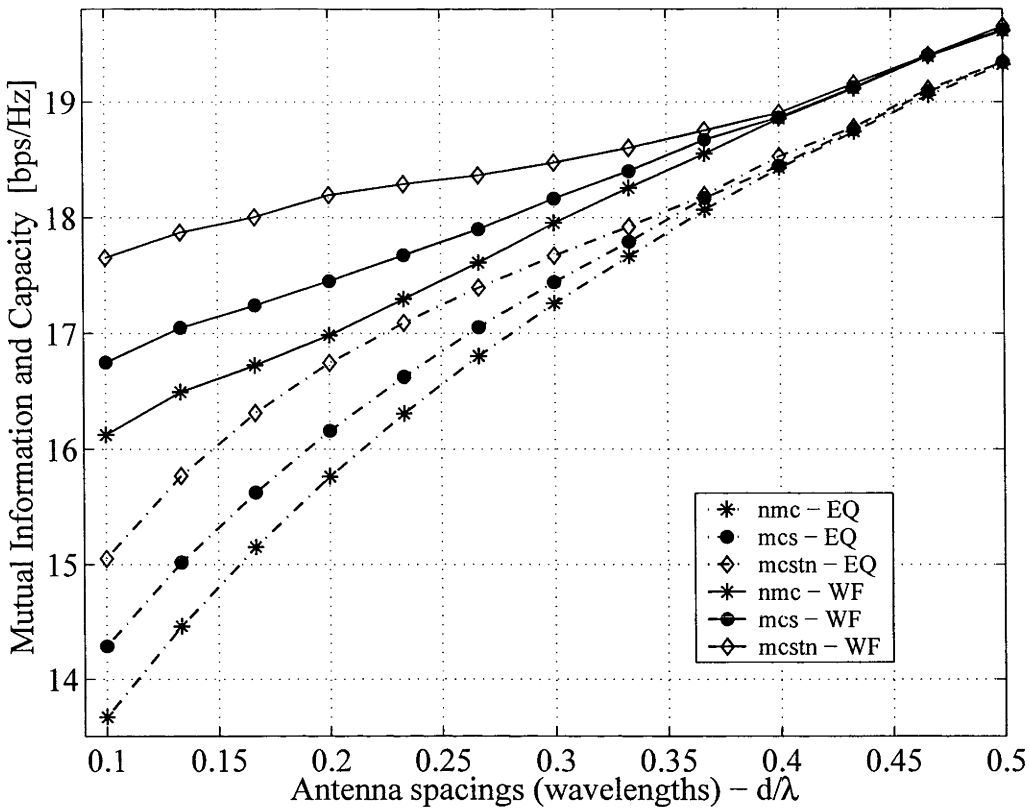

Figure 6.2: Mean (ergodic) capacity with water-filling C_{wf} and equal-power allocation C_{eq} versus antenna element spacings, for 3×3 MIMO Systems

respectively (see Fig. 6.1).

Fig. 6.2 depicts the 3×3 MIMO channel capacity as a function of antenna element spacing. We study the capacity distribution under two power allocation schemes: the ergodic channel capacity when the equal-power allocation scheme is used at the transmitter C_{eq} (6.5) and the ergodic channel capacity with the water-filling power allocation scheme C_{wf} (6.11). We estimate the capacity under three assumptions: 1) the mutual coupling affects both the signal and thermal noise (mcstn), 2) we consider the mutual coupling on the signal only (mcs) and finally, 3) we omit the mutual coupling effect on both the signal and noise (nmc). Simulation results shown in Fig. 6.2 confirm that the mutual coupling decorrelates the signals. This leads to the increase in the transmission rate of the MIMO system with coupled antennas (mcs) [38]

in comparison with the information rate calculated when the mutual coupling effect is not accounted for (nmc). Also, we confirmed that the mean capacity of a MIMO system with water-filling power allocation scheme at the transmitter is higher than the mutual information obtained by applying the equal power allocation scheme in all three cases (nmc, mcs and mcstn).

Fig. 6.2 shows that a higher information rate over the MIMO system can be obtained, if the noise coupling is taken into account. In fact, the calculated information rate is a more realistic estimation as both the signal and noise are accounted for. The conclusion is derived by estimating the capacity distribution for both the equal power and water-filling power allocation schemes.

6.3 Outage MIMO Channel Capacity Analysis

Outage capacity is defined as the data rate that can be guaranteed with high level of certainty. While the outage capacity is defined in Section 5.3.2 for the general case, the outage capacity of the MIMO systems with the closely spaced antennas at the receiver side is analyzed in [30, 79]. The signal and noise correlation are taken into account in order to provide a comprehensive analysis of the channel capacity.

In addition, analysis of the CDF of the channel capacity can be very useful in order to gain better insights into achievable information rate over random wireless channels as was illustrated in [30, 79].

Fig. 6.3 depicts the outage capacity $C_{0.01}$. The outage capacity $C_{0.01}$ means that there is a probability of 0.01 that the capacity is less than what is displayed on the figure. We compute the outage capacity with no mutual coupling (nmc), mutual coupling for the signal only (mcs) and mutual coupling for both the signal and thermal noise (mcstn). One can see that the outage capacity can be underestimated by up to 5% in the 2×2 MIMO system if the noise correlation due to the mutual coupling is not taken into account. The result is valid for antenna spacing up to 0.4λ.

Fig. 6.4 shows the CDF for three cases: (1) when mutual coupling is con-

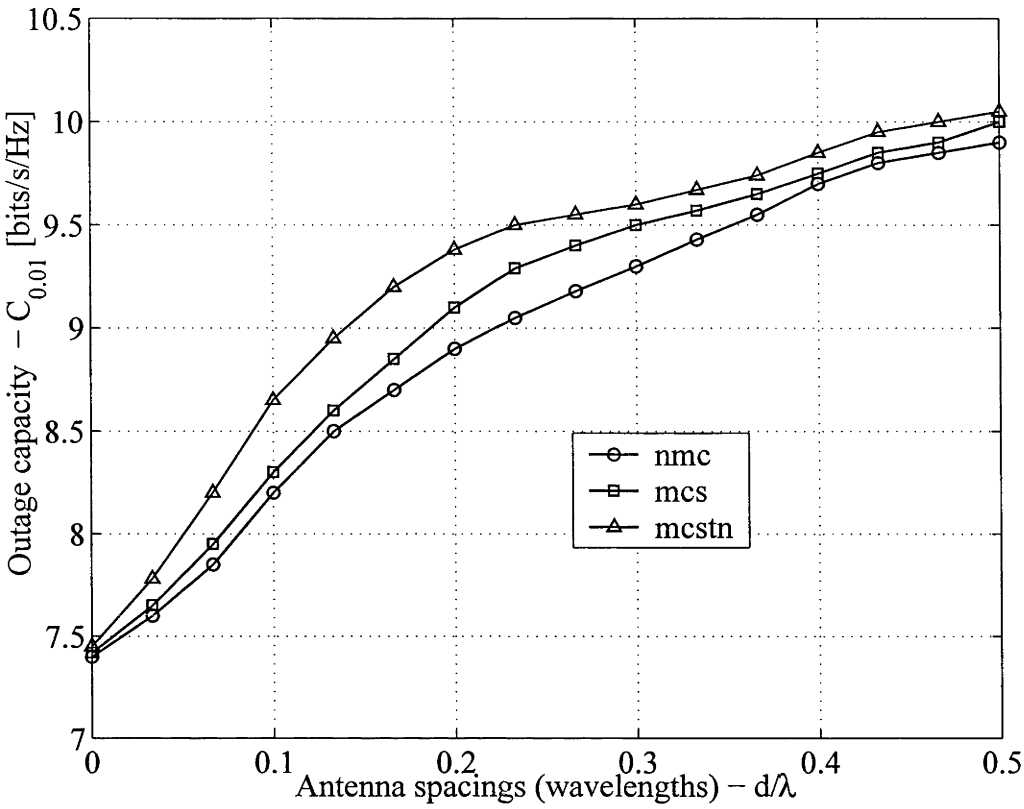

Figure 6.3: Outage MIMO channel capacity versus antenna element spacings for 2 × 2 MIMO Systems

sidered on both the signal and thermal noise (mcstn); (2) mutual coupling is considered on the signal (mcs); (3) mutual coupling is omitted on both the signal and thermal noise (nmc). Further, CDF's is presented for two cases of antenna separation at the receiver side $d = \lambda/6$ and $d = \lambda/3$. Fig. 6.4 illustrates that the guaranteed information rate is actually significantly higher for small antenna spacing $\lambda/6$ when the noise coupling is accounted for. On the other hand, for the larger antenna spacing $\lambda/3$ this difference is negligible.

Fig. 6.5 depicts the 1% outage capacity $C_{0.01}$ in case when the transmitter possesses full knowledge of the channel characteristics. We compute the outage capacity with no mutual coupling (nmc), mutual coupling for the signal only (mcs) and mutual coupling on both the signal and thermal noise (mcstn). From Fig. 6.5, one can conclude that the outage capacity can be

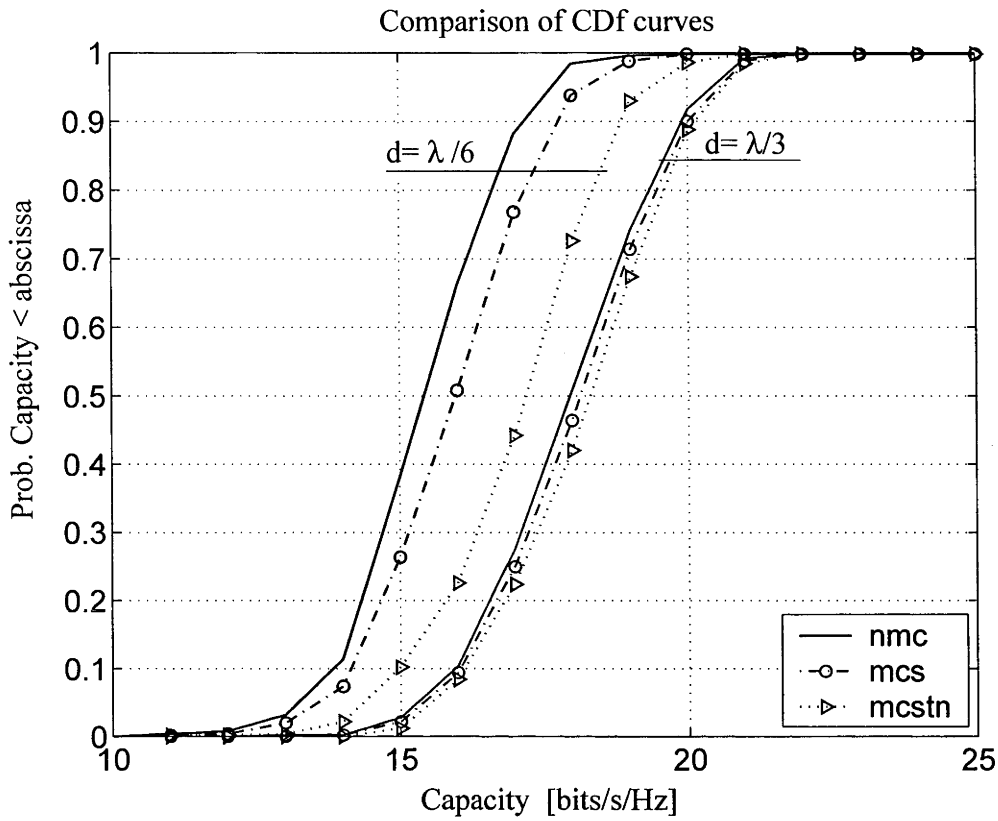

Figure 6.4: Capacity cdf with 2×2 MIMO model for $\lambda/6$ and $\lambda/3$ antenna spacings

underestimated by up to 5.5% in the 3×3 MIMO system if the noise correlation due to the mutual coupling is not taken into account. The result is valid for antenna spacing up to 0.4λ, while for antenna spacing $0.4 \leq d \leq 0.5$ all curves merge into one.

Fig. 6.6 shows the CDF for three cases: with mutual coupling on both the signal and thermal noise, with mutual coupling on the signal and without mutual coupling on either the signal or thermal noise. We present CDF's for two antenna separations at receiver side $d = \lambda/6$ and $d = \lambda/3$ for 2×2 and 3×3 MIMO systems. If one ignores the effect of mutual coupling on both the signal and noise, it can be seen that one significantly underestimates the channel capacity. The channel capacity underestimation increases with decreasing inter-element separation and with a higher order of signal and

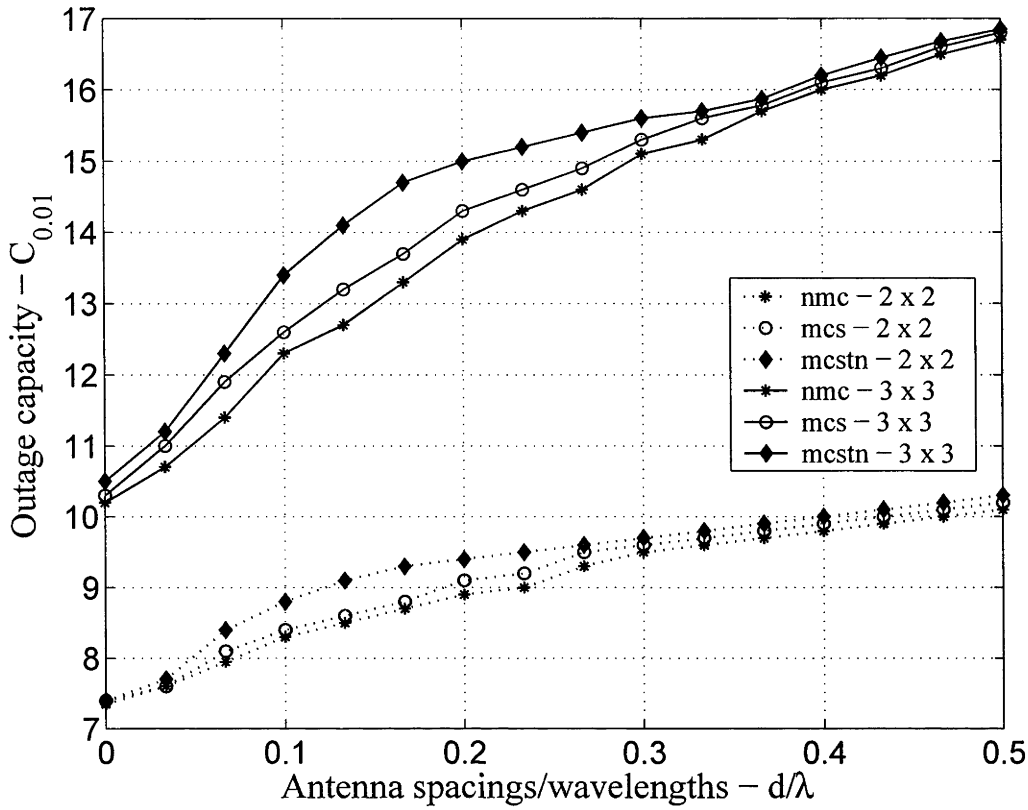

Figure 6.5: $C_{0.01}$- 1% Outage capacity versus antenna element spacings for the 2×2 and 3×3 MIMO Systems

noise correlation.

In addition, Fig. 6.5 and Fig. 6.6 investigate the capacity performance under the correlated noise in the uniform linear antenna array when the number of antennas is increased. One can see from Fig. 6.5 that by increasing the number of the receive antennas in the ULA, the underestimation becomes worse. This is due to the fact that the antennas in the three-antenna ULA are asymmetrically affected by the electromagnetic coupling. Namely, the antenna positioned in the middle is more affected than the other two.

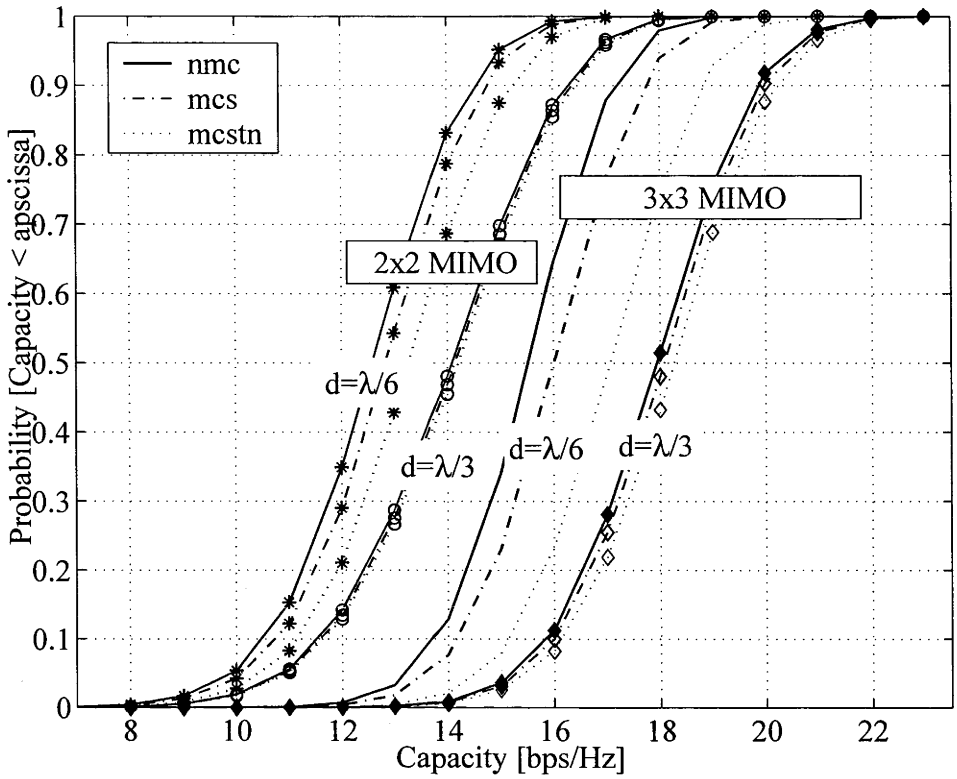

Figure 6.6: Cumulative distribution function (CDF) of channel capacity for the 2×2 and 3×3 MIMO systems for antenna spacing $d = \lambda/6$ and $d = \lambda/3$

6.4 Effective Degrees of Freedom

To get a better insight into subchannel decorrelation (separation) due to mutual coupling effect on thermal noise, we calculate the effective degrees of freedom (EDOF's) of the channel [6]. It represents the number of effective subchannels that can be decomposed into wireless channels.

$$\text{EDOF} = \frac{dC(x)}{d(\log_2 x)}\bigg|_{x=\text{SNR}} \tag{6.12}$$

For the high SNR regime, the EDOF is approximately equal to the channel matrix rank. For low SNR, however, "bad" subchannels carry an insignificant amount of information and, therefore, they are not considered as effective subchannels.

We use simulation to present the variation in the effectively active number

of degree of freedoms when the antenna spacing in the receiving antenna array is varied in the range $[0, \lambda/2]$ [78].

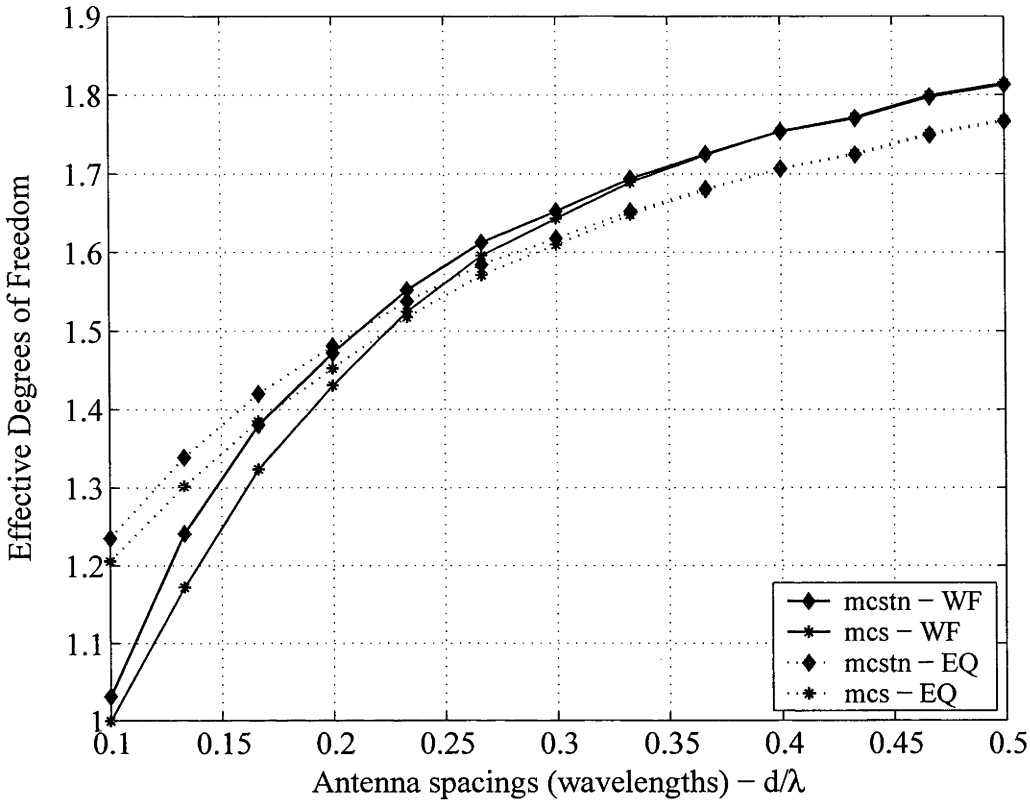

Figure 6.7: Effective degrees of freedom versus antenna element spacings for 2×2 MIMO Systems

Fig. 6.7 verifies that the MIMO system with closely spaced antenna elements exhibits a higher effective degrees of freedom (EDOF), if the noise correlation due to the mutual coupling is taken into account than the case where the noise coupling is neglected. We compute the EDOF with (mcstn) and without (mcs) noise correlation, in both cases the signal is correlated due to the mutual coupling effect. Additionally, from Fig. 6.7, we confirm that the water-filling power allocation scheme performs better, even for antenna spacing $d \rightarrow 0$ when we have only one effective receiving antenna element (overlapping case), where the EDOF converges to 1. In that case the multiple antenna system collapses to a single antenna system, and the effective

number of MIMO-subchannels drops to one.

6.5 Noise Correlation Factor

In this Section, we derive the noise correlation factor and an upper bound of the channel capacity of the MIMO systems with the coupled receiving antennas [81]. The noise factor quantifies the noise correlation contribution to the channel capacity, while the upper bound of channel capacity represents the theoretical limits that might be reached when the noise is correlated.

In order to derive the noise factor, the derivation of the channel capacity of MIMO systems, presented in Section 5.2 will be partially repeated.

The capacity is given in terms of the mutual information rate between $\mathcal{I}(\mathbf{x}, \mathbf{y})$ the channel input vector $\mathbf{x}$ and output vector $\mathbf{y}$ as

$$C = \max_{\mathbf{Q}_x} \mathcal{I}(\mathbf{x}, \mathbf{y}) = \max_{\mathbf{Q}_x} \big(\mathcal{H}(\mathbf{y}) - \mathcal{H}(\mathbf{y}|\mathbf{x})\big) \tag{6.13}$$

where $\mathcal{H}(\mathbf{y})$ and $\mathcal{H}(\mathbf{y}|\mathbf{x})$ are the entropies in $\mathbf{y}$ and $\mathbf{y}|\mathbf{x}$, respectively and $\mathbf{Q}_x$ is the covariance matrix of $\mathbf{x}$.

Components of transmitted signal $\mathbf{x}$ are taken to be statistically independent Gaussian [1]. Thus, entropy rate $\mathcal{H}(\mathbf{x})$ of $\mathbf{x}$ is given by

$$\mathcal{H}(\mathbf{x}) = \log_2((2\pi e)^{\frac{n}{2}}|\mathbf{Q}_x|)$$

From the definition of entropy rate yields that $\mathcal{H}(\mathbf{y}|\mathbf{x}) = h(\mathbf{n})$, where $h(\mathbf{n})$ is the noise entropy. The entropy rate is then

$$\mathcal{H}(\mathbf{n}) = \mathcal{H}(\mathbf{y}|\mathbf{x}) = \log_2\left((2\pi e)^{\frac{n}{2}}|\mathbf{Q}_n|\right) \tag{6.14}$$

and

$$\mathcal{H}(\mathbf{y}) = \log_2((2\pi e)^{\frac{n}{2}}|\mathbf{Q}_y|) \tag{6.15}$$

are decided by covariance matrices $\mathbf{Q}_n$ and $\mathbf{Q}_y = \hat{\mathbf{H}}\mathbf{Q}_x\hat{\mathbf{H}}^\dagger + \mathbf{Q}_n$, respectively. Then (6.13) becomes [16]

$$C = \max_{\mathbf{Q}_x}\left(\log_2\left(\frac{|\mathbf{Q}_n + \hat{\mathbf{H}}\mathbf{Q}_x\hat{\mathbf{H}}^\dagger|}{|\mathbf{Q}_n|}\right)\right) \tag{6.16}$$

where $|\cdot|$ denotes the determinant of a matrix.

We assume equal power allocation scheme at the transmitter, and the covariance matrix of $\mathbf{x}$ is then a diagonal matrix $\mathbf{Q}_x = \frac{P_T}{n_T} \times \mathbf{I}_{n_T}$, where P_T is the total emitted power and $\mathbf{I}_{nT}$ is the identity matrix of order n_T. Additionally, $\mathbf{N}_c$ is the noise correlation matrix and $\hat{\mathbf{H}}$ is the channel matrix.

Now, the ergodic channel capacity may be defined as

$$C = E_{\hat{\mathbf{H}}}\left\{ \log_2 \left(\frac{|\mathbf{N}_c + \frac{P_T}{n_T}\hat{\mathbf{H}}\hat{\mathbf{H}}^\dagger|}{|\mathbf{N}_c|} \right) \right\} \tag{6.17}$$

where the expectation $E_{\mathbf{H}}\{\cdot\}$ is taken with respect to $\hat{\mathbf{H}}$ and $(\cdot)^\dagger$ denotes the conjugate transpose of a matrix.

Expression (6.17) can be simplified as:

$$C = E_{\hat{\mathbf{H}}}\left\{ \log_2 \left| \mathbf{I}_{n_R} + \frac{P_T}{n_T}\mathbf{N}_c^{-1}\hat{\mathbf{H}}\hat{\mathbf{H}}^\dagger \right| \right\} \tag{6.18}$$

Furthermore, by applying the noise coupling matrix defined in Section 2.5, the channel capacity (6.18) becomes

$$C = E_{\hat{\mathbf{H}}}\left\{ \log_2 \left| \mathbf{I}_{n_R} + \frac{\rho}{n_T}\hat{\mathbf{N}}_c^{-1}\hat{\mathbf{H}}\hat{\mathbf{H}}^\dagger \right| \right\} \tag{6.19}$$

where $\rho = \frac{P_T}{N}$.

By applying the eigenvalue decomposition, the expression (6.19) may be rewritten as

$$C = E_{\hat{\mathbf{H}}}\left\{ \log_2 \prod_{i=1}^{r_H} (1 + \frac{\rho}{n_T}\lambda_i\mu_i) \right\} \tag{6.20}$$

$$= E_{\hat{\mathbf{H}}}\left\{ \sum_{i=1}^{r_H} \left(\log_2(1 + \frac{\rho}{n_T}\lambda_i\mu_i) \right) \right\} \tag{6.21}$$

where λ_i is the i^{th} eigenvalue of matrix $\hat{\mathbf{H}}\hat{\mathbf{H}}^\dagger$ and μ_i is the i^{th} eigenvalue of matrix $\hat{\mathbf{N}}_c^{-1}$.

Now, by recalling the inequality (6.6)

$$\mu_i \geq 1 \tag{6.22}$$

which holds true for antenna spacing $d \leq 0.4$

Furthermore, the following Corollary can be defined

Corollary 6.1.

$$\left(1+\frac{\rho}{n_T}\lambda_i\mu_i\right) \leq \left(1+\frac{\rho}{n_T}\lambda_i\right)\mu_i$$

Then, the ergodic channel capacity (6.20) of the MIMO systems with coupled antennas can be bounded

$$C^{corr} = E_{\mathbf{H}_c}\left\{\sum_{i=1}^{n_R}\log_2\left(1+\frac{\rho}{n_T}\lambda_i\mu_i\right)\right\} \tag{6.23}$$

$$\leq E_{\hat{\mathbf{H}}}\left\{\sum_{i=1}^{n_R}\log_2\left((1+\frac{\rho}{n_T}\lambda_i)\mu_i\right)\right\} \tag{6.24}$$

Then, the expression (6.23) can be rewritten as:

$$C^{corr} \leq E_{\hat{\mathbf{H}}}\left\{\sum_{i=1}^{n_R}\log_2\left(1+\frac{\rho}{n_T}\lambda_i\right)\right\} + \sum_{i=1}^{n_R}\log_2(\mu_i) \tag{6.25}$$

Expression (6.25) represents the upper bound on MIMO channel capacity in the presence of correlated noise. The first term in (6.25) is the ergodic channel capacity of MIMO systems with white Gaussian (uncorrelated) noise [1, 2], while the second term is the noise correlation factor ζ_{cn}. Thus, expression (6.25) is equivalent to

$$C^{corr} \leq C^{wgn} + \zeta_{cn} \tag{6.26}$$

where the noise correlation factor ζ_{cn} is defined by

$$\zeta_{cn} = \sum_{i=1}^{n_R}\log_2(\mu_i) \tag{6.27}$$

In the case of the white Gaussian (uncorrelated) noise, the noise correlation factor ζ_{cn} drops to 0, since the noise coupling matrix turns into the identity matrix $\hat{\mathbf{N}}_c = I_{n_R}$. Thus, the inequality (6.25) becomes equality, i.e., the well-know formula for the MIMO channel capacity.

By using (6.26), we isolate the noise correlation factor in the formula for upper bound on MIMO channel capacity in the presence of correlated noise. This enables quantitative investigation of the noise correlation contribution on the channel capacity. The derived noise correlation factor ζ_{cn} represents the measure of the capacity increase due to the noise correlation effect.

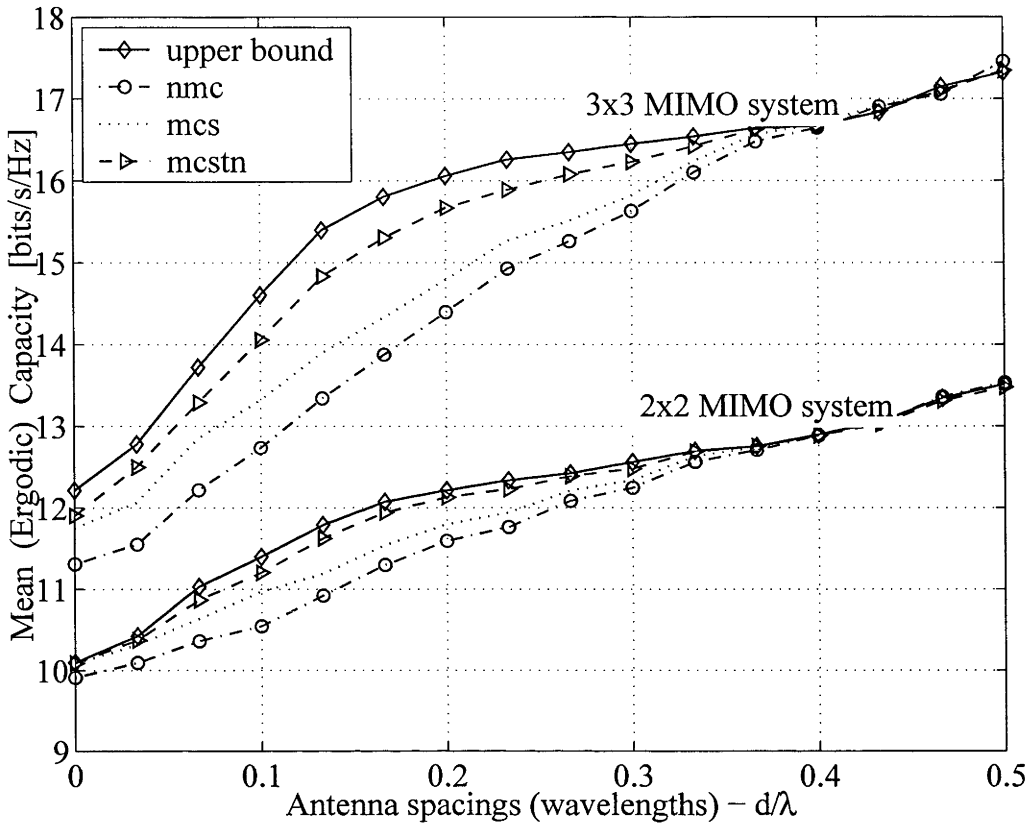

Figure 6.8: Upper bound and mean (ergodic) MIMO channel capacity versus antenna element spacings for 2×2 and 3×3 MIMO Systems

Expression (6.26) shows that we can bound the MIMO channel capacity as the sum of the MIMO channel capacity in the presence of white Gaussian (uncorrelated) noise and the noise correlation factor. This approach may significantly reduce the calculation complexity of MIMO channel capacity in the presence of correlated noise, avoiding the complex matrix multiplications, which are time-consuming for large numbers of antenna elements.

Fig. 6.8 shows the mean (ergodic) channel capacity of 2×2 and 3×3 MIMO systems. The mean channel capacity is calculated under the assumption that mutual coupling affects both the signal and thermal noise (mcstn). For the purpose of comparison, the capacity is computed when mutual coupling is considered on the signal only, and it is denoted by (mcs). Then, the capacity is computed when the multiple antennas are closely spaced but

the signal and noise coupling are neglected from the analysis. It is denoted by (nmc) in Fig. 6.8. Fig. 6.8 also illustrates an upper bound on MIMO channel capacity.

We observe the channel capacity performance when the inter-element spacing at the receiver side is within the range [0, 0.5λ], for which the mutual interactions between antennas are considerable. Further, if the signal correlation due to the scattering is very high, the signal coupling actually reduces the equivalent signal correlation [82], and hence enhances the channel capacity performances. One can observe this effect by comparing the (mcs) and (nmc) curves.

Fig. 6.8 depicts that the upper bound can be used for a rough estimation of MIMO channel capacity. Moreover, the use of the upper bound formula for the rough channel capacity estimation is justified by the fact that the complex matrix multiplications are substituted with simple additions.

Fig. 6.8 also shows how ergodic MIMO channel capacity evolves as the number of the transmit and receive antennas increases. The increase of the achievable information rate of MIMO systems due to the noise correlation rises even more as the number of the transmit and receive antennas increases. Although the conclusion is drawn based on the asymmetrical antenna arrangement in a three-dipole array, it is true in general for any asymmetrical arrangements. In symmetrical arrangement the signal-to-noise ratio per antenna is not affected by the position of the antenna.

6.6 Summary and Contributions

In this chapter, a thorough analysis of the channel capacity performance of MIMO systems with coupled antennas from different aspects is presented. It has been shown that the noise correlation significantly affects the channel capacity performance of the MIMO systems. Furthermore, the MIMO systems with small antenna spacing ($d < 0.4\lambda$) actually performs betters in terms of the channel capacity if the noise and signal correlations due to mutual coupling are taken into account.

Some specific contributions made in this chapter are:

1. We show that the ergodic capacity of MIMO systems is underestimated if the noise correlation due to the mutual coupling effect on thermal noise is neglected. We confirm the result by applying both the equal and water filling transmitted power allocation schemes.

2. We provide numerical investigation of the outage capacity, and confirm that the multi-antenna systems with the small antenna spacing 0.2λ provides almost $4-6\%$ better performance in outage capacity if mutual coupling on the noise and signal are accounted for. We investigate the CDF's for the small antenna spacings of 0.3 λ and 0.6 λ. We use the antenna spacing 0.6 λ as the inter-element distance which provides the uncorrelated noise and signal in the multiple antennas.

3. We apply an eigenvalue decomposition to determine the effect of noise correlation on the channel capacity. The advantage of the eigenvalue decomposition is that it directly provides information about the MIMO channel capacity co-factors: the intensity of each MIMO sub-channel (evaluated by signal-to-noise ratio level) and the effective number of MIMO sub-channels.

4. We provide an analysis of the effective degrees of freedom in the MIMO systems with closely spaced antennas, for both equal and water filling transmitted power allocation schemes, and it confirms the superior behavior of the water filling allocation scheme. Namely, we show that for the WF scheme, the total power is better distributed especially for very small antenna spacing ($d \rightarrow 0$), when the number of effectively subchannels drops to 1.

5. We derive the noise correlation factor which enables a significant reduction in the calculation complexity of MIMO channel capacity in the presence of correlated noise, avoiding complex matrix multiplications, which are time-consuming for large numbers of antenna elements.

6. We present an upper bound on channel capacity of MIMO system in the presence of correlated noise.

In summary, we confirm that in order to provide a thorough analysis of the electromagnetic coupling effects on MIMO channel capacity we need to consider noise correlation in addition to signal correlation due to mutual coupling. We show that the mutual coupling effect which correlates both signal and thermal noise could be a beneficial factor in the achievable information rate over the MIMO systems. The statement is valid for the case when the small inter-element separation ($d < 0.4\lambda$) is enforced due to limited size of hand-held devices.

Chapter 7

Termination dependance

7.1 Introduction

The previous chapters have shown that the noise coupling significantly affects the channel capacity performance of MIMO systems, and that the channel capacity might be considerable underestimated if the noise coupling is omitted from the analysis.

In this chapter the impedance mismatching effect due to the mutual coupling of thermal noise is considered. The design of passive and lossless decoupling and matching networks has been suggested in [83–85] in order to improve the transmitting and receiving capability of antenna arrays [3]. Recently, it has been reported in [39,86] that the choice of termination network might have significant impact on the performance of multi-antenna systems in terms of the transmitted and received signal powers [86] as well as the capacity [39]. Furthermore, an algorithm to come up with an adjusted network matrix that counteracts the mismatching effect on power is presented in [87]. Additionally, the impact of matching network on the antenna correlation, matching efficiency and bandwidth in compact antenna arrays used for wideband wireless systems has been investigated in [88]. However, the noise power was omitted from those discussions, even though the noise power level is closely related to the apparent resistive part of the antenna impedance.

Here, we provide an analysis of the mismatching effect on thermal noise. Further, we estimate the channel capacity of MIMO system when different

matching networks are employed. This analysis represents the most logical extension to our study of noise coupling effect in the multi-antenna system, presented in Chapter 2 and its impact on the channel capacity presented in Chapter 6. The analytical results are corroborated by the simulation results [89]

7.2 Matching Network Specification

There are many coupling networks that can be used to connect the transmission lines to the antenna elements and which can be designed to provide acceptable diversity and capacity performances. A general block diagram of the receive subsystem with an associated matching network is presented in Fig. 7.1, where the equivalent matching load is denoted by $\mathbf{Z}_M$.

In the following, we introduce three most common matching networks found in the literature.

The *characteristic impedance matching network* is considered as it can be often found in practical applications. On the other hand, in order to satisfy the maximal delivered power condition, the *optimal hermitian match*(or multiport conjugate match) with non-zero off-diagonal terms is usually proposed [39, 84, 86, 90]. Although a practical implementation of the multi-port conjugate match for two coupled antennas is proposed in [91], it is still difficult to accomplish the match for larger numbers of antennas. Thus, the *self-impedance matching network* as a satisfactory sub-optimal solution in terms of maximal power delivery is additionally considered.

Although the matching network conditions are explained in the context of the receive mode, they are equally applicable to the transmit mode.

7.2.1 Characteristic Impedance Match

The characteristic impedance match is achieved when antennas are terminated by the characteristic impedances Z_c. In other words, there is no matching network. It can be modeled by removing of the matching network

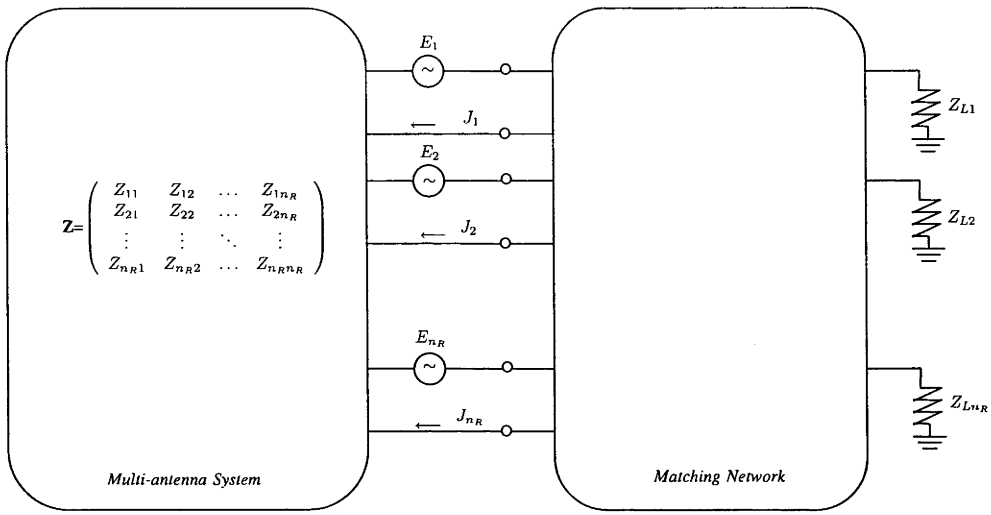

Figure 7.1: Block diagram of the receive subsystem including mutually coupled array, matching network and loads

in Fig. 7.1. In such a way, it can be defined as

$$\mathbf{Z}_M = Z_c \mathbf{I}_{n_R} \tag{7.1}$$

where Z_c is the characteristic impedance.

The degree of mismatch depends on the difference between the antenna self and mutual impedances and the characteristic impedance.

7.2.2 Self-Impedance Match

A relatively simple way to accomplish impedance matching, although sub-optimal, is when the antenna elements are terminated by
self-impedances. Then, the self-impedance match can be defined as

$$\mathbf{Z}_M = \text{diag}(\mathbf{Z}^*) \tag{7.2}$$

where $\mathbf{Z}$ is the mutual impedance matrix, and diag$(\cdot)$ operator retains only the diagonal elements of the matrix operand.

For isolated antennas, the self-impedance match is also known as the complex conjugate match [92]. Theoretically, it facilities maximum power

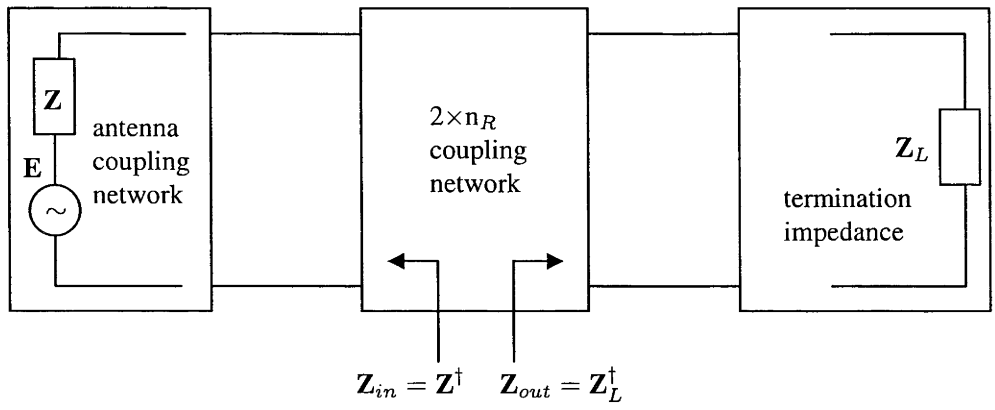

Figure 7.2: Multiport Conjugate Match

transfer to the load when there is no mutual coupling, i.e., the array antennas are infinitely far apart. At finite antenna separation, however, the goodness of the match depends on the behavior of the mutual impedance which is not taken into account.

7.2.3 Multiport Conjugate (MC) Match

The so-called multi-port conjugate [39] (or optimal Hermitian [86]) match takes account of the mutual coupling among the antenna ports. In the modeling of MC match, the interconnections between all ports on the two sides of the network are permitted. Furthermore, the MC match requires one side of the matching network to be *conjugate-matched* to the antennas and the other side to the loads, as illustrated in Fig. 7.2. While the condition for optimum matching of multiple antennas (or MC match) is well known [39, 45, 86], its practical implementation is a subject of current interest [91, 93].

7.3 Noise Power Analysis

For the system shown in Fig. 7.1, the noise current covariance matrix (2.26), originally derived in chapter 2, can be written as

$$\mathbf{N}_j(f) = 2kTB(\mathbf{Z}+\mathbf{Z}_M)^{-1}\big((\mathbf{Z}+\mathbf{Z}_M)+(\mathbf{Z}+\mathbf{Z}_M)^*\big)((\mathbf{Z}+\mathbf{Z}_M)^{-1})^\dagger \quad (7.3)$$

where k is the Boltzmann constant, T is the absolute temperature, B is the bandwidth, $\mathbf{Z}$ is the mutual impedance matrix of the multi-antenna systems and $\mathbf{Z}_M$ is the impedance matrix of the equivalent matching load.

In the following, we show how the different matching network transforms the noise current covariance matrix.

Characteristic Impedance Match

By substituting $\mathbf{Z}_M = \mathbf{Z}_c^*$ and $\mathbf{Z}_c = Z_c\mathbf{I}_{n_R}$ in (7.3), the noise current covariance matrix takes the following form

$$\begin{aligned}\mathbf{N}_j &= \mathbf{j}\mathbf{j}^\dagger \\ &= 2kTB(\mathbf{Z}+\mathbf{Z}_c^*)^{-1}\big((\mathbf{Z}+\mathbf{Z}_c^*)+(\mathbf{Z}+\mathbf{Z}_c^*)^*\big)((\mathbf{Z}+\mathbf{Z}_c^*)^{-1})^\dagger \end{aligned} \quad (7.4)$$

The noise voltage covariance matrix is

$$\begin{aligned}\mathbf{N}_{cov} &= \mathbf{v}\mathbf{v}^\dagger \\ &= 2kTB\big((\mathbf{Z}+\mathbf{Z}_c^*)+(\mathbf{Z}+\mathbf{Z}_c^*)^*\big)((\mathbf{Z}+\mathbf{Z}_c^*)^{-1})^\dagger(\mathbf{Z}+\mathbf{Z}_c^*) \end{aligned} \quad (7.5)$$

Then, the corresponding correlated noise power matrix can be written as

$$\mathbf{N}_c = kTB\mathrm{diag}\Big((\mathbf{Z}_c+\mathbf{Z}_c^*)\big((\mathbf{Z}+\mathbf{Z}_c^*)^{-1}\big((\mathbf{Z}+\mathbf{Z}_c^*)+(\mathbf{Z}+\mathbf{Z}_c^*)^*\big)((\mathbf{Z}+\mathbf{Z}_c^*)^{-1})^\dagger\big)\Big) \quad (7.6)$$

The degree of mismatch depends on the difference between the antenna self and mutual impedances and the characteristics impedance.

Self-Impedance Match

For the self-impedance match, the noise current covariance matrix can be calculated as

$$\begin{aligned}\mathbf{N}_j &= E\{\mathbf{j}\mathbf{j}^\dagger\} \\ &= 2kTB(\mathbf{Z}+\mathrm{diag}(\mathbf{Z}^*))^{-1}\big((\mathbf{Z}+\mathrm{diag}(\mathbf{Z}^*)) \\ &\quad +(\mathbf{Z}+\mathrm{diag}(\mathbf{Z}^*))^*\big)((\mathbf{Z}+\mathrm{diag}(\mathbf{Z}^*))^{-1})^\dagger \end{aligned} \tag{7.7}$$

For widely spaced antennas, the self-impedance match is actually the optimal (complex conjugate) match [92]. The mutual impedance matrix is diagonal, and the condition (7.2) can be simplified as

$$\mathbf{Z}_\mathrm{M} = \mathrm{diag}(\mathbf{Z}^*) = \mathbf{Z}^*$$

In such a way, the noise covariance matrix can be written as

$$\begin{aligned}\mathbf{N}_{cov} &= E\{\mathbf{v}\mathbf{v}^\dagger\} \\ &= 2kTB\big((\mathbf{Z}+\mathbf{Z}^*)+(\mathbf{Z}+\mathbf{Z}^*)^*\big)((\mathbf{Z}+\mathbf{Z}^*)^{-1})^\dagger(\mathbf{Z}+\mathbf{Z}^*) \\ &= 2kTB(\mathbf{Z}+\mathbf{Z}^*) \\ &= 4kTB\mathfrak{Re}\{\mathbf{Z}\} \end{aligned} \tag{7.8}$$

The noise power matrix becomes

$$\begin{aligned}\mathbf{N}_c &= kTB\mathrm{diag}\Big((\mathbf{Z}+\mathbf{Z}^*)\big((\mathbf{Z}+\mathbf{Z}^*)^{-1}((\mathbf{Z}+\mathbf{Z}^*)+(\mathbf{Z}+\mathbf{Z}^*)^*)((\mathbf{Z}+\mathbf{Z}^*)^{-1})^\dagger\big)\Big) \\ &= 2kTB\mathbf{I}_{n_R} \end{aligned} \tag{7.9}$$

The total multi-port thermal noise power is then

$$P_\mathrm{n} = kTB\mathrm{Tr}(\mathbf{I}_{n_R}) = 4n_RkTB \tag{7.10}$$

The total multi-port thermal noise power becomes the sum of n_R uncorrelated noise powers which represents the maximum noise power.

Multiport Conjugate (MC) Match

In the MC conjugate match, one side of the matching network is *conjugate-matched* to the antenna and the other side is *conjugate-matched* to the load.

Ideally, the matching network is formed with passive, reactive elements so that it is lossless and reciprocal.

Further, it has been shown in [90] that the eigenvalues of the characteristic noise matrix are invariant to a lossless transformation if the number of terminal pairs is preserved. Then, for the lossless n_R-port network, the noise current covariance matrix becomes

$$\mathbf{N}_j = 2kTB(\mathbf{Z}+\mathbf{Z}^*)^{-1}\big((\mathbf{Z}+\mathbf{Z}^*)+(\mathbf{Z}+\mathbf{Z}^*)^*\big)((\mathbf{Z}+\mathbf{Z}^*)^{-1})^\dagger \tag{7.11}$$

while it has been taken that antennas are looking at impedance $\mathbf{Z}_M = \mathbf{Z}^*$.

Then, the noise covariance matrix at the load becomes

$$\begin{aligned}\mathbf{N}_{cov} &= E\{\mathbf{v}\mathbf{v}^\dagger\}\\ &= 2kTB\big((\mathbf{Z}+\mathbf{Z}^*)+(\mathbf{Z}+\mathbf{Z}^*)^*\big)((\mathbf{Z}+\mathbf{Z}^*)^{-1})^\dagger(\mathbf{Z}+\mathbf{Z}^*)\\ &= 2kTB(\mathbf{Z}+\mathbf{Z}^*)\\ &= 4kTB\mathfrak{Re}\{\mathbf{Z}\}\end{aligned} \tag{7.12}$$

The noise power matrix can be written as

$$\begin{aligned}\mathbf{N}_c &= 2kTB\mathrm{diag}\Big((\mathbf{Z}+\mathbf{Z}^*)\big((\mathbf{Z}+\mathbf{Z}^*)^{-1}\big((\mathbf{Z}+\mathbf{Z}^*)+(\mathbf{Z}+\mathbf{Z}^*)^*\big)((\mathbf{Z}+\mathbf{Z}^*)^{-1})^\dagger\big)\Big)\\ &= 4kTB\mathbf{I}_{n_R}\end{aligned} \tag{7.13}$$

The total receive thermal noise power is

$$\begin{aligned}P_n &= \mathrm{Tr}\Big(kTB(\mathbf{Z}+\mathbf{Z}^*)^{-1}\big((\mathbf{Z}+\mathbf{Z}^*)+(\mathbf{Z}+\mathbf{Z}^*)^*\big)((\mathbf{Z}+\mathbf{Z}^*)^{-1})^\dagger\Big)\\ &= 2kTB\mathrm{Tr}(\mathbf{I}_{n_R})\\ &= 4n_RkTB\end{aligned} \tag{7.14}$$

where Tr(.) is the trace operator.

Thus, the multi-port conjugate match transforms the coupled thermal noise into uncorrelated noise.

The following remarks can be made:

1. The presented analysis of the mismatching effect on the noise power in the multi-antenna system shows that mismatching affect thermal noise power in addition to the signal power;

2. Further, the signal and noise powers are affected by the mismatching in the coupled antenna array. Hence, it is suggested that matching condition should be based on the SNR observation instead on the signal power only;

3. Finally, one can conclude that the multi-port conjugate match acts not only as optimal in terms of the minimal reflections and maximal power transfer, but also performs as the whitening-filter for coupled thermal noise.

7.4 Capacity Analysis

In this section, the channel capacity performance of MIMO systems with different matching networks are presented. The aim is to indicate on the possible error introduced when the mismatching effect is not accounted for in the thermal noise power in addition to the signal power in the coupled antenna system.

Here, we provide an analysis of the MIMO channel capacity with closely spaced antenna elements when transmitter does not have any knowledge about the channel characteristics (CSI is not available at transmitter). Then, the most reasonable strategy is to equally distribute the transmit power to all n_T transmit antenna elements. Transmitted signals are taken to be independent and their covariance matrix is

$$\mathbf{Q} = \frac{P_T}{n_T}\mathbf{I}_{n_T} \tag{7.15}$$

where P_T is the total radiated power and $\mathbf{I}_{n_T}$ is the identity matrix of order n_T.

The channel capacity of MIMO system is given by

$$C = E_{\hat{\mathbf{H}}}\left\{ \log_2 \left[\det\left(\mathbf{I}_{n_R} + \mathbf{N}_c^{-1}\hat{\mathbf{H}}\mathbf{Q}\hat{\mathbf{H}}^{\dagger}\right)\right]\right\} \tag{7.16}$$

where the channel matrix $\hat{\mathbf{H}}$, used in this analysis, is defined in Section 5.4, and $E_{\hat{\mathbf{H}}}\{\cdot\}$ is the expectation over the random channel realizations. Further, $\mathbf{N}_c$ is the noise correlation matrix as defined in previous section for different matching network.

By applying the noise coupling matrix (2.32) as defined in Chapter 2, the capacity can be rewritten as

$$C = E_{\mathbf{H}}\left\{ \log_2 \left[\det \left(\mathbf{I}_{n_R} + \frac{\rho}{n_T} \hat{\mathbf{N}}_c^{-1} \hat{\mathbf{H}} \hat{\mathbf{H}}^{\dagger} \right) \right] \right\} \tag{7.17}$$

where ρ/n_T is the average received (SNR) signal-to-noise ratio of one sub-channel and ρ is defined by $\rho = P_T/P_n$.

If an eigenvalue decomposition is carried out on the matrix $\hat{\mathbf{H}}\hat{\mathbf{H}}^{\dagger}$ and noise coupling matrix $\hat{\mathbf{N}}_c$, the channel capacity can be rewritten in the following form

$$\begin{aligned} C &= E_{\hat{\mathbf{H}}}\left\{ \log_2 \prod_{i=1}^{r_{\mathbf{H}}} \left(1 + \frac{\rho}{n_T} \frac{\lambda_i}{\nu_i} \right) \right\} \\ &= E_{\hat{\mathbf{H}}}\left\{ \sum_{i=1}^{r_{\mathbf{H}}} \left(\log_2 \left(1 + \frac{\rho}{n_T} \frac{\lambda_i}{\nu_i} \right) \right) \right\} \end{aligned} \tag{7.18}$$

where λ_i is the i^{th} eigenvalue of matrix $\hat{\mathbf{H}}\hat{\mathbf{H}}^{\dagger}$, ν_i is the i^{th} eigenvalue of matrix $\hat{\mathbf{N}}_c$ and

$$r_{\mathbf{H}} = \operatorname{rank}(\hat{\mathbf{N}}_c^{-1}\hat{\mathbf{H}}\hat{\mathbf{H}}^{\dagger}) \leq \min(n_{\mathrm{T}}, n_{\mathrm{R}}). \tag{7.19}$$

The eigenvalues ν_i of the noise coupling matrix $\hat{\mathbf{N}}_c$ are defined by inequality (6.6) in Chapter 6

$$\nu_i \leq 1 \;\Rightarrow\; \frac{1}{\nu_i} \geq 1 \tag{7.20}$$

where there is strict inequality for antenna spacings lower than 0.4λ as illustrated in Fig. 2.4.

Based on (7.18) and (7.20), one can conclude that as the eigenvalues of channel matrix represent virtual channel gains, the eigenvalues of noise correlation matrix may be considered as an additional increment to the channel gains. We show that this additional increment of channel gain is the consequence of the noise coupling. In the case of the ideally matched lossless termination network this increment drops to zero.

Care should be taken about the potentially beneficial effect of mismatching on thermal noise, and in such a way on the capacity performance. The outcome is a result of the combined mismatching effect on both signal and thermal noise. In such a way, the mismatching conditions should be defined based on the SNR observation rather than on the signal power only.

The result is especially relevant for wireless systems operating in the low SNR regime such as mobile handheld devices. Furthermore, it can be exploited to design RF front-end part of mobile handheld devices with lower transmit output power while preserving the same information rate performance.

7.4.1 Simulation Results

To confirm results of the presented analytical analysis, we use simulation models consisting of ULA's with two and three half-wave dipoles. The mutual impedance matrices are calculated by using the $SONNET^{®}$ [32] software. The transmitting antennas are taken to be widely spaced in most cases, if not specified otherwise. The receiving multi-antenna system with interelement distance d is used, where d is varied within the range $[0, \lambda]$. The outdoor channel is simulated by using the MIMO outdoor channel model given in Section 5.4.2. The channel capacity is calculated over 10000 channel realizations.

Fig. 7.3 depicts the thermal noise power of a coupled antenna normalized by thermal noise power of an isolated antenna. Here, coupled thermal noise power is calculated for two cases: antennas are terminated by the characteristic impedance match (Ch. imped.) and the self-impedance match (Self-imped.). The decrease of the coupled noise power is closely related to the impedance mismatching effect on thermal noise. Namely, due to the mismatching effect the resistive part of impedance is transformed, and hence the dissipated noise power is affected. In the case of uniform linear dipole array, we have found that the actual coupled noise power is lower than that of the isolated antennas.

Intuitively, the decrease in the noise power can be explained by using the antenna radiation pattern. Namely, it has been found in [41, 72] that the mutual coupling distorts the antenna radiation pattern. Since the receiver noise is partly generated from its own load resistance and partially from the environment (isotropic noise), the distortion of the antenna radiation pattern will affect the thermal noise power in addition to the reported distortion of signal power. Thus, the radiation pattern degradation and the fact that the

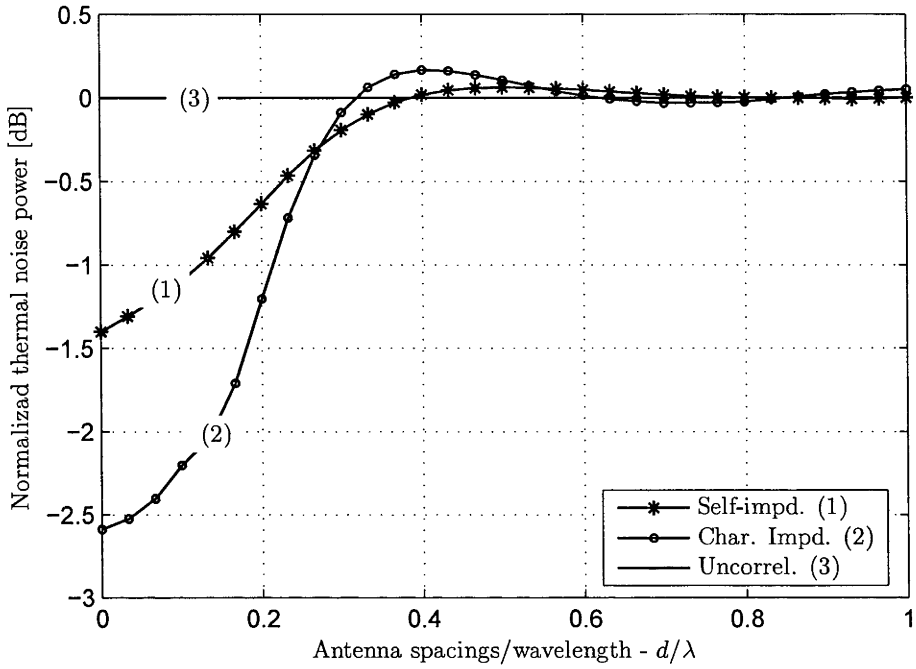

Figure 7.3: Mutual coupling effect on thermal noise; Thermal noise power of coupled antenna element in two-antenna array with: (1) characteristic impedance match and (2) self-impedance match normalized by the uncorrelated thermal noise power (3)

neighboring antenna acting as the electromagnetic reflector cause the noise power decrement of the coupled antenna for the antenna spacing $d < 0.4\lambda$.

Our simulation results show that for antenna spacing $d < 0.4\lambda$, the effect of antenna mismatch due to mutual coupling decreases thermal noise in the case of the non-optimal match (characteristic and self-impedance). Beyond this distance (0.4λ) and up to $d = 1\lambda$, one can observe that the coupled thermal noise power slightly oscillates around the uncorrelated thermal noise level. For the $d > 1\lambda$ antenna spacing, coupled thermal noise power and thermal noise power level of isolated antennas merges into one curve as the effect of mutual coupling diminishes. This confirms our analytical results that the thermal noise power is affected by the mismatching impedance effect.

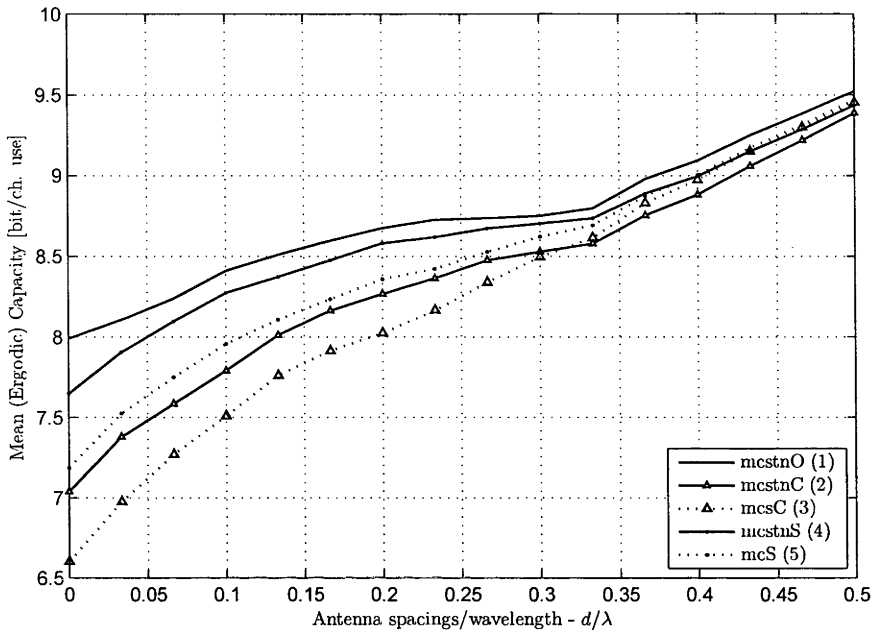

Figure 7.4: Mean (ergodic) capacity versus antenna spacings for 2×2 MIMO system

Furthermore, we confirm that for the optimal MC lossless matching network, the noise appears uncorrelated at the output of the coupled antennas.

Another interesting conclusion that could be drawn from the result in Fig. 7.3 is that within the antenna spacing range $d < 0.4\lambda$, the coupled thermal noise power level is always below the uncorrelated noise power. Thus, the MC match does not only maximize delivered signal power, but it acts as decoupling network for thermal noise as well [90]. Although the power maximization and reflection minimization properties of multi-port conjugate match is well known for signals, here we confirm its whitening property on the thermal noise.

Fig. 7.4 depicts the mean channel capacity of a 2×2 MIMO system for different levels of mutual coupling (or antenna spacings). We provide channel capacity estimation for closely spaced receive antennas. We neglect the transmit signal spatial correlation presupposing wide inter-element spacing

at the transmitter side. In order to get perceptibly clearer representation of our analysis, we provide the simulation results for antenna spacings up to 0.5λ, as the thermal noise mutual coupling is considerable for antenna spacing up to 0.4λ.

Further, in Fig. 7.4, an investigation of the noise correlation effect on channel capacity has been done for the multi-antennas terminated by: the MC match, the self-impedance and the characteristic impedance matching network. We compare the case where mutual coupling is accounted for in both the signal and thermal noise against the case when only the signal coupling is taken into account.

Further, an estimate of the mean channel capacity is calculated for: (1) (mcstnO) the receive antennas systems is simulated with the MC match; the receive antenna system is terminated by the self-impedance match and antenna systems is simulated with mutual coupling on the signal and thermal noise (2) (mcstnS) and only on the signal (3) (mcsS). Then, the multi-antenna system terminated by the characteristic-impedance match and antenna system is simulated with mutual coupling on both the signal and thermal noise (4) (mcstnC) and on the signal only (5) (mcC).

From Fig. 7.4, one can conclude that MC match prevails as the optimal match for the combined mutual coupling effect on signal and thermal noise. For antenna spacing below 0.4λ mutual coupling on thermal noise provides an obvious capacity benefit for both self- and characteristic impedance match. While the self- and characteristic impedance match yields a modest capacity degradation in comparison with the optimal match, the results in Fig. 7.4 show that the actual degradation is lower than that in [39] when the thermal noise mutual coupling was neglected. Fig. 7.5 demonstrates the combined effect of mutual coupling at transmitter and receiver side. The transmit and receive antenna spacing are equal and the mean capacity is estimated for the self-impedance match (TxRxS) and optimal match (TxRxO). Fig. 7.5 shows that the optimal match (TxRxO) performs better than the sub-optimal match even for the case when receive and transmit antennas are coupled and both the signal and thermal noise mutual coupling are considered. Furthermore, it was confirmed that the transmit mutual coupling (TxRxS) degrades the capacity performance comparing with the case with no con-

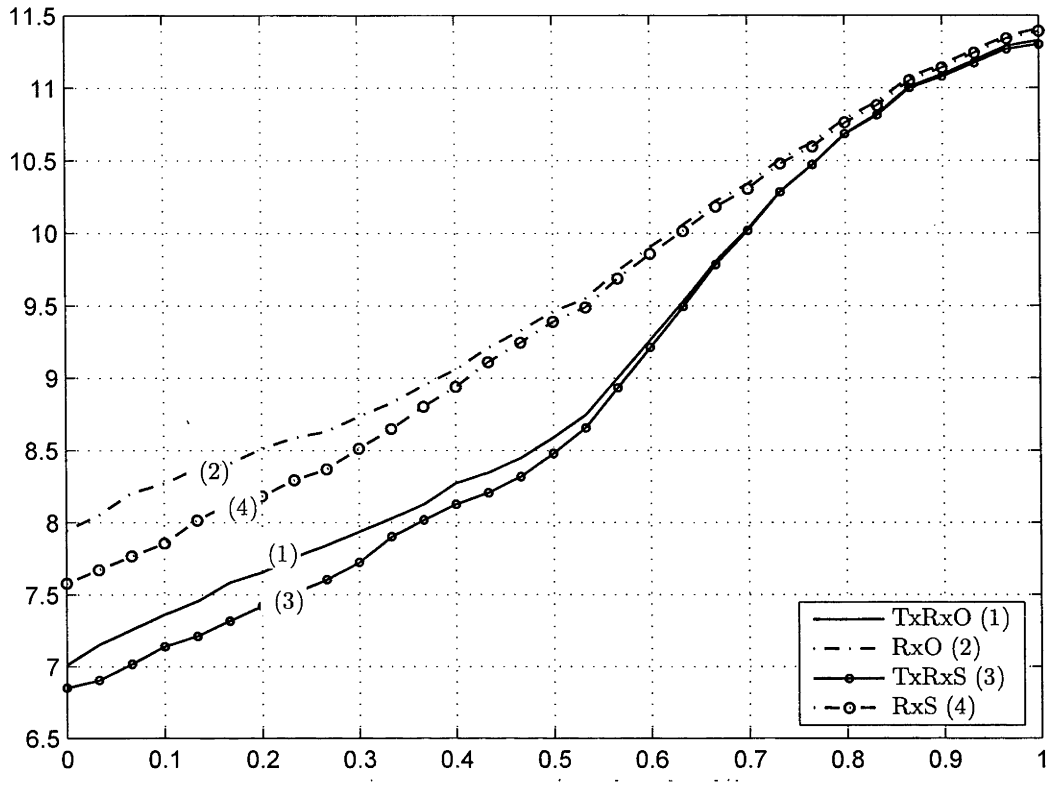

Figure 7.5: Mean (ergodic) capacity versus transmit and receive antenna spacing for different antenna coupling assumption

straint on the emitted power (RxS). Therefore, Fig. 7.5 represents a more realistic estimation of the channel capacity of MIMO systems with small antenna spacings as we present the case when small antenna spacings is only enforced at the receiver and compare it with the case when both the receive and transmit multiple antennas are closely spaced.

7.5 Summary and Contributions

In this chapter, we provide an analysis of the effect of mutual coupling on the channel capacity of MIMO systems with different matching networks. The results indicate that an additional factor — the spatial electromagnetic noise correlation — must be included into the analysis in order to correctly evaluate the effect of the matching networks for the particular multi-antenna

systems.

Some specific contributions made in this chapter are:

1. We provide an analysis of the termination-dependant noise covariance matrix for three most common matching networks. We show that the impedance mismatching effect does affect the thermal noise in addition to the previously reported effect on the signal.

2. We show that the MC match acts not only as the optimal match in terms of maximal delivered signal power, but also as the whitening filter for the coupled thermal noise.

3. We show that an accurate matching network design should be based on the signal-to-noise ratio analysis rather than on the signal power analysis. This is especially important for wireless systems operating in the low SNR regime, such as mobile handheld devices.

4. We confirm that the transmit coupling degrades the capacity performance comparing with the case with no constraint on the emitted power.

In summary, we show that an adequate consideration of the noise coupling effect could improve the design of the matching networks. Further, we show that the multiple antennas with inter-element separations less than 0.4λ performs better in terms of capacity, if mutual coupling is accounted for in both the signal and noise. This result indicates the possibility to conserve the transmit output power, which is an important issue for battery operated devices.

Chapter 8

Conclusions and Future work

This chapter states the conclusions drawn from Part II of the thesis. Following this, some possible future directions are proposed.

8.1 Conclusions

This part of thesis has been concerned with the potential practical and theoretical limitations on the achievable information rate over the MIMO systems with closely spaced multiple antennas. As it has been discussed, small inter-element separation between the multiple antennas results in a high level of correlation. In particular, the correlation due to the mutual coupling is the main focus of this thesis.

By introducing the previously ignored noise coupling effect into the channel capacity analysis, we more accurately estimated the channel capacity. In particular, we outlined the following:

- In order to provide a more comprehensive insight into the effect of noise coupling on the MIMO channel capacity, we analyzed the ergodic channel capacity under different assumptions based on the availability of the channel state information at the transmitter. In particular, we analyzed the ergodic channel capacity with equal power allocation and water-filling power allocation schemes of the transmitted power. We showed that the ergodic capacity of MIMO systems is underestimated if the noise correlation due to the mutual coupling on the thermal noise is

neglected. Furthermore, we confirmed that the water-filling allocation scheme is superior to the equal-power allocation scheme, and this superiority is greater when multiple antennas with non-uniformly spaced antennas are used at the receiver. In that case, the noise coupling affects the signal-to-noise ratio of individual antennas differantly, and the water-filling scheme better allocates the total transmitted power.

- To better understand the characteristics of realistic information transmission over fading channels, it is important to analyze the distribution of mutual information over realizations of fading. In such a way, outage capacity provides information about the variance of the mutual information, the smaller the variance, the lower the probability of outage error when transmitting at the fixed rate. Therefore, we provided numerical investigation of the outage capacity, and showed that the multi-antenna systems with small antenna spacing up to 0.2λ provides almost $4-6\%$ better performance in outage capacity if the mutual coupling on the noise is accounted for. In addition, we confirmed the result by investigating the CDF's for small antenna spacing of 0.3 λ and 0.6 λ, where the large spacing closely approximates the case of uncorrelated signal and noise.

- By introducing the concept of the effective degrees of freedom, we attempted to isolate and study the effect of correlation in the MIMO systems. Especially, we emphasized the noise correlation effect on the channel capacity. We showed how the number of effective degrees of freedom decreases with the reduction of the inter-element separation. Further, we showed that for very small antenna spacing ($d \rightarrow 0$) when the number of effective subchannels drops to 1 the water-filling allocation scheme is superior as it reconfigures to the optimal situation of allocating the total power to only one receiving antenna.

- We isolated the contribution from the noise correlation in the channel capacity formula by deriving the noise correlation factor. It enables a significant reduction in the calculation complexity of MIMO channel capacity in the presence of correlated noise by avoiding complex matrix

multiplications, which are time-consuming for large numbers of antenna elements.

- We derived an upper bound on the channel capacity of MIMO system in the presence of correlated noise. This is a significant result as it enables the channel capacity estimation of the multiple antennas with closely spaced antennas which avoids complex matrix computations.
- In order to accurately calculate the received correlated noise power, it is essential to take account of the antenna mismatching impedance effect in the analysis. Therefore, we provided the analysis of the noise covariance matrix for three most common antenna terminated matching networks. We presented the impact of different termination matching networks on the noise covariance matrix, and the corresponding received thermal noise power. We showed that the MC match acts not only as the optimal match in terms of maximal delivered signal power, but also as the whitening filter for the coupled thermal noise.
- Finally, the results of our termination network analysis implied that an accurate matching network design should be based on the SNR analysis rather than on the signal power analysis. This is especially important for wireless systems operating in the low SNR regime, such as mobile handheld devices.

8.2 Future Directions of Research

Although this thesis has given valuable insights into the function of the multi-antenna systems with small antenna spacing, and the achievable channel capacity of such systems, there are many more research directions one could follow to further broaden the understanding and implementation of such systems. Outlined below is a small subset of a much larger group of possible research projects pertinent to this thesis.

Channel modeling The channel model used in this thesis is based on the separable correlation model. However we are fully aware of its limitations especially for indoor environments. To fully understand and

exploit all properties that a wireless channel offers, there is a need to further extend the modeling of the scattering environment. In particular, a significant amount of work is required to fully develop a channel model which includes the spatial correlation due to the mutual coupling and the scattering effect from scatterers in the far-field as well as the near-field region of the antenna.

In addition, channel modeling should be extended to the millimeter-wave frequency band (30 GHz-300 GHz) as new wireless applications are appearing in those frequency bands. Although the channel model for the 60 GHz frequency band is well on the way, a significant amount of work is still needed in this area. Especially, for the case when the signal wavelength approaches the size of a rain drop, the scattering modeling and spatial correlation should be reconsidered. Furthermore, the spatial noise correlation due to scattering, particulary in the indoor environment, should be reviewed.

Signal processing theory This thesis has focused on the front-end part of receiver, an obvious extension is to include the digital signal processing (DSP) unit in our analysis. In such a way, the behavior of a minimum mean squared error (MMSE) receiver should be examined in the presence of the coupled noise. Different adaptive algorithm schemes will be exploited in order to propose an adequate solution for the DSP unit.

In this thesis, we examined the multi-antenna systems which are used as spatial multiplexers. A logical extension of our analysis will be to investigate the noise coupling effect on the beamforming performance of adaptive antenna arrays. The aim of such analysis is to propose an adaptive scheme that maximizes the information rate over the wireless links with adaptive antenna arrays in the presence of correlated noise.

In addition, recent studies have indicated that a new degree of freedom might be introduced by exploiting polarization diversity. Following that, the mobile hand-held devices with orthogonally polarized antennas closely spaced to each other might be a possible solution in order to achieve a high information data rate. The channel capacity of such systems should be analyzed, and, based on that, the optimal antenna

arrangement for the mobile hand-held devices might be proposed.

Implementation The practical implementation of MIMO systems has been the subject of several standardization efforts, such as the high-speed packet data mode of third-generation cellular systems IMT-2000, as well as the high-throughput wireless Local Area Networks (LANs) (IEEE 802.11n). However, further improvements in the implementation of MIMO systems is possible only when all effects arising from the application of multiple antennas are theoretically accounted for, and practically verified. In such a way, the experimental validation of the results presented in this thesis might be the next step.

Bibliography

[1] G. J. Foschini, "On limits of wireless communication in fading environment when using multiple antennas," *Wireless Personal Communication*, no. 6, pp. 311–335, Mar. 1998.

[2] E. Telatar, "Capacity of multi-antenna gaussian channels," *Eur. Trans. Telecommun*, vol. 10, no. 6, pp. 585–595, Nov/Dec. 1999.

[3] S. Stein, "On cross-coupling in multiple-beam antennas," *IEEE Trans. Antennas Propag.*, vol. AP-10, no. 5, pp. 548–557, 1962.

[4] C. A. Balanish, *Antenna Theory: Analysis and Design.* New York: John Wiley and Sons, Inc., 1997.

[5] W. L. Stutzman and G. L. Thiele, *Antenna Theory and Design*, 2nd ed. New York: John Wiley and Sons INC, 1998.

[6] D. Shiu, G. Foschini, M. Gans, and J. Kahn, "Fading correlation and its effect on the capacity of multi-element antenna system," *IEEE Trans. on Communications*, vol. 48, pp. 502–513, Mar. 2000.

[7] L. Schumacher, K. I. Pedersen, and P. E. Mogensen, "From antenna spacings to theoretical capacities - guidelines for simulating MIMO systems," in *13th IEEE International Symposium on Personal Indoor Mobile and Radio Communications, Proceedings PIMRC*, vol. 2, Lisbon, Portugal, Sep. 2002, pp. 587 – 592.

[8] P. D. Teal, T. D. Abhayapala, and R. A. Kennedy, "Spatial correlation for genaral distibution of scatterers," *IEEE Signal Processing Letters*, vol. 9, no. 10, pp. 305–308, Oct. 2002.

[9] Y. Yamada, K. Kogoshima, and K. Tsenekawa, "Diversity antennas for base and mobile station in land mobile communication systems," *IEICE Trans.*, vol. E 74, no. 10, Oct. 1991.

[10] J. Richmond, "Coupled linear antennas with skew orientations," *IEEE Trans. on Antennas and Propagations*, vol. 18, no. 5, pp. 694–696, 1970.

[11] T. Sventenson and M. Vibergs, "Mutual coupling in antenna array: effects and cures," in *Proc. PCC Workshop*, Stocholm, Sweden, Nov 1998, pp. 99–103.

[12] H. E. King, "Mutual impednace of unequal length antennas in echelon," *IEEE Trans. on Antennas and Propagation*, vol. 5, pp. 306–313, July. 1951.

[13] R. Harrington, *Field Computation by Moment Method.* New York: MacMillan, 1968.

[14] J. C. Rautio, "Planar electromagnetic analysis," *IEEE Microwave Magazine*, vol. 4, pp. 35–41, 2003.

[15] S. Verdu, *Multi-user detection.* Cambrige University Press, 1998.

[16] P. B. Rapajic, "Information capacity of the space division multiple access mobile communication system," *Wireless Personal Communication*, vol. 11, pp. 131–159, 1999.

[17] A. F. Molish, *Wireless Communications.* West Sussex, England, UK: John Wiley and Sons Ltd., 2005.

[18] J. Lawson and G. H. Uhlenback, *Threshold signals.* New York: Massachusetts Institute of Technology Radiation Laboratory Series, McGraw-Hill, 1950, vol. 24.

[19] J. Bernamont, "Fluctuations de potentiel auz bornes d'un conducteur metallique de faible volume parcouru par un courant," *Ann. phys.*, vol. 71, no. 9, 1937.

[20] C. J. Bekker and G. Heller, "On the brownian motion in electrical resistances," *Physica*, vol. 6, no. 262, 1939.

[21] E. Spenke, "Wiss. veroffentl," *Siemens-Werken*, vol. 18, no. 54, 1939.

[22] H. Nyquist, "Thermal agitation of electric charge in conductors," *Phys. Rev.*, vol. 32, pp. 110–113, 1928.

[23] F. C. Williams, "Thermal fluctuations in complex networks," *Journal of IEE*, vol. 81, p. 751, 1937.

[24] D. Middleton, *Introduction to Statistical Communication Theory.* Los Alotos, California: Peninsula Publishinga, 1987.

[25] F. C. Williams, "Fluctuation noise in vacuum tubes which are not temperature limited," *Journal of IEE*, vol. 78, p. 326, 1936.

[26] S. M. Rytov, Y. A. Krastov, and V. Tatarskii, *Principles of Statistical Radiophysics 3: Elements of Random Fields.* Berlin, Heidelberg, New York: Springer, 1987.

[27] R. Q. Twiss, "Nyquist's and thevenin's generalized for nonreciprocal linear networks," *J. Applied Phys.*, vol. 26, pp. 559–602, May 1955.

[28] G. E. Valley and H. Wallman, *Vacuum Tube Amplifier, Volume 18 of MIT Radiation Laboratory Series.* New York: McGraw-Hill, 1948.

[29] S. Krusevac, P. B. Rapajic, and R. A. Kennedy, "Mutual coupling effect on thermal noise in multi-element antenna systems," *Progress in Electromagnetics Research (PIER)*, vol. 59, pp. 325–333, 2006.

[30] S. Krusevac, P. B. Rapajic, and R. A. Kennedy, "Channel capacity estimation for MIMO systems with correlated noise," in *Proc. 2005 IEEE Global Telecommunications Conference, IEEE GLOBECOM 2005*, St. Louis, MO, USA, Dec. 2005, pp. 2812–2816.

[31] S. M. Rytov, Y. A. Krastov, and V. Tatarskii, *Principles of Statistical Radiophysics 2: Correlation Theory of Random Fields.* Berlin, Heidenberg, New York: Springer, 1987.

[32] SONNET, *Full wave 3D electromagnetic simulator*, www.sonnet.com.

[33] G. J. Foschini, "Layered space-time architecture for wireless communication in a fading environment when using multi-element antennas," *Bell Labs Technical Journal*, vol. 1, pp. 41–59, 1996.

[34] T. S. Rappaport, *Wireless Communications - Principles and Practice.* New Yor, USA: Prentice Hall, Inc., 2002.

[35] F. Agnelli, G. Albasini, I. Bietti, A. Gnudi, A. Lacatia, D. Mansstretta, R. Rovatti, E. Sacchi, P. Savazzi, F. Svelto, E. Temporti, S. Vitali, and R. Castello, "Wireless multi-standard terminals: System analysis and design of a reconfigurable rf front-end," *IEEE Circuit and System Magazine*, vol. 6, no. 1, pp. 38–59, 2006.

[36] M. C. Leifer, "Signal correlations in coupled cell and MIMO antennas," in *Proc. IEEE Antennas and Propag. Society Int. Symp.*, vol. 3, San Antonio, TX, Jun. 2002, pp. 194–197.

[37] I. J. Gupta and A. A. Ksienski, "Effect of the mutual coupling on the performance of the adaptive arrays," *IEEE Trans. on Antennas and Propagation*, vol. 31, no. 5, pp. 785–791, Sep. 1983.

[38] T. Sventenson and A. Ranheim, "Mutual coupling effects on the capacity of the multielement antenna system," in *Proc. IEEE ICASSP'2001*, vol. 4, Salt Lake City, UT, May 2001, pp. 2485–2488.

[39] J. W. Wallace and M. A. Jensen, "Mutual coupling in MIMO wireless systems: A rigorous network theory analysis," *IEEE Trans. on Wireless Communications*, vol. 3, pp. 1317–1325, Jul. 2004.

[40] C. Waldschmidt, S. Schulteis, and W. Wiesbeck, "Complete RF system model for analysis of compact mimo arrays," *IEEE Trans. on Vehicular Technology*, vol. 53, no. 3, pp. 579–586, May 2004.

[41] V. Jungnickel, V. Pohl, and C. von Helmolt, "Capacity of MIMO systems with closely spaced antennas," *IEEE Communications Letters*, vol. 7, no. 8, pp. 361–363, Aug. 2003.

[42] D. Gesbert, H. Bolcskei, D. Gore, and A. Paulraj, "Outdoor MIMO wireless channel: Model and performance prediction," *IEEE Trans. on Communications*, vol. 50, no. 12, pp. 1926–1935, Dec. 2002.

[43] W. C. Jakes, *Microwave Mobile Communications.* New York: Wiley, 1974.

[44] K. Tsunekawa and K. Kagoshima, "Analysis of correlation coeficient of built-in diversity antennas for a portable telephone," in *Proc. IEEE Antennas and Propagation Society International Symposium, 1990. AP-S. 'Merging Technologies for the 90's'. Digest.*, vol. 1, Dalas, TX, USA, May. 1990, pp. 543 – 546.

[45] R. G. Vaughan and N. L. Scott, *Channels, Propagation and Antennas for Mobile Communications.* London, UK: Institution of Electrical Engineers, 2003.

[46] W. Y. C. Lee, "Effects on correlation between two mobile radio base-station antennas," *IEEE Trans. on Communications*, vol. COMM-21, pp. 1214–1244, Nov. 1973.

[47] J. Fuhl, A. F. Molish, and E. Bonek, "Unified channel model for mobile radio systems with smart antennas," *IEEE Proceedings - Radar, Sonar Navigation*, vol. 145, pp. 32–41, Feb. 1998.

[48] F. Adachi, M. T. Feeney, A. G. Williamson, and J. D. Parsons, "Cross-correlation between the envelopes of 900 mhz signals received at a mobile base station site," *IEE Proc. Pt. F*, vol. 133, pp. 506–512, Oct. 1986.

[49] J. Salz and J. Winters, "Effect of fading correlation on adaptive arrays in digital mobile radio," *IEEE Trans. on Vehicular Technology*, vol. 43, pp. 1049–1057, Nov. 1994.

[50] K. I. Pederson, P. E. Mogerson, and B. H. Fleury, "Spatial channel characteristics in outdoor environments and their impact on BS antenna system performance," in *Proc. IEEE Vehicular Technology Confernce VTC'1998*, vol. 2, Ottawa, Canada, 1998, pp. 437–447.

[51] M. K. Ozdemir, E. Arvas, and H. Arslan, "Dynamics of spatial correlation and implications on MIMO systems," *IEEE Communications Magazine*, vol. 42, no. 6, pp. S14–S19, Jun. 2004.

[52] R. Janaswamy, *Radiowave Propagation and Smart Antennas for Wireless Communications.* Boston, MA: Kluwer, 2000.

[53] R. Janaswamy, "Effects of element mutual coupling on the capacity of fixed length linear arrays," *IEEE Antennas and Wireless Propagation Letters*, vol. 1, pp. 157–160, 2002.

[54] S. Krusevac, P. B. Rapajic, and R. A. Kennedy, "Effect of mutual coupling on the performance of multi-element antenna systems," in *Proc. 2005 IEEE International Symposium on Antennas and Propagation, ISAP05*, Seoul, Korea, Aug. 2005, pp. 565–568.

[55] S. Krusevac, P. B. Rapajic, and R. A. Kennedy, "SNR estimation for multi-antenna communication systems with closely spaced antenna elements," in *Proc. The Eight IEEE International Symposium on Signal Processing and Its Applications, ISSPA 2005*, Sydney, Australia, Aug. 2005, pp. 423–426.

[56] M. Andrews, P. Mitre, and R. deCarvalho, "Tripling the capacity of wireless communication using electromagnetic polarization," *Nature*, vol. 409, no. 6818, pp. 316–318, 2001.

[57] N. K. Das, T. Inoue, T. Taniguichi, and Y. Korasawa, "An experimental on mimo system having three orthogonal polarization diversity branches in multipath-rich environment," in *Proc. IEEE Vehicular Technology Conference, VTC2004-Fall.*, vol. 2, Los Angeles, California, USA, Sep. 2004, pp. 1528–1532.

[58] A. Paulraj and T. Kailath, "Increasing capacity in wireless broadcas systems using distributed tranmission/directional reception," *U.S. Patent no:*, no. 5345599, 1994.

[59] J. H. Winters, "On the capacity of radio communications systems with diversity in rayleigh fading environment," *IEEE Journal on Selected Areas in Communications*, vol. 5, pp. 871–878, Jun 1987.

[60] T. Cover and J. Thomas, *Elements of Information Theory.* New york: Wiley, 1991.

[61] A. Goldsmith, *Wireless Communications.* Cambridge University Press, 2005.

[62] P. B. Rapajic and D. Popescu, "Information capacity of random signature multiple-input multipe-output channel," *IEEE Trans. on Communications*, vol. 48, no. 8, pp. 1245–1248, 2000.

[63] A. Lozano, F. R. Farokhni, and R. A. Valenzuela, "Lifting the limits of high speed data acess using antenna arrays," *IEEE Communications Magazine*, vol. 39, no. 9, pp. 156–162, 2001.

[64] P. Drissen and G. J. Foschini, "On the capacity formula for multiple-input multiple-output communication channels: a geometric interpretation," *IEEE Trans. on Communications*, vol. 47, no. 2, pp. 173–176, 1999.

[65] E. Biglieri, J. Proakis, and S. Shamai, "Fading channels: Information-theoretic and communication aspects," *IEEE Trans. Inform. Theory*, vol. 44, pp. 2619–2692, Oct. 2004.

[66] F. R. Farrokhi, G. J. Foschini, A. Lazano, and R. A. Valenzuela, "Link-optimal space-time processing with multiple transmit and receive antennas," *IEEE Communications Letters*, vol. 5, no. 3, pp. 85–87, 2001.

[67] D. S. Shiu, *Wireless communication using dual antenna arrays.* Kluwer Academic: Kluwer International Series in Engineering and Computer Science, 1999.

[68] V. D.N., D. N. C. Tse, and V. Anantharam, "Asympthotically optimal water-filling in vector multiple-access channels," *IEEE Trans. on Information Theory*, vol. 47, no. 1, pp. 241–267, 2001.

[69] D. W. Bliss, K. W. Forsythe, A. O. Hero, and A. F. Yegulalp, "Environmental issues for mimo capacity," *IEEE Trans. on Signal Processing*, vol. 50, no. 9, pp. 2128–2142, 2002.

[70] H. Ozcelik, M. Herdin, W. Weichselberger, J. Wallace, and E. Bonek, "Deficiencies of the kronecker mimo radio channel model," *IEEE Electronics Letters*, vol. 39, pp. 1209–1210, Aug. 2003.

[71] W. Weichselberger, H. Ozcelik, M. Herdin, and E. Bonek, "A novel stochastic mimo channel model and its physical interpretation," in *Proc. International Symposium on Wireless Personal Multimedia Communications, WPMC*, Yokosuka, Japan, Oct. 2003.

[72] B. Clerckx, D. Vanhonacker-Janvier, C. Oestegs, and L. Vanderdorpe, "Mutual coupling effect on the channel capacity on the space-time processing of MIMO communication systems," in *Proc. IEEE International Conference on Communications,(ICC'03)*, Anchorage, AK, May 2003, pp. 2638–2642.

[73] P. N. Fletcher, M. Dean, and A. R. Nix, "Mutual coupling in multi-element array antenna and its influence on mimo channel capacity," *IEE Electronics Letters*, vol. 39, no. 4, pp. 342–344, Feb. 2003.

[74] B. Lindmark, "Capacity of a 2 x 2 MIMO antenna system with mutual coupling losses," in *IEEE Antenna and Propagation Society Symposium*, vol. 2, Banff, Alberta, Canada, Jun. 2004, pp. 1720–1723.

[75] P. S. Kildal and K. Rosengren, "Correlation and capacity of mimo systems and mutual coupling, radiation efficiency, and diversity gain of their antennas: simulations and measurements in a reverberation chamber," *IEEE Communications Magazine*, vol. 42, pp. 104 – 112, Dec. 2004.

[76] G. Delisle, M. Pelletier, and J. Cummins, "Signal-to-noise ratios of array receiving systems with internal losses," *IEEE Transactions on Antennas and Propagation*, vol. 29, no. 1, pp. 600–608, 1981.

[77] M. L. Morris and M. A. Jensen, "Network model for MIMO systems with coupled antennas and noisy amplifiers," *IEEE Trans. on Antennas and Propagation*, vol. 53, pp. 545–552, 2005.

[78] S. Krusevac, P. B. Rapajic, and R. A. Kennedy, "Channel capacity of multi-antenna communication systems with closely spaced antenna elements," in *Proc. The 16th Annual IEEE International Symposium on Personal Indoor and Mobile Radio Communications, IEEE PIMRC 2005*, Berlin, Germany, Sep. 2005, pp. 2366–2370.

[79] S. Krusevac, R. A. Kennedy, and P. B. Rapajic, "Effect of signal and noise mutual coupling on mimo channel capacity," *Wireless Personal Communications*, vol. 40(3), pp. 317–328, 2007.

[80] S. Loyka and A. Kouki, "Dimensionality loss in MIMO communication systems," in *3rd IASTED International Conference on Wireless and Optical Communications (WOC 2003)*, Banff, Alberta, Canada, Jul. 2003, pp. 138–143.

[81] S. Krusevac, P. B. Rapajic, and R. A. Kennedy, "Mutual coupling effect on thermal noise in multi-antenna wireless communication systems," in *Proc. 8th International Symposium on Communication Theory and Applications, ISCTA05*, Ambelside, UK, Jul. 2005, pp. 298–303.

[82] M. K. Ozdemir, H. Arslan, and E. Arvas, "Mutual coupling effect in multi-antenna wireless communication systems," in *Proc. IEEE GLOBECOM '2003*, vol. 2, Dec. 2003, pp. 829–833.

[83] A. C. Ludwig, "Mutual coupling, gain, and directivity of an array of two identical antennas," *IEEE Trans. Antennas Propag.*, vol. AP-24, no. 6, pp. 837–841, Nov. 1976.

[84] J. B. Andersen and H. H. Rasmussen, "Decoupling and descattering networks for antennnas," *IEEE Trans. Antennas Propag.*, vol. AP-24, no. 6, pp. 841–846, Nov. 1976.

[85] V. Riech, "Remarks on decoupling- and matching-networks for small antenna arrays," *Arch. Elektron. Uebertrag.*, vol. 30, no. 5, pp. 204–208, 1976.

[86] J. W. Wallace and M. A. Jensen, "Termination-dependant diversity performance of coupled anatennas: Network theory analysis," *IEEE Trans. on Antennas and Propagation*, vol. 52, no. 1, pp. 98–105, Jan. 2004.

[87] J. Weber, C. Volmer, K. Blau, R. Stepna, and M. A. Hein, "Miniaturized antenna array using decoupling networks with realistic elements," *IEEE Trans. on Microwave Theory and Tech.*, vol. 54, no. 6, pp. 2733–2740, Jun. 2006.

[88] B. K. Lau, J. B. Andersen, G. Kristensson, and A. F. Molish, "Impact of matching network on bandwidth of compact antenna array," *IEEE Trans. on Antennas and Propag.*, vol. 54, no. 11, pp. 3225–3238, Nov. 2006.

[89] S. Krusevac and P. B. Rapajic, "Channel Capacity of MIMO Systems with Closely Spaced Terminated Antenna," in *Proc. 2007 IEEE International Symposium on Information Theory, IEEE ISIT 2007*, Nice, France, Jun. 2007, pp. 1076–1080.

[90] H. A. Haus and R. B. Adler, *Circuit Theory of Linear Noisy Network.* New York: John Wiley and Sons, Inc., 1959.

[91] S. Dossche, S. Blanch, and J. Romeu, "Optimum antenna matching to minimize signal correlation on a two-port antenna diversity system," *IEE Electronics Letters*, vol. 40, no. 19, pp. 1164–1165, Sep. 2004.

[92] D. M. Pozar, *Microwave Engineering.* New York: Wiley, 1998.

[93] H. J. Chaloupka and X. Wang, "On the properties of small arrays with closely spaced antenna elements," in *Proc. IEEE Antennas Propag. Soc. int. Symp.,*, Monterey, CA, Jun. 2004, pp. 2699–2702.